

## Climate data and their characterisation for hydrological scenario modelling across northern Australia

LingTao Li, Randall J Donohue, Tim R McVicar, Tom G Van Niel, Jin Teng, Nick J Potter, Ian N Smith, Dewi GC Kirono, Janice M Bathols, Wenju Cai, Steve P Marvanek, Simon N Gallant, Francis HS Chiew and Andrew J Frost

December 2009

A report to the Australian Government from the CSIRO Northern Australia Sustainable Yields Project

## **Northern Australia Sustainable Yields Project acknowledgments**

Prepared by CSIRO for the Australian Government under the Raising National Water Standards Program of the National Water Commission (NWC). Important aspects of the work were undertaken by the Northern Territory Department of Natural Resources, Environment, The Arts and Sport (NRETAS); the Queensland Department of Environment and Resource Management (QDERM); the New South Wales Department of Water and Energy; Sinclair Knight Merz; Environmental Hydrology Associates and Jolly Consulting.

The Project was guided and reviewed by a Steering Committee (Kerry Olsson, NWC – co-chair; Chris Schweizer, Department of the Environment, Water, Heritage and the Arts (DEWHA) – co-chair; Tom Hatton, CSIRO; Louise Minty, Bureau of Meteorology (BoM); Lucy, Vincent, Bureau of Rural Sciences (BRS); Tom Crothers, QDERM; Lyall Hinrichsen, QDERM; Ian Lancaster, NRETAS; Mark Pearcey, Department of Water; Michael Douglas, Tropical Rivers and Coastal Knowledge (TRaCK); Dene Moliere, Environmental Research Institute of the Supervising Scientist (*eriss*); secretariat support by Angus MacGregor, DEWHA) and benefited from additional reviews by a Technical Reference Panel and other experts, both inside and outside CSIRO.

### **Northern Australia Sustainable Yields Project disclaimers**

Derived from or contains data and/or software provided by the Organisations. The Organisations give no warranty in relation to the data and/or software they provided (including accuracy, reliability, completeness, currency or suitability) and accept no liability (including without limitation, liability in negligence) for any loss, damage or costs (including consequential damage) relating to any use or reliance on the data or software including any material derived from that data or software. Data must not be used for direct marketing or be used in breach of the privacy laws. Organisations include: the Northern Territory Department of Natural Resources, Environment, The Arts and Sport; the Queensland Department of Environment and Resource Management; the New South Wales Department of Water and Energy.

CSIRO advises that the information contained in this publication comprises general statements based on scientific research. The reader is advised and needs to be aware that such information may be incomplete or unable to be used in any specific situation. No reliance or actions must therefore be made on that information without seeking prior expert professional, scientific and technical advice. To the extent permitted by law, CSIRO (including its employees and consultants) excludes all liability to any person for any consequences, including but not limited to all losses, damages, costs, expenses and any other compensation, arising directly or indirectly from using this publication (in part or in whole) and any information or material contained in it. Data are assumed to be correct as received from the organisations.

### **Citation**

Li LT, Donohue RJ, McVicar TR, Van Niel TG, Ten J, Potter NJ, Smith IN, Kirono DGC, Bathols JM, Cai W, Marvanek SP, Gallant SN, Chiew FHS and Frost AJ (2009) Climate data and their characterisation for hydrological scenario modelling across northern Australia. A report to the Australian Government from the CSIRO Northern Australia Sustainable Yields Project. CSIRO Water for a Healthy Country Flagship, Australia. 63pp.

### **Publication Details**

Published by CSIRO © 2009 all rights reserved. This work is copyright. Apart from any use as permitted under the Copyright Act 1968, no part may be reproduced by any process without prior written permission from CSIRO.

ISSN 1835-095X

Cover photograph: Victoria River Research Station, at Kidman Springs, lies just over 200 km south-west of Katherine. These photos were taken on the 11<sup>th</sup> (top) and 12<sup>th</sup> (bottom) of December 2007.

Courtesy of Bruce Doran.

# Preface

This is a report to the Australian Government from CSIRO. It is an output of the CSIRO Northern Australian Sustainable Yields Project which, together with allied projects for Tasmania and south-west Western Australia, will provide a nationwide expansion of the assessments that began with the CSIRO Murray-Darling Basin Sustainable Yields Project.

The projects are the first rigorous attempt to estimate the impacts of catchment development, changing groundwater extraction, climate variability and anticipated climate change on water resources at a whole-of-region scale, explicitly considering the connectivity of surface and groundwater systems. The CSIRO Northern Australian Sustainable Yields Project has undertaken the most comprehensive hydrological modelling ever attempted for the region, using rainfall-runoff models, groundwater recharge models, river system models and groundwater models, and considering all upstream-downstream and surface-subsurface connections.

## Summary

This report describes the climate data for the three climate scenarios used for the hydrological modelling in the project. The three climate scenarios are historical climate, recent climate, and future climate. The climate scenarios have 77 years of daily climate data at  $0.05^\circ \times 0.05^\circ$  (~ 5 km x 5 km) resolution grid cells across northern Australia. This report documents the data sources and methods implemented to develop the three climate scenarios, being historical climate (Scenario A), recent climate (Scenario B), and future climate (Scenario C). It also provides key climate characteristics of the three scenarios that allow water resource managers to better understand the current and projected climate of the systems they manage.

The historical climate scenario (Scenario A) is the baseline against which other scenarios are compared. Scenario A is a 77-year record of daily rainfall and evapotranspiration data from 1 September 1930 to 31 August 2007, and is based on the SILO database developed and maintained in real-time by the Queensland Climate Change Centre of Excellence.

The recent climate scenario (Scenario B) is used to assess future water availability should the climate in the future prove to be similar to that of the most recent 11 years (i.e. 1 September 1996 to 31 August 2007). The future climate scenario (Scenario C) is used to assess a range of possible climate conditions around the year 2030. Forty-five future climate variants, each with 77 years of daily climate sequences, were used. The future climate variants came from scaling the historical climate data to represent ~2030 climate, based on analyses of 15 global climate models (GCMs) and three global warming scenarios from the Fourth Assessment Report (AR4) of the Intergovernmental Panel on Climate Change.

The historical (77-year) mean annual rainfall for the entire project area is 850 mm/year. Rainfall is highest in northern near-coastal areas, with some isolated locations receiving a mean annual rainfall in excess of 3000 mm/year. The lowest rainfall occurs in the south of the project area, where mean annual rainfall is less than 350 mm/year. Over the entire area, 94 percent of the rainfall occurs in the wet season (November to April). The 77-year mean annual areal potential evapotranspiration averaged across the project area is 1954 mm/year, varying from 2116 mm/year in the south to 1584 mm/year in the north. As mean annual potential evapotranspiration is greater than mean annual rainfall over most of the project area, the project area is largely a water-limited landscape. Note, however, that there are pockets where rainfall is greater than potential evapotranspiration on a mean annual basis, so hydrologically are considered energy-limited. Intense rainfall in the wet season leads to significant river flows. Over the 77-year period rainfall trends are increasing, and this is primarily due to an increase in rainfall intensity, with the number of rain-days per year being fairly constant.

The recent (11-year) mean annual rainfall for the project area is 1001 mm/year, 17.8 percent higher than the historical mean. The increases are seen primarily in the Timor Sea Drainage Division (the western part of the study area). Recent annual rainfall is similar to historical annual rainfall for much of the Gulf of Carpentaria Drainage Division and the northern portion of the North-East Coast Drainage Division.

There is considerable uncertainty in the global warming projections and in the predictions of how global warming affects local rainfall, while simulations of potential evapotranspiration have less variance. In the wet season months, regional

projections of rainfall vary by up to 100 mm/month. Over the whole project area, projected water-year rainfall varies between 758 and 873 mm/year compared to its historical average of 850 mm/year. Projected potential evapotranspiration ranges between 1920 and 1972 mm/year compared to a historical mean of 1954 mm/year.

Under a wet ~2030 climate, rainfall increases by 3 percent and potential evapotranspiration decreases by 2 percent, compared to Scenario A. Under a median ~2030 climate, rainfall decreases by 3 percent and potential evapotranspiration increases by 1 percent. Under a dry ~2030 climate rainfall decreases by 11 percent and potential evapotranspiration increases by 1 percent. As most rainfall occurs in the wet season, these months are likely to experience the greatest changes in rainfall. Changes in potential evapotranspiration are projected to occur more uniformly across the whole year. The range between wet ~2030 climate and dry ~2030 climate rainfall projections varied between 50 and 200 mm/year between regions, while the regional variation for potential evapotranspiration was less than 50 mm/year. Future climate projections are problematic as the output from the 15 GCMs are not in agreement. However, it is important to note that the majority of the GCMs show increases in rainfall in ~2030 compared to the ~1990 levels – particularly in near-coastal areas. This suggests that the frequency of intense rainfall events in these areas will increase, leading to similar increases in runoff which could lead to an increase in flood recurrence.

The Bureau of Meteorology's (BoM) network of stations form the underlying input to the SILO database. An assessment of this network was undertaken at each grid-cell by coupling the distance to the ten nearest stations with the decadal completeness of the records for those stations. This analysis shows that the coverage of the BoM's stations has increased over time, with only small areas having 'distance-completeness index' values less than <0.5 since the 1970s.

# Table of Contents

<b>1</b>	<b>Introduction</b> .....	<b>1</b>
<b>2</b>	<b>Historical climate (Scenario A)</b> .....	<b>2</b>
2.1	Data source.....	2
2.2	Calculating areal potential evapotranspiration (APET).....	6
2.3	General climate characterisation .....	10
2.4	Rainfall, rainday and intensity trends .....	18
<b>3</b>	<b>Recent climate (Scenario B)</b> .....	<b>23</b>
3.1	Rainfall recurrence intervals .....	26
<b>4</b>	<b>Future climate (Scenario C)</b> .....	<b>29</b>
4.1	Global warming and the Fourth Assessment Report of the Intergovernmental Panel on Climate Change .....	29
4.2	Methods used to simulate a 2030 climate.....	31
4.3	Characterising simulated climate change.....	36
4.3.1	Characterising simulated air temperature change.....	36
4.3.2	Characterising simulated rainfall change .....	38
4.3.3	Characterising simulated APET change .....	42
4.4	Identifying three representative 2030 climates—Cwet, Cmid and Cdry .....	46
<b>5</b>	<b>Confidence levels</b> .....	<b>59</b>
<b>6</b>	<b>Conclusions</b> .....	<b>62</b>
<b>7</b>	<b>References</b> .....	<b>63</b>

## Tables

Table 1. General rainfall characteristics of northern Australia, reported for the 17 areas. All units are mm, with differing periods of integration being discussed in the text above. The exceptions are the column labelled '% wet of total' which is the ratio of the total wet season rainfall to the total water year rainfall (expressed as a percentage), and the columns labelled 'year' which is the end of the water year when either the maximum or minimum rainfall was experienced. Note that the sum of the seasonal values do not always equal the water year values because the combined wet season–dry season period (Nov–Oct) is different to the water year period (Sep–Aug) .....	11
Table 2. General monthly rainfall characteristics of northern Australia, reported for the 17 areas. The long-term monthly mean rainfall is calculated for the 77-years (from 1 September 1930 to 31 August 2007) .....	12
Table 3. General APET characteristics of northern Australia, reported for the 17 areas. All units are mm, with differing periods of integration being discussed in the text above. The exceptions are the column labelled '% wet of total' which is the ratio of the total wet season APET to the total water year APET (expressed as a percentage), and the columns labelled 'year' which is the end of the water year when either the maximum or minimum APET was experienced. Note that the sum of the seasonal values do not always equal the water year values because the combined wet season–dry season period (Nov–Oct) is different to the water year period (Sep–Aug) .....	13
Table 4. General monthly APET characteristics of northern Australia, reported for the 17 areas. The long-term monthly mean APET is calculated for the 77-years (from 1 September 1930 to 31 August 2007) .....	14
Table 5. Scenario B rainfall characteristics of northern Australia, for the 17 areas. All units are mm, with the exception of the column labelled '% wet of total' which is the ratio of the total wet season rainfall to the total water year rainfall (expressed as a percentage). Note that the sum of the seasonal values do not equal the water year values because the combined wet season–dry season period (Nov–Oct) is different to the water year period (Sep–Aug) .....	25
Table 6. Scenario B APET characteristics of northern Australia, for the 17 areas. All units are mm, with the exception of the column labelled '% wet of total' which is the ratio of the total wet season APET to the total water year APET (expressed as a percentage). Note that the sum of the seasonal values do not always equal the water year values because the combined wet season–dry season period (Nov–Oct) is different to the water year period (Sep–Aug) .....	25
Table 7. Number of rainfall stations passing completeness thresholds in each region, all the project area and an associated buffered area .....	26
Table 8. Storylines from the Intergovernmental Panel on Climate Change (2000) Special Report on Emission Scenarios (SRES) .....	30
Table 9. List of 15 Global Climate Models used .....	32
Table 10. Mean annual rainfall and percent rainfall change over the project area for the 15 GCMs using the high, medium and low global warming scenarios. The rainfall percent change is calculated as (GCM rainfall – historical rainfall) / historical rainfall and expressed as a percentage. The historical rainfall value is derived from Scenario A results and is 850 mm/year (see Table 1). The mean annual rainfall change data are plotted in Figure 32. Scenario Cwet (high scenario GCM = ccma_t63) Cmid (medium scenario GCM = cnrm) and the Cdry (high scenario GCM = gfdl) are bolded. The spatial distributions of P percent simulated change for the 15 GCMs for the medium warming scenario are shown in Figure 26 .....	47

Table 11. Mean annual APET and percent APET change over the project area for the 15 GCMs using the high, medium and low global warming scenarios. The APET percent change is calculated as (GCM APET – historical APET) / historical APET and expressed as a percentage. The historical APET value is derived from Scenario A and is 1954 mm/year (see Table 3). The mean annual APET change data are plotted in Figure 33. Scenario Cwet (high scenario GCM = cccma\_t63) Cmid (medium scenario GCM = cnrm) and the Cdry (high scenario GCM = gfdl) are bolded; noting this decision is based on P not APET. The spatial distributions percent simulated change for the 15 GCMs for the medium warming scenario are shown in Figure 31 .....48

Table 12. Annual and seasonal averaged P and APET for historical conditions and for scenario Cwet, Cmid and Cdry 2030 climate simulations. Note that the sum of the seasonal values do not always equal the water year values because the combined wet season–dry season period (Nov–Oct) is different to the water year period (Sep–Aug).....49

## Figures

Figure 1. Location map of northern Australia, showing the 13 reporting regions. The Timor Sea Division is comprised (from west to east) by the Fitzroy (WA), Kimberley, Ord-Bonaparte, Daly, Van Diemen, Arafura regions. The Gulf of Carpentaria Division contains (again from west to east) the Roper, South-West Gulf, Flinders-Leichhardt, South-East Gulf, Mitchell, Western Cape regions. The Northern Coral region is located in the North-East Coast Division ..... 1

Figure 2. Geographic neat-lines (units are decimal degrees) and grid-cells locations for the SILO dataset held on the CSIRO-WRON computing facility for all-Australia and the Northern Australia Sustainable Yields Project area .....2

Figure 3. Decadal analysis of the location and completeness of Bureau of Meteorology stations measuring daily rainfall used in the SILO database. The decade labelled 1910 is defined from 1 January 1910 to 31 December 1919, and so on. At a station, a decade is 100 percent complete if there are observations for every day in that decade .....4

Figure 4. Decadal analysis of the location and completeness of Bureau of Meteorology stations measuring daily maximum air temperature used in the SILO database. The decade labelled 1910 is defined from 1 January 1910 to 31 December 1919, and so on. At a station, a decade is 100 percent complete if there are observations for every day in that decade .....5

Figure 5. Long-term daily mean maximum air temperatures (Tmax) for: (a) the water year (1 September to 31 August), (b) the wet season (1 November to 30 April); and (c) the dry season (1 May to 31 Oct). The same periods are shown for daily mean minimum air temperature (Tmin) in (d) to (f). Note there are different legends for the maximum and minimum daily mean air temperature.....7

Figure 6. Long-term daily mean incoming shortwave radiation for: (a) the water year (1 September to 31 August), (b) the wet season (1 November to 30 April) and (c) the dry season (1 May to 31 Oct).....7

Figure 7. Long-term daily mean relative humidity for (a) the water year (1 September to 31 August), (b) the wet season (1 November to 30 April) and (c) the dry season (1 May to 31 October).....8

Figure 8. Water year mean rainfall and rainfall divergence: (a) shows water year rainfall (calculated as the spatial mean of the all-project-area); and (b) shows the annual rainfall divergence from the long-term mean (i.e. 1 September 1930 to 31 August 2007) .....11

Figure 9. Long-term mean rainfall, Morton’s areal potential evapotranspiration, and the difference: (a) shows the water year (1 September to 31 August) mean rainfall, (b) the wet season (1 November to 30 April) mean rainfall and (c) the dry season (1 May to 31 October) mean rainfall. The same periods are shown for APET in (d) to (f), and the difference (calculated as rainfall - potential evapotranspiration) is shown for the same periods in (g) to (i) ..... 15

Figure 10. Long-term 77-year monthly (a) rainfall and (b) APET showing the project area maximum, minimum, mean and  $\pm$  one standard deviation of monthly rainfall and APET, respectively. The maximum and minimum values are the upper and lower bounds of the range, respectively..... 16

Figure 11. Decadal mean wet season rainfall. The decade labelled 1930 is the 1930/31 to 1939/40, and so on ..... 17

Figure 12. Coefficient of variation of rainfall for (a) water year; (b) wet season and (c) dry season..... 18

Figure 13. Spatial distribution of long-term rainfall trends for (a) the water year (1 September to 31 August), (b) the wet season (1 November to 30 April) and (c) the dry season (1 May to 31 October)..... 19

Figure 14. Spatial distribution of long-term number of rainy days for (a) the water year (1 September to 31 August), (b) the wet season (1 November to 30 April) and (c) the dry season (1 May to 31 October)..... 19

Figure 15. Spatial distribution of long-term rainfall intensity for (a) the water year (1 September to 31 August), (b) the wet season (1 November to 30 April); and (c) the dry season (1 May to 31 October).....20

Figure 16. Spatial distribution of long-term trends in number of rain days for (a) the water year (1 September to 31 August); (b) the wet season (1 November to 30 April) and (c) the dry season (1 May to 31 October) .....21

Figure 17. Spatial distribution of long-term trends in rainfall intensity for (a) the water year (1 September 31 August); (b) the wet season (1 November to 30 April) and (c) the dry season (1 May to 31 October).....21

Figure 18. Historical and recent mean rainfall for the project area. Figure (a) is the historical rainfall calculated for the 77 years from 1 September 1930 to 31 August 2007 and figure (b) is the recent rainfall for the 11 years from 1 September 1996 to 31 August 2007 .....23

Figure 19. Comparison of ‘historical\*’ and ‘recent’ mean water year rainfall for the project area. Figure (a) shows the percentage relative differences between the ‘historical\*’ and ‘recent’ periods. Figure (b) is the statistical significance results between the ‘historical\*’ and ‘recent’ periods, calculated using a two-sided, non-overlapping two-sample t-test. The ‘historical\*’ period is from 1 September 1930 to 31 August 1996 (i.e. 66 years) and the ‘recent’ period is from September 1996 to 31 August 2007 (i.e. 11 years) .....24

Figure 20. Average recurrence intervals for rainfall for the Scenario B period relative to the Scenario A period at the locations of BoM stations.....27

Figure 21. Surface of average recurrence intervals for rainfall for the Scenario B period relative to the Scenario A period.....28

Figure 22. Global average temperature over the last 150 years (from IPCC, 2007).....30

Figure 23. Diagram summarising the methods used to calculate Scenario C data. The inter-relationships with the historical data used in Scenario A and B are highlighted .....33

Figure 24. Schematic explaining the daily scaling factors for rainfall from three grid-cells (NASY points 1, 2 and 3) for summer. Daily rainfall exceedance plots comparing the 1982-2000 GCM simulation with the 2046 to 2065 GCM simulation are shown in (a), (c) and (e). The functions used to fit the binned data are shown in (b), (d) and (f) .....	35
Figure 25. Change in mean annual near-surface air temperature for ~2030 relative to ~1990 for the project area from the 15 GCMs for the medium global warming scenario.....	37
Figure 26. Percent change in mean annual rainfall for ~2030 relative to ~1990 for the project area from the 15 GCMs for the medium global warming scenario.....	39
Figure 27. Number of GCMs showing decreases (or increases) in:(a) future mean annual rainfall; (b) highest 1 percent of rainfall (c) highest 5 percent of rainfall and (d) highest 10 percent of rainfall, when simulated ~2030 outputs are compared to ~ 1990 rainfall levels. All 15 GCMs are used .....	40
Figure 28. Spatial distribution of percent change in mean summer rainfall for ~2030 relative to ~1990 for the project area from the 15 GCMs for the medium global warming scenario. Summer is defined by the months December, January and February .....	41
Figure 29. Percent change in mean annual near-surface relative humidity for ~2030 relative to ~1990 for the project area from the 15 GCMs for the medium global warming scenario .....	43
Figure 30. Percent change in mean annual near-surface incoming solar radiation for ~2030 relative to ~1990 for the project area from the 15 GCMs for the medium global warming scenario .....	44
Figure 31. Percent change in mean annual areal potential evapotranspiration for ~2030 relative to ~1990 for the project area from the 15 GCMs for the medium global warming scenario .....	45
Figure 32. Percent change in mean annual rainfall for the 15 GCMs using the high, medium and low global warming scenarios for the project area. The GCMs are ordered by their percent change for the high global warming scenario from lowest (on the left) to highest (on the right). The values for this data are provided below in Table 10, and the spatial distributions of P percent simulated change for the 15 GCMs for the medium warming scenario are shown in Figure 26 .....	46
Figure 33. Percent change in mean annual APET for the 15 GCMs using the high, medium and low global warming scenarios for the project area. The GCMs are ordered by their percent change for the high global warming scenario from lowest (on the left) to highest (on the right). The values for these data are provided below in Table 11, and the spatial distributions of APET percent simulated change for the 15 GCMs for the medium warming scenario are shown in Figure 31.....	47
Figure 34. Water year, wet season and dry season rainfall for the project area under historical climate and scenarios Cwet, Cmid and Cdry 2030 climate projections .....	51
Figure 35. Water year, wet season and dry season APET for the project area under historical climate and scenarios Cwet, Cmid and Cdry 2030 climate projections .....	52
Figure 36. The relative difference in rainfall and areal potential evapotranspiration under scenarios Cwet, Cmid and Cdry relative to historical climate .....	53
Figure 37. Mean monthly rainfall across northern Australia, reported for the 17 areas under historical climate (i.e. Scenario A – labelled A) and Scenario C. The range of Scenario C values (C range) is the highest and lowest value from all 45 future ~2030 climate variants (i.e. the 15 GCMs and the high, medium and low emission scenarios) .....	55
Figure 38. Mean monthly APET across northern Australia, reported for the 17 areas under historical climate (i.e. Scenario A – labelled A) and Scenario C. The range of Scenario C values (C range) is the highest and lowest value from all 45 future ~2030 climate variants (i.e. the 15 GCMs and the high, medium and low emission scenarios) .....	57
Figure 39. Decadal maps of the distance-completeness index for rainfall. A value of 1.0 means the location is at a station with a complete rainfall record, and the index decreases with distance away from stations and/or with decreasing completeness of rainfall record. The decade labelled 1910 is defined from 1 January 1910 to 31 December 1919, and so on .....	60
Figure 40. Decadal maps of the distance-completeness index for maximum air temperature. A value of 1.0 means the location is at a station with a complete record, and the index decreases with distance away from stations and/or with decreasing completeness of record. The decade labelled 1910 is defined from 1 January 1910 to 31 December 1919, and so on.....	61



# 1 Introduction

This report is one in a series of technical reports from the CSIRO Northern Australia Sustainable Yields Project. The terms of reference for the project are to estimate current and future water availability in each catchment and aquifer in northern Australia considering climate change, other risks, and surface-groundwater interactions; and compare the estimated current and future water availability to that required to meet the current levels of extractive use. Results from the project have been reported progressively for the three Drainage Divisions that constitute the area.

The project area covers the entire tropical region of Australia, see Figure 1. The area is defined by the surface water drainage divisions (as defined by the Australian Water Resources Council) flowing to the seas north of Australia: the Timor Sea Drainage Division (comprised of reporting regions 01 to 06 in Figure 1), the Gulf of Carpentaria Drainage Division (reporting regions 07 to 12 in Figure 1) and the northern portion of the North-East Coast Drainage Division (region 13 in Figure 1). The area is over 1,200,000 km<sup>2</sup> in size.

The CSIRO Northern Australia Sustainable Yields Project considered three climate scenarios impacting water resources. Broadly speaking they are: (1) Scenario A is historical climate; (2) Scenario B is recent climate; (3) Scenario C is projected climate conditions around the year 2030 relative to approximate 1990 climatology. The historical climate scenario (Scenario A) is the baseline against which other scenarios are compared.

This report describes the sources of climate data and their characterisation for use in the CSIRO Northern Australia Sustainable Yields Project. Input climate data for the rainfall-runoff modelling are needed for scenarios A, B and C. The following three sub-sections describe: (1) the sources and methods used to generate the input climate data; and (2) characterisation of that data for scenarios A, B and C, respectively. Following this, some discussion of climate scenario estimation confidence levels are provided.

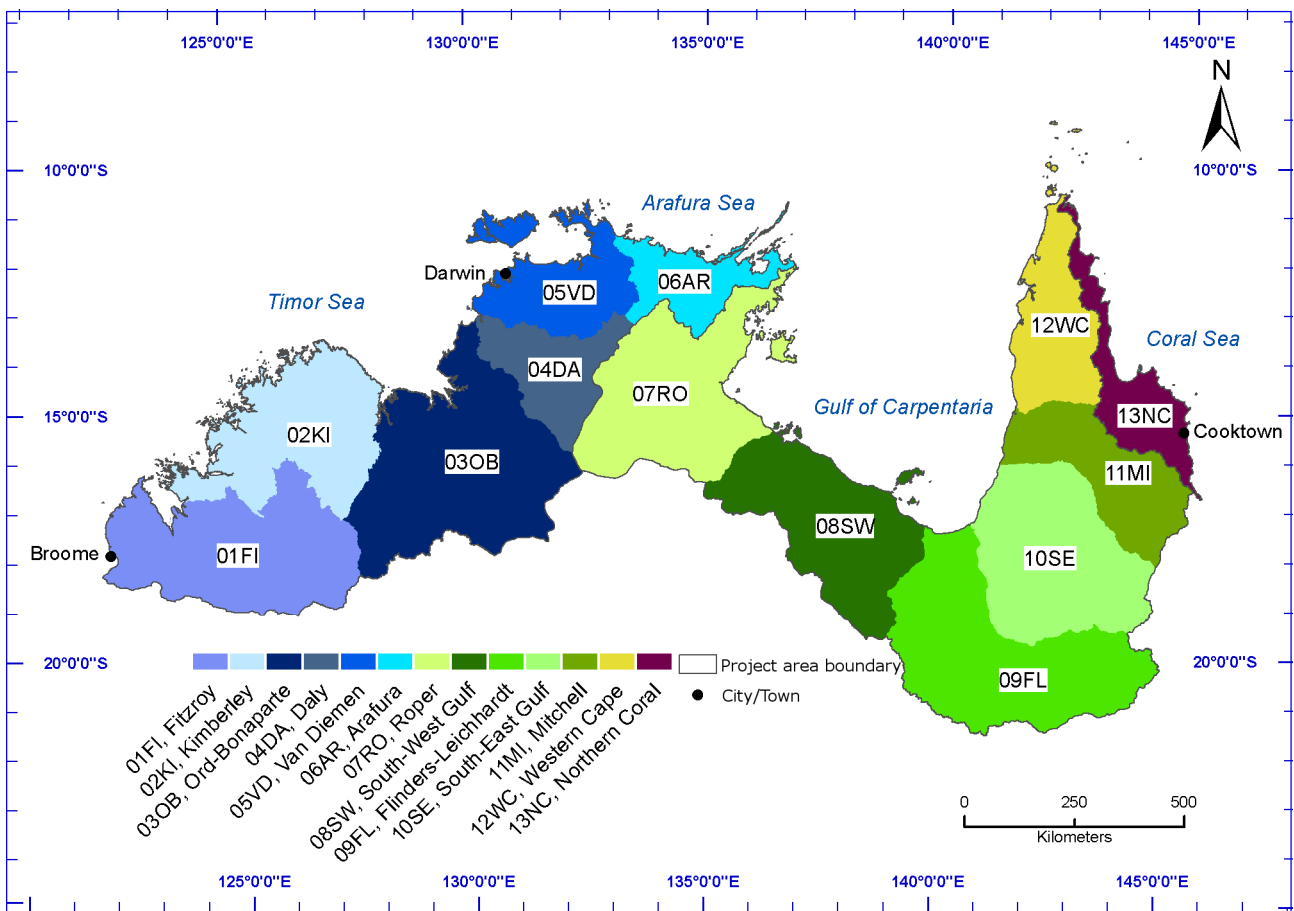


Figure 1. Location map of CSIRO Northern Australia, showing the three drainage divisions and 13 reporting regions. The Timor Sea Division is comprised (from west to east) by the Fitzroy (WA), Kimberley, Ord-Bonaparte, Daly, Van Diemen, Arafura regions. The Gulf of Carpentaria Division contains (again from west to east) the Roper, South-West Gulf, Flinders-Leichhardt, South-East Gulf, Mitchell, Western Cape regions. The Northern Coral region is located in the North-East Coast Division

## 2 Historical climate (Scenario A)

### 2.1 Data source

Historical daily climate data in the form of  $0.05^\circ \times 0.05^\circ$  (~ 5 km x 5 km) resolution grids are used as the primary information input, spanning 1 September 1930 to 31 August 2007. The source of the data was the SILO database developed and maintained in real-time by the Queensland Climate Change Centre of Excellence <<http://www.longpaddock.qld.gov.au/silo/>> and (Jeffrey, 2006; Jeffrey et al., 2001). SILO provides surfaces of daily climate data interpolated from point measurements made by the observation network developed and maintained by the Bureau of Meteorology. The variables used were rainfall (referred to as P in this report), incoming shortwave solar radiation ( $R_s$ ), vapor pressure ( $e_a$ ), maximum air temperature ( $T_{max}$ ) and minimum air temperature ( $T_{min}$ ).

The dominant weather patterns that bring rainfall to the project area are tropical cyclones and thunderstorms, the effects of which are highly localised. Due to this, and as the point observations of rainfall are highly discontinuous in space and time, interpolation of rainfall is particularly challenging. To maximise the accuracy of the SILO rainfall surfaces, Jeffrey (2006) implemented an interpolation strategy where a rainfall normalisation parameter was interpolated with ordinary Kriging, and after removal of stations with large residuals, the revised dataset was re-interpolated and the normalisation reversed. To capture air temperature lapse rates, and other near-surface elevation dependent processes (McVicar et al., 2007), surfaces for the other climatic variables were interpolated using a tri-variate thin plate spline as a function of longitude, latitude and elevation (Jeffrey et al., 2001).

The all-Australian SILO database held on the CSIRO Water Resources Observation Network (WRON) computing facility has the geographic neat-lines and grid-cells as shown in Figure 2. The geographical data extents refer to the cell-centres of the SILO grid-cells, to calculate the outer neat-lines  $0.025^\circ$  (i.e. half of the  $0.05^\circ$  grid-cell resolution) needs to be added (or subtracted as appropriate) to the geographic values provided below.

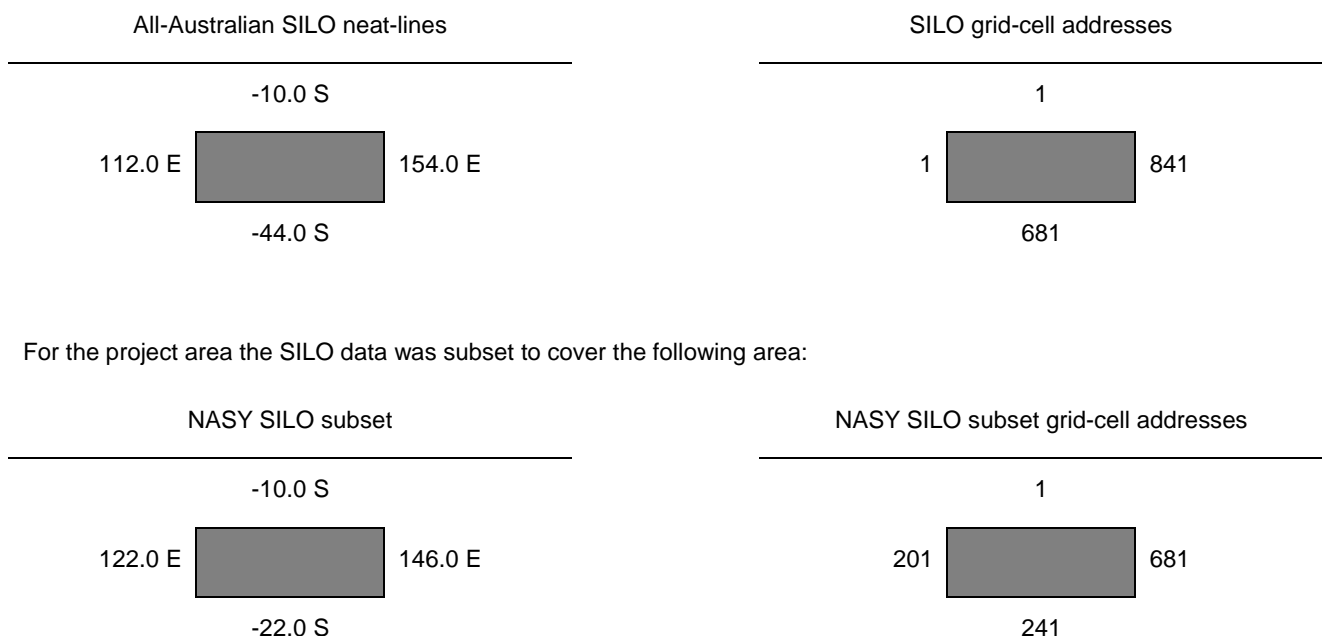


Figure 2. Geographic neat-lines (units are decimal degrees) and grid-cells locations for the SILO dataset held on the CSIRO-WRON computing facility for all-Australia and the CSIRO Northern Australia Sustainable Yields Project area

The gridded climate data are derived from observations that have been quality checked by the Bureau of Meteorology and have been subject to additional error checking by the Queensland Climate Change Centre of Excellence (Jeffrey et al., 2001). Nevertheless, it is inevitable that there will still be errors in the data. Interpolation routines also introduce errors. In general, the data accuracy was expected to be lower in areas where the observation density was low relative to the climate gradients. In this context, it should be noted that rainfall has lower spatial and temporal auto-correlation than other climate variables; and this has been compensated for by the Bureau of Meteorology purposefully establishing the rainfall observation network with a higher density than for other climate variables (compare Figure 3 to Figure 4), noting that the observing densities of both rainfall and maximum air temperature have increased over time (Figure 3 and Figure 4).

In the project area SILO subset, of the 115,921 grid-cells, calculated as 481 (the number of SILO grid-cells in the east-west direction of the subset) times 241 (the number of SILO grid-cells in the north-south direction of the subset), there are 86,806 that are over land – the remaining grid-cells are located in the surrounding oceans. When the 86,806 grid-cells are intersected with the project area boundary, defined using the Australian Surface Water Management Areas (ASWMA) 2000 boundaries, there are 44,679 0.05°x 0.05° resolution grid-cells that comprise the project area. It should be noted that for this project all ASWMA 2000 boundaries correspond to Geoscience Australia's Australia River Basins 1997 boundaries data, and that the exact project area was determined with additional consultation with the CSIRO Northern Australia Sustainable Yields Project steering committee.

For the rainfall-runoff and groundwater models used in the CSIRO Northern Australia Sustainable Yields Project, which use only time-series point data, the time series of daily climate surfaces were converted to a 77-year long time-series of point files for each 0.05°x 0.05° resolution grid. These 44,679 files were stored in CSV format, with the longitude and latitude decimal-degree cell-centre stored in the file name (noting that the negative sign for the southern hemisphere was omitted, which made file naming easier and was suitable as all of Australia is located in the southern hemisphere). For example, 13550\_1775.CSV is the file for 135.50 °E and -17.75 °S, or 135°30' E and -17°45' S.

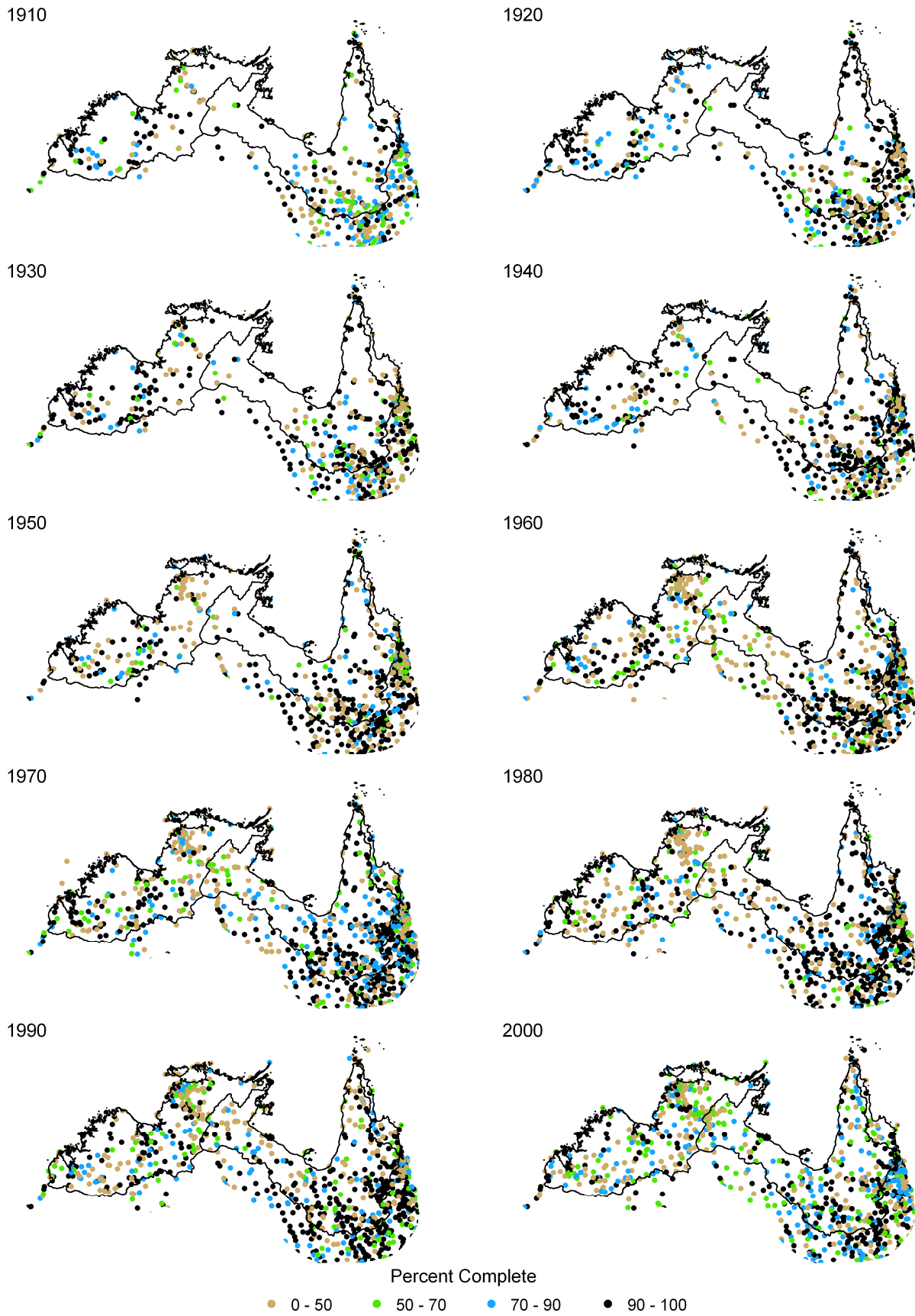


Figure 3. Decadal analysis of the location and completeness of Bureau of Meteorology stations measuring daily rainfall used in the SILO database. The decade labelled 1910 is defined from 1 January 1910 to 31 December 1919, and so on. At a station, a decade is 100 percent complete if there are observations for every day in that decade

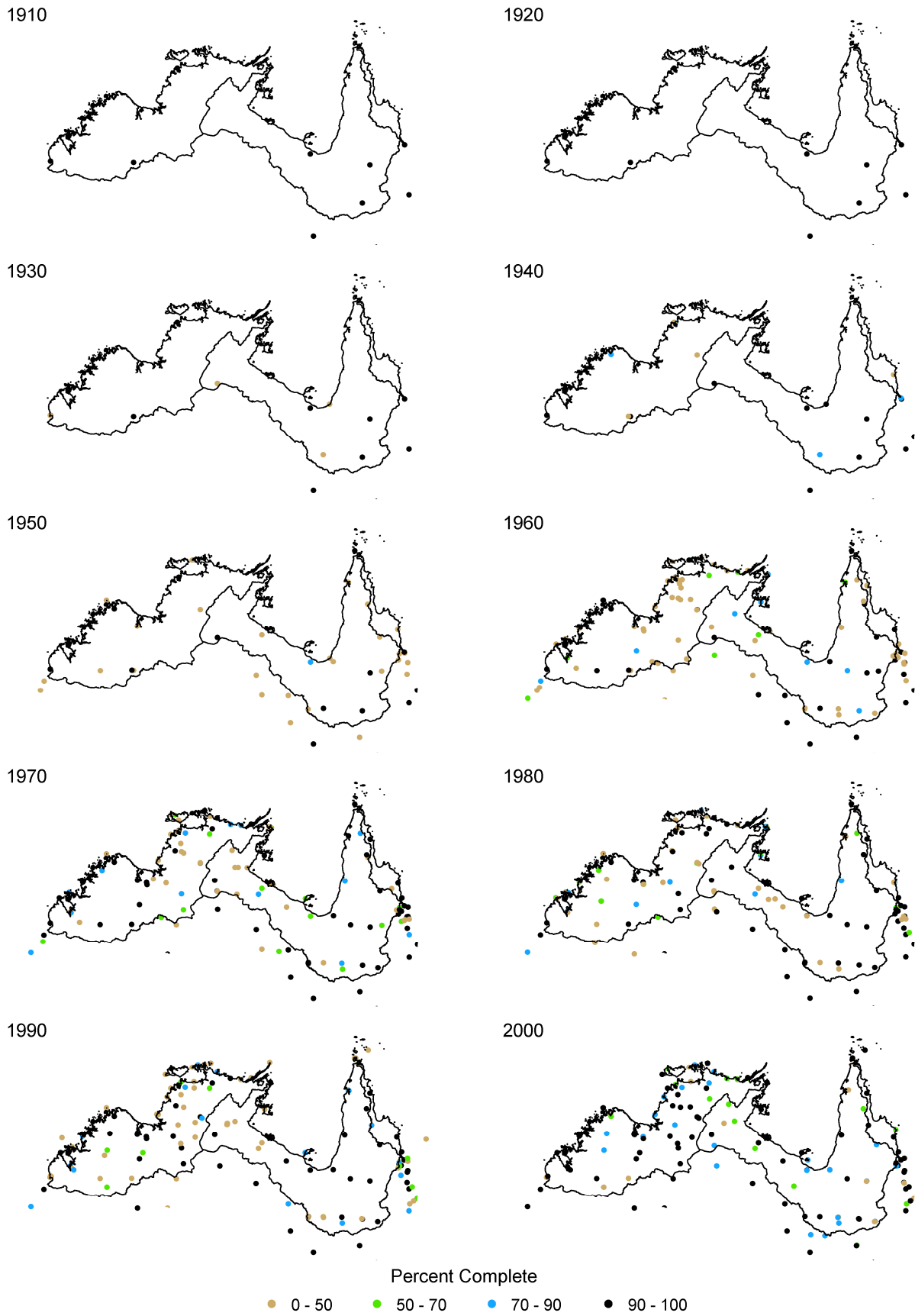


Figure 4. Decadal analysis of the location and completeness of Bureau of Meteorology stations measuring daily maximum air temperature used in the SILO database. The decade labelled 1910 is defined from 1 January 1910 to 31 December 1919, and so on. At a station, a decade is 100 percent complete if there are observations for every day in that decade

## 2.2 Calculating areal potential evapotranspiration (APET)

In addition to daily rainfall data, the surface-water and ground-water models require estimates of potential evapotranspiration (PET). PET represents the atmospheric demand for water under given meteorological conditions and provides an upper limit to the actual evapotranspiration in the hydrological modelling. Morton's wet environment areal PET (APET) (Chiew and Leahy, 2003; Morton, 1983) was calculated for the daily  $0.05^\circ \times 0.05^\circ$  grids using the following SILO data: maximum and minimum air temperature; incoming solar radiation, and atmospheric vapor pressure, (converted to relative humidity using the SILO actual vapour pressure divided by the saturation vapour pressure at the daily air temperature extremes). Long-term mean maximum and minimum air temperature, incoming solar radiation and relative humidity are shown in Figure 5, Figure 6 and Figure 7 respectively.

Relative humidity (percent) was calculated from the SILO atmospheric water vapor pressure ( $e_a$ ) data as follows:

$$\text{Rel Humidity} = 100 (e_a / e_s) \quad (1)$$

where Rel Humidity is the daily relative humidity (percent);  $e_a$  is the atmospheric water vapor pressure (kPa); and  $e_s$  is the saturation atmospheric water vapor pressure (kPa). The saturation vapor pressure ( $e_s$ ) is calculated for the two daily air temperatures Tmax or Tmin as:

$$e_s (T) = 0.6108 \exp \left[ \frac{17.27 \times T}{T + 237.3} \right], \quad (2)$$

and then averaged for use in equation (1) above.

APET represents the evapotranspiration that would take place from a continually saturated surface that is large enough to render the effects of any upwind boundary transitions negligible, thus integrating local variations to an areal average. In water-limited environments, daily hydrological modelling results are much less sensitive to errors in the PET data than they are to errors in the rainfall data. It is also easier to provide reliable PET data for the hydrological modelling as PET has lower spatial variance with smaller day-to-day variation when compared to rainfall. In other words, PET is relatively conservative in both space and time relative to rainfall.

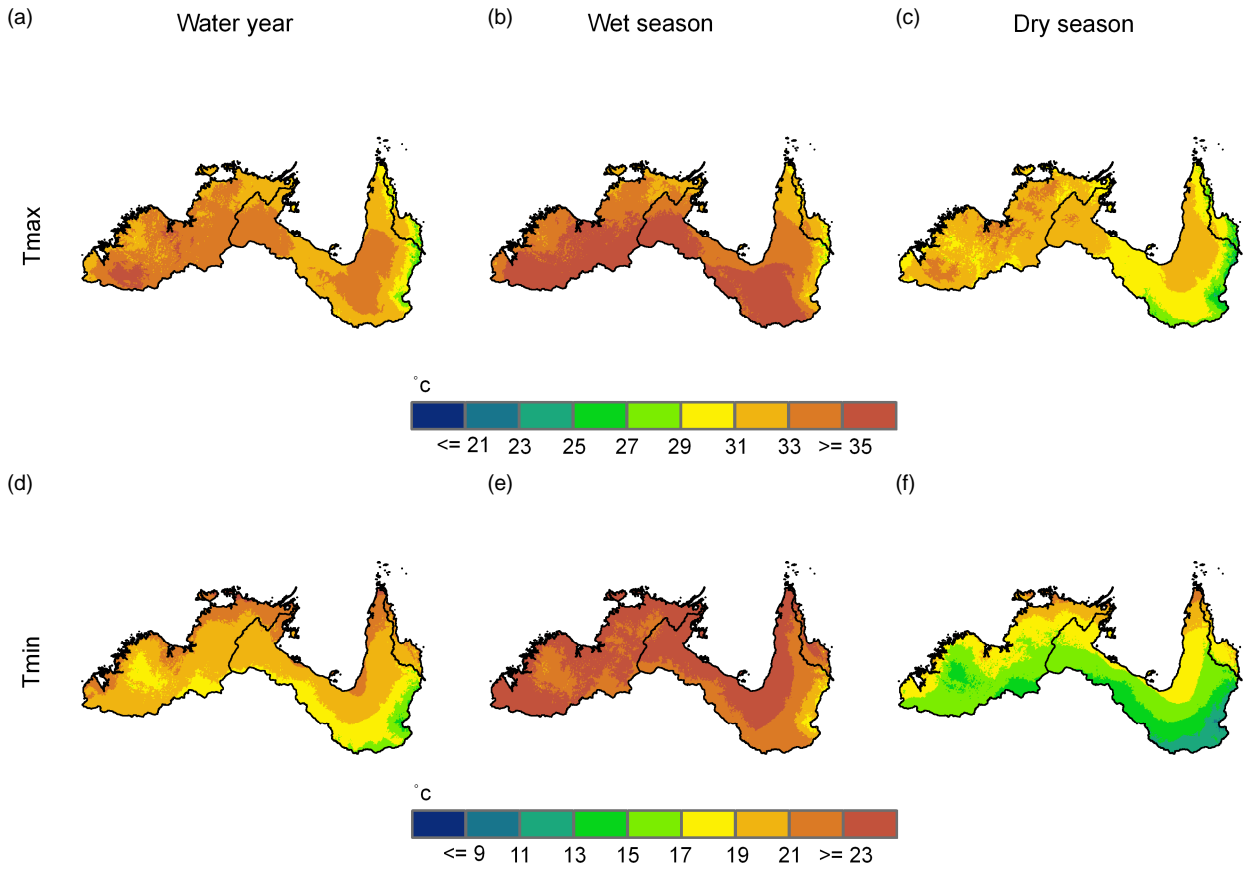


Figure 5. Long-term daily mean maximum air temperatures (Tmax) for: (a) the water year (1 September to 31 August), (b) the wet season (1 November to 30 April); and (c) the dry season (1 May to 31 Oct). The same periods are shown for daily mean minimum air temperature (Tmin) in (d) to (f). Note there are different legends for the maximum and minimum daily mean air temperature

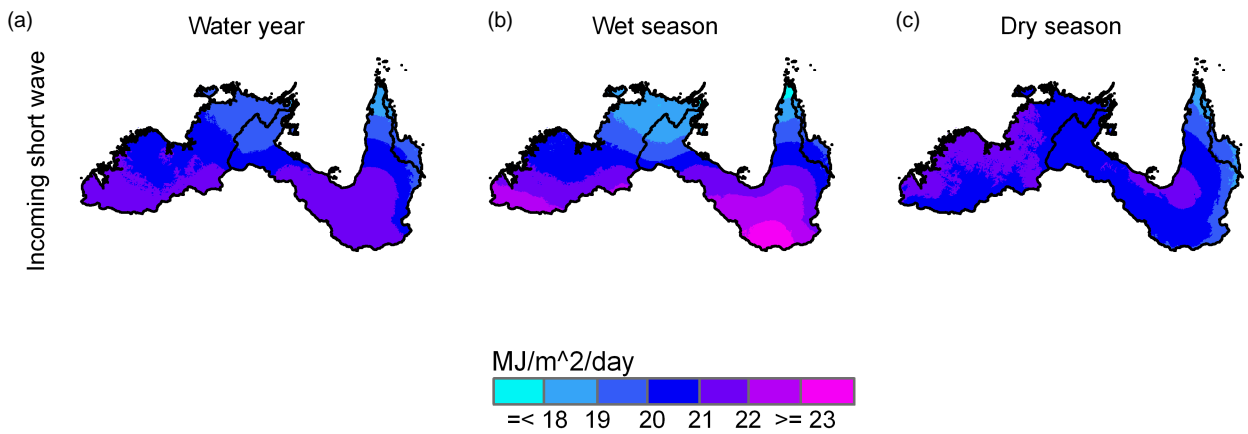


Figure 6. Long-term daily mean incoming shortwave radiation for: (a) the water year (1 September to 31 August), (b) the wet season (1 November to 30 April) and (c) the dry season (1 May to 31 Oct)

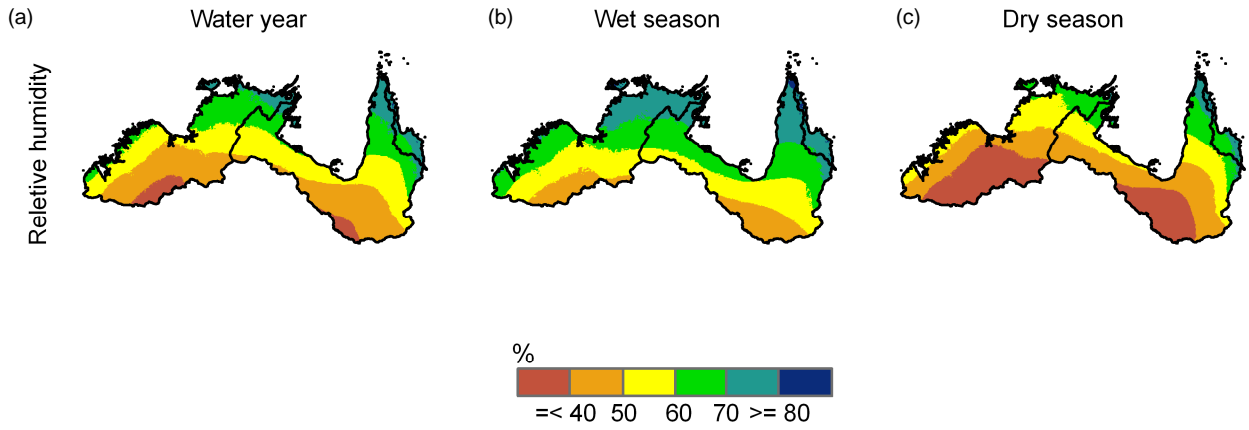


Figure 7. Long-term daily mean relative humidity for (a) the water year (1 September to 31 August), (b) the wet season (1 November to 30 April) and (c) the dry season (1 May to 31 October)

In most formulations of PET net radiation is needed as it is the primary source of energy for driving evaporation. Net radiation ( $R_n$  units of MJ/m<sup>2</sup>/day) is defined here as the sum of the component longwave and shortwave fluxes:

$$R_n = R_{s\downarrow} - R_{s\uparrow} + R_{L\downarrow} - R_{L\uparrow} \quad (3)$$

where  $R_{s\downarrow}$  is the incoming shortwave radiation,  $R_{s\uparrow}$  is outgoing shortwave radiation,  $R_{L\downarrow}$  incoming longwave radiation, and  $R_{L\uparrow}$  outgoing longwave radiation (all with units of MJ/m<sup>2</sup>/day).  $R_{s\downarrow}$  was obtained from the SILO database and  $R_{s\uparrow}$  was calculated as:

$$R_{s\uparrow} = R_{s\downarrow} \times \alpha \quad (4)$$

Where albedo ( $\alpha$ ) was set to 0.23 following Allen et al. (1998).

The net longwave ( $R_{nL}$ ) radiation was calculated using the following formulation, derived from Allen et al. (1998).

$$R_{nL} = \sigma \left[ \frac{T_{\max}^4 + T_{\min}^4}{2} \right] \left( 0.34 - 0.14 \sqrt{e_a} \right) \left( 0.10 + 0.9 \frac{n}{N} \right) \quad (5)$$

Where  $n$  is the bright sunshine hours and  $N$  is the number of daylight hours, with the ratio ( $n/N$ ) being a measure of the atmospheric transmittance. The ratio  $n/N$  is calculated by inverting the Ångström–Prescott equation (Prescott 1940).

$$\frac{n}{N} = (R_{s\downarrow} / R_a - a) / b \quad (6)$$

Where  $R_a$  is the extraterrestrial (or top-of-Earth atmosphere) solar radiation measured on a horizontal surface (MJ/m<sup>2</sup>/day), with  $a$  and  $b$  being semi-empirical coefficients;  $a$  being the regression constant relating  $R_{s\downarrow}$  to  $R_a$  for totally overcast days ( $n = 0$ ); and  $a + b$  being the atmospheric transmittance for totally clear days ( $n = N$ ). Following Allen et al. (1998)  $a = 0.25$ , and as McVicar and Jupp (1999) showed that maximum Australian clear-sky atmospheric transmittance was 0.81, an Australian-specific value for  $b$  of 0.56 (calculated as  $0.81 - 0.25 = 0.56$ ) was used.

$R_a$  was calculated as follows:

$$R_a = \frac{I_0}{\pi} d_r [\omega_s \sin(\varphi) \sin(\delta) + \cos(\varphi) \cos(\delta) \sin(\omega_s)] \quad (7)$$

Where  $I_0$  is the solar constant (118.1 MJ/m<sup>2</sup>/day),  $d_r$  is the inverse relative earth-sun distance ( $d_r = 1 + 0.033 \cos(0.0172 \text{DOY})$ ), where DOY is the Day Of Year from 1 (1 January) to 366 (31 December in a leap year);  $\omega_s$  is the sunset hour angle in radians (given by  $\omega_s = \arccos[-\tan(\varphi) \tan(\delta)]$ ), where  $\varphi$  is the latitude and  $\delta$  is the solar declination, both in radians.

The method used to calculate  $\delta$  is:

$$\delta = 0.409 \sin\left(\frac{2\pi}{365} \text{DOY} - 1.39\right) \quad (8)$$

Implementing the above equations produces daily  $R_n$  suitable for use in modelling APET as described below.

Morton's wet environment APET is calculated for an 'equilibrium' temperature that is iteratively determined by simultaneously solving the vapour transfer and energy balance equations. Potential evaporation is then calculated for the equilibrium temperature. The first step (equations 9 to 11) is to calculate three coefficients. The stability factor ( $\xi$ ) is:

$$\frac{1}{\xi} = 0.28 \left(1 + \frac{e_a}{e_s}\right) + \frac{\Delta R_n}{\gamma (P_s/P)^{0.5} f_z (e_s - e_a)} \quad (9)$$

Here  $e_a$  is the actual vapor pressure (kPa),  $e_s$  is the saturated vapor pressure (kPa) (Eq. 2),  $R_n$  (MJ/m<sup>2</sup>/day) (Eq. 3),  $P_s$  is mean sea level pressure (101.3 kPa),  $P$  is surface pressure given by  $101.3 * (293 - 0.0065z/293)^{5.26}$ , where  $z$  (elevation, m) is derived from a national 9-second DEM, and  $f_z$  is 24.19 MJ/m<sup>2</sup>/day/kPa for air temperature ( $T_a$ ) at or above 273.16 K and 27.82 MJ/m<sup>2</sup>/day/kPa for  $T_a$  below 273.16 K.

The vapour transfer coefficient ( $F$ , MJ/m<sup>2</sup>/day/kPa) is

$$F = \left(\frac{P_s}{P}\right)^{0.5} \frac{f_z}{\xi} \quad (10)$$

and the heat transfer coefficient ( $H$ , kPa/°C) is

$$H = \gamma + \frac{1.804 \times 10^{-8} (T_a + 273.16)^3}{F} \quad (11)$$

Where  $\gamma$  is the psychrometric constant (kPa/°C) and the coefficient  $1.804 \times 10^{-8}$  is the value of  $4 \mathcal{E} \sigma$  where  $\mathcal{E}$  is the land surface emissivity (here taken to be 0.92) and  $\sigma$  is the Stefan-Boltzmann constant ( $4.903 \times 10^{-9}$  MJ/K<sup>4</sup>/m<sup>2</sup>/day).

The second step (equations 12 to 17) is to iteratively calculate the equilibrium temperature,  $T_p$  (°C). This is done by initially setting  $T_p$  to  $T_a$  (°C), setting the equilibrium vapour pressure  $e_p$  to  $e_a$  and setting the equilibrium vapour pressure slope  $\Delta p$  to  $\Delta$  (the slope of the saturation vapor pressure curve). A temperature increment ( $\delta T$ ) is calculated according to:

$$\delta T = \frac{R_n/F + H(T_a - T_p) + e_a - e_p}{\Delta_p + H} \quad (12)$$

Estimates of equilibrium temperature ( $T_p'$ ), vapour pressure ( $e_p'$ ) and vapour pressure slope ( $\Delta p'$ ) are derived in each iteration:

$$T_p' = \delta T + T_p \quad (13)$$

$$e_p' = 0.6108 e^{\left(\frac{17.27 T_p'}{T_p' + 237.3}\right)} \quad (14)$$

and

$$\Delta_p' = \frac{4098e_p'}{(T_p' + 237.3)^2} \quad (15)$$

However, if  $T_p'$  is below 0.0 °C (an unlikely event in northern Australia yet documented here for completeness), then

$$e_p' = 0.6108 e^{\left(\frac{21.88T_p'}{T_p' + 265.5}\right)} \quad (16)$$

and

$$\Delta_p' = \frac{5809e_p'}{(T_p' + 265.5)^2} \quad (17)$$

$T_p$  is then set to  $T_p'$ ,  $e_p$  to  $e_p'$  and  $\Delta p$  to  $\Delta p'$  and the iteration (contained in equations 12 to 17) is repeated until the absolute value of  $\delta T$  is less than 0.01 °C. Morton's point potential evapotranspiration (PPET units of MJ/m<sup>2</sup>/day) is calculated as follows:

$$PPET = R_n - HF(T_p - T_a) \quad (18)$$

Then  $R_{np}$  (MJ/m<sup>2</sup>/day) is calculated, this is the net radiation that would occur at the equilibrium temperature

$$R_{np} = PPET + \gamma F(T_p - T_a) \quad (19)$$

Then APET (MJ/m<sup>2</sup>/day) is calculated as follows:

$$APET = 1.2096 + 1.2R_{np} \left( \frac{\Delta_p}{\Delta_p + \gamma} \right) \quad (20)$$

Finally the APET is converted from energy units of MJ/m<sup>2</sup>/day to depth of mm/day by multiplying this term by 0.408. This is determined by dividing the energy unit by the latent heat of vaporisation (2.45 MJ/kg) and density of water 1000 (kg/m<sup>3</sup> – at a standard atmosphere); see Allen et al. (1998) for full details. Temporal and spatial characteristics of the resultant APET surfaces, and rainfall, are described in the following sub-section.

## 2.3 General climate characterisation

For each of the 17 areas (i.e. the all-project-area, the three divisions and the 13 regions) general statistics characterising northern Australia's climate have been generated for both rainfall and APET. The statistics have been generated by adding all the daily surfaces to monthly total values, then calculating a water-year long-term average surface for the 77 years. The 'mean' is the mean value of the spatial surface, and the standard deviation, maximum and minimum are the spatial (not temporal) statistics determined for each of the 17 areas, in turn. The units of the statistics reported under the heading 'long-term annual' are mm/year, with a year defined as the northern Australia water year (1 September to the following 31 August). The statistics reported under the heading 'wet / dry seasonal information' are the mean seasonal rainfall, so they have units of mm/season. The wet-season is defined as the 6-month period from 1 November to following 30 April and the dry-season is defined as the 6-month period from 1 May to 31 October. Under the heading 'extreme year' the units are mm/year – again for a water year, with the year reported being the calendar year of the last 8 months of the water-year. For example, the Gulf of Carpentaria Division received 1611 mm/year (spatially averaged) in the period 1 September 1973 to 31 August 1974, so this is reported as occurring in 1974 in Table 1.

Table 1 shows that the all-project-area mean rainfall is 850 mm/year. Over 90 percent of this rainfall is received in the wet season, for the all-project-area and for each of the 13 reporting regions. The spatial coefficient of variation (CV – calculated as the standard deviation divided by the mean) is 0.38 for the all-project-area, and as the areas decrease in size the CV accordingly decreases and for the regions CV ranges from 0.30 (for the Ord-Bonaparte region) to 0.08 (for

the Arafura Sea region). On average the Western Cape region is the wettest (1417 mm/year), however there are small pockets in the Northern Coral region (around Cape Tribulation in the Daintree) that have a 3640 mm/year average. There is considerable temporal variation in the rainfall received by the area, this is seen by the all-project-area mean maximum rainfall (1539 mm/year being received from 1 September 1973 to 31 August 1974) being almost 4 times the all-project-area mean minimum rainfall (431 mm/year being received from 1 September 1951 to 31 August 1952). At a regional level this 'maximum-to-minimum water year rainfall' ratio ranges from 7.01 (for the Flinders-Leichhardt region) to 2.54 (for Van Diemen region). The all-project-area annual water year rainfall amounts are shown in Figure 8a, and the anomaly compared to the long-term mean is provided in Figure 8b.

Table 1. General rainfall characteristics of northern Australia, reported for the 17 areas. All units are mm, with differing periods of integration being discussed in the text above. The exceptions are the column labelled '% wet of total' which is the ratio of the total wet season rainfall to the total water year rainfall (expressed as a percentage), and the columns labelled 'year' which is the end of the water year when either the maximum or minimum rainfall was experienced. Note that the sum of the seasonal values do not always equal the water year values because the combined wet season–dry season period (Nov–Oct) is different to the water year period (Sep–Aug)

Areas	Long-term annual				Wet / dry seasonal information			Extreme year			
	Mean	Std	Max	Min	Wet mean	Dry mean	% wet of total	Max	Year	Min	Year
	mm						percent	mm		mm	
NASY*	850	324	3640	331	802	48	94%	1539	1974	431	1952
TS	868	303	1688	383	822	46	95%	1412	2000	421	1952
GC	779	289	1806	334	735	44	94%	1611	1974	384	1952
NE	1338	376	3640	917	1233	105	92%	2143	1974	769	1961
01FI	577	119	963	383	534	43	93%	1127	2000	249	1953
02KI	950	155	1223	628	898	53	94%	1679	2000	477	1936
03OB	730	218	1486	441	689	41	94%	1248	1974	316	1952
04DA	1019	189	1493	667	975	44	96%	1640	1974	498	1952
05VD	1390	113	1695	1155	1327	63	95%	1942	2000	765	1952
06AR	1186	100	1383	920	1140	46	96%	1821	2001	595	1952
07RO	843	163	1357	592	805	38	96%	1477	2001	347	1952
08SW	670	161	1168	405	631	39	94%	1460	2001	289	1952
09FL	493	86	812	331	437	56	89%	1326	1974	189	1952
10SE	750	129	1078	490	710	40	95%	2126	1974	329	1952
11MI	965	147	1615	714	917	48	95%	1945	1974	525	1952
12WC	1417	200	1809	1054	1370	47	97%	2033	1999	735	1961
13NC	1338	376	3640	917	1233	105	92%	2143	1974	769	1961

\*the all-project-area

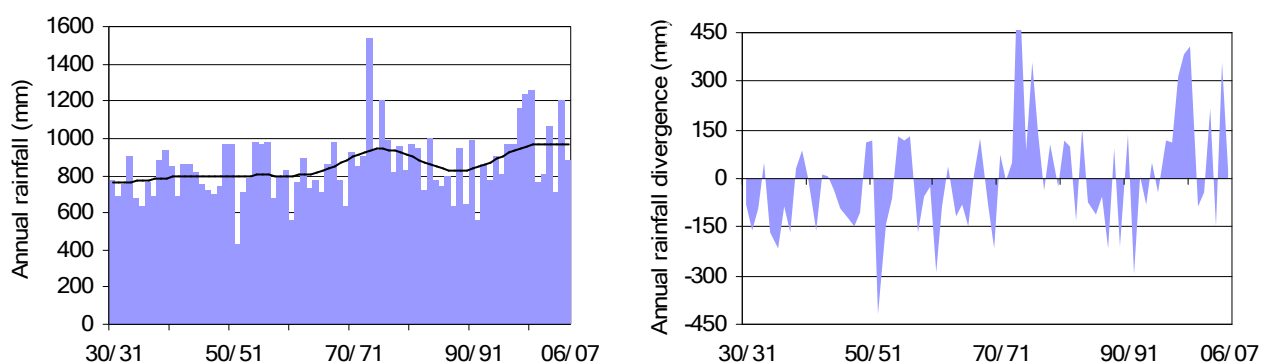


Figure 8. Water year mean rainfall and rainfall divergence: (a) shows water year rainfall (calculated as the spatial mean of the all-project-area); and (b) shows the annual rainfall divergence from the long-term mean (i.e. 1 September 1930 to 31 August 2007)

Table 2 reports the long-term monthly mean rainfall statistics for each of the 17 areas comprising the project area study site. These statistics underpin the wet-season dry-season analysis reported previously.

Table 2. General monthly rainfall characteristics of northern Australia, reported for the 17 areas. The long-term monthly mean rainfall is calculated for the 77-years (from 1 September 1930 to 31 August 2007)

Areas	Jan	Feb	Mar	Apr	May	Jun	Jul	Aug	Sep	Oct	Nov	Dec
	mm/month											
NASY*	214	207	157	43	14	8	4	2	4	17	53	127
TS	219	207	159	41	13	6	4	1	3	19	59	136
GC	199	196	141	36	11	8	4	2	4	16	47	115
NE	295	313	282	122	37	20	13	10	8	17	60	161
01FI	165	153	96	22	17	10	6	1	2	7	21	77
02KI	257	231	177	37	19	9	5	1	2	17	54	143
03OB	182	183	126	23	7	4	4	1	3	22	58	117
04DA	247	237	187	37	5	2	2	1	5	29	90	177
05VD	324	300	271	88	14	2	2	1	7	37	117	226
06AR	271	248	252	126	24	6	2	1	2	11	61	181
07RO	200	190	174	59	12	5	2	1	2	15	54	129
08SW	170	167	125	26	9	7	2	1	3	17	41	103
09FL	125	120	71	16	14	11	7	3	4	16	32	73
10SE	208	202	119	22	8	8	4	2	4	14	47	111
11MI	245	262	167	37	11	8	4	4	4	16	62	144
12WC	358	365	294	98	17	6	4	3	3	14	68	187
13NC	295	313	282	122	37	20	13	10	8	17	60	161

\*the all-project-area

Table 3 shows that the all-project-area mean APET is 1954 mm/year, which is approximately double the all-project-area mean rainfall of 850 mm/year reported in Table 1. This means on an annual basis the project area is water-limited, however, due to the extreme seasonality of rainfall stream flow occurs each wet season. The all-project-area wet-season APET is 55 percent of the annual total, and on a regional basis this value ranges from 50 percent (for both the Van Diemen and Arafura Sea regions) to 58 percent (for the Flinders-Leichhardt region). The high spatial auto-correlation of the APET surfaces is shown by the all-project-area spatial CV only being 0.03 (compared to 0.38 for rainfall). The region with the largest water year APET (2023 mm/year) is the Fitzroy (WA) region and the lowest is the Northern Coral region (1853 mm/year); so there is only a relatively small difference across the study area. When compared to the same statistics provided for rainfall in Table 1, both of the above findings confirm, as previously discussed, the low spatial variability of APET compared to the high spatial variability of rainfall. There is little temporal variation in the APET for the area; this is seen by the all project-area mean maximum APET (2050 mm/year in the year from 1 September 1991 to 31 August 1992) being only 1.12 times the all-project-area minimum mean APET (1826 mm/year in the year from 1 September 1973 to 31 August 1974). It is interesting to note that the water year that received the maximum rainfall (1539 mm/year in 1974, see Table 1) is the same year that had the lowest APET (1826 mm/year in 1974, see Table 3). This is expected, as periods receiving high rainfall are associated with high amounts of cloud cover, which results in the incoming radiation received at the surface being relatively lower, thereby reducing the APET. At a regional level this 'maximum-to-minimum water year APET' ratio ranges from 1.21 (for the Van Diemen region) to 1.22 (for the Ord-Bonaparte region). These findings confirm the previous discussion regarding the low temporal variability of APET compared to the high temporal variability of rainfall.

Table 3. General APET characteristics of northern Australia, reported for the 17 areas. All units are mm, with differing periods of integration being discussed in the text above. The exceptions are the column labelled ‘% wet of total’ which is the ratio of the total wet season APET to the total water year APET (expressed as a percentage), and the columns labelled ‘year’ which is the end of the water year when either the maximum or minimum APET was experienced. Note that the sum of the seasonal values do not always equal the water year values because the combined wet season–dry season period (Nov–Oct) is different to the water year period (Sep–Aug)

Areas	Long-term annual				Wet / Dry seasonal information			Extreme year			
	Mean	Std	Max	Min	Wet Mean	Dry Mean	% Wet of total	Max	Year	Min	Year
	mm				percent			mm		mm	
NASY*	1954	64	2116	1584	1068	886	55%	2050	1992	1826	1974
TS	1979	51	2116	1801	1068	911	54%	2086	1992	1848	1945
GC	1939	61	2054	1592	1076	863	56%	2023	1992	1796	1974
NE	1853	55	1933	1584	989	864	53%	1974	1992	1692	1945
01FI	2023	39	2080	1803	1140	883	56%	2158	1992	1884	1974
02KI	1994	48	2111	1818	1069	926	54%	2113	1992	1823	2000
03OB	1988	31	2116	1812	1092	896	55%	2093	2005	1865	1945
04DA	1942	28	1982	1838	1015	927	52%	2064	1998	1752	1945
05VD	1936	26	1973	1801	972	964	50%	2071	1998	1712	1945
06AR	1898	23	1952	1825	958	941	50%	2015	1992	1675	1945
07RO	1928	29	1984	1820	1023	906	53%	2040	2005	1783	1945
08SW	1961	19	1999	1897	1103	858	56%	2067	1992	1814	1974
09FL	1939	54	2024	1736	1134	805	58%	2023	1935	1771	1974
10SE	1980	71	2054	1695	1109	871	56%	2075	1931	1804	1974
11MI	1905	88	2005	1592	1036	870	54%	2003	1992	1772	1974
12WC	1874	47	1972	1690	974	900	52%	2003	1992	1696	1944
13NC	1853	55	1933	1584	989	864	53%	1974	1992	1692	1945

\*the all-project-area

Table 4 reports the long-term monthly mean APET statistics for each of the 17 areas comprising the project area. These statistics underpin the wet / dry season analysis reported previously. It is interesting to note that the maximum all-project-area mean APET (203 mm/month) is recorded in October, when the amount of incoming solar radiation is high due to the relative solar position, the relatively higher atmospheric transmittances associated with the previous 6-month dry season, and relatively higher vapor pressure deficits. In contrast, in February when a similar relative solar position occurs, being in the midst of the wet season with high amounts of cloud cover associated with rainfall, meaning both the atmospheric transmittance and vapor pressure deficit are relatively lower, the APET is only 157 mm/month. The minimum monthly APET occurs in June, at the time of the winter solstice, when incoming radiation received at the surface is at its lowest.

Table 4. General monthly APET characteristics of northern Australia, reported for the 17 areas. The long-term monthly mean APET is calculated for the 77-years (from 1 September 1930 to 31 August 2007)

Areas	Jan	Feb	Mar	Apr	May	Jun	Jul	Aug	Sep	Oct	Nov	Dec
	mm/month											
NASY*	183	157	171	154	134	113	120	145	171	203	203	199
TS	180	156	173	158	138	116	124	149	176	207	205	197
GC	188	160	171	151	130	109	116	140	167	201	204	204
NE	170	145	155	142	131	115	123	143	163	190	190	187
01FI	196	168	184	160	131	108	116	142	174	212	218	214
02KI	177	154	173	161	140	119	127	151	179	210	208	196
03OB	188	161	176	158	135	112	120	146	175	207	207	201
04DA	169	146	165	156	141	120	128	153	179	204	195	184
05VD	157	139	159	157	150	131	140	162	181	201	187	174
06AR	156	136	153	150	145	129	136	157	175	198	188	175
07RO	172	147	162	152	138	117	125	149	174	203	198	190
08SW	194	164	175	154	130	107	114	139	167	202	206	209
09FL	206	174	180	149	119	97	103	129	159	198	208	217
10SE	195	164	176	154	130	108	116	141	170	206	209	210
11MI	179	151	163	146	130	112	120	142	167	199	199	196
12WC	163	139	154	146	137	121	130	149	169	194	191	181
13NC	170	145	155	142	131	115	123	143	163	190	190	187

\*the all-project-area

An increasing trend of rainfall over much of northern Australia (particularly the north-west) has been reported for recent decades (e.g. Suppiah and Hennessy, 1998; Donohue et al., 2009) and this is evident in the NASY project area (see Figure 8). These trends are possibly caused by increases in anthropogenic aerosol over Asia affecting air temperature gradients and atmospheric circulation (Rotstayn et al., 2007; Rotstayn et al., 2008). There is a strong north-south rainfall gradient across the area (Figure 9), with a marked seasonality (Figure 10a), associated with the relative latitudinal position of the Inter-Tropical Convergence Zone (Suppiah, 1992). Figure 10c shows the long-term variability around the mean shown in Figure 10a. Decadal mean wet-season rainfall (94 percent of the water year rainfall, Table 1) shows the spatial pattern of the generally increasing rainfall across the region (Figure 11). Note the location of the yellow band, signifying rainfall of approximately 1000 mm per wet season, has generally moved southward illustrating that wet seasons are becoming wetter, as well as the extremely wet 1970s over the northern portion of the Cape York clearly evident (Figure 11).

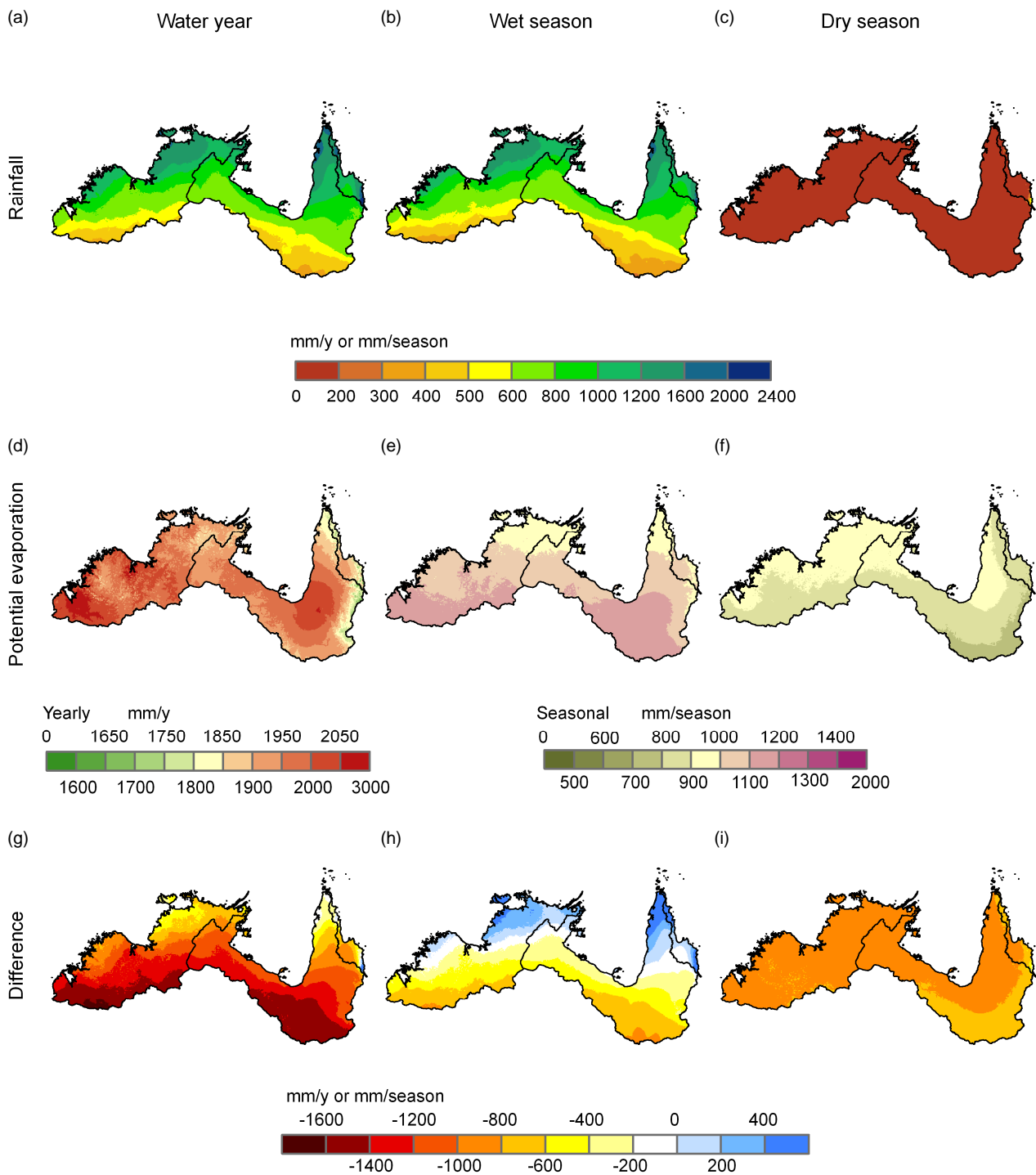
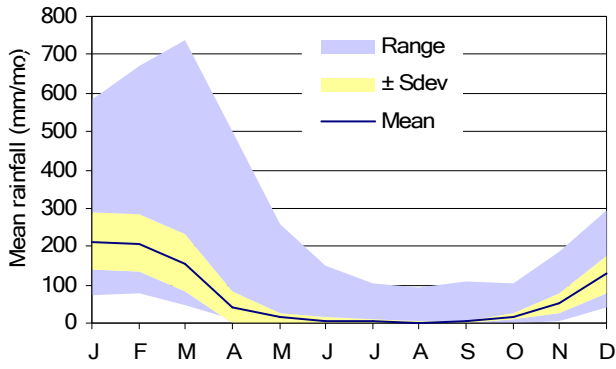


Figure 9. Long-term mean rainfall, Morton's areal potential evapotranspiration, and the difference: (a) shows the water year (1 September to 31 August) mean rainfall, (b) the wet season (1 November to 30 April) mean rainfall and (c) the dry season (1 May to 31 October) mean rainfall. The same periods are shown for APET in (d) to (f), and the difference (calculated as rainfall - potential evapotranspiration) is shown for the same periods in (g) to (i)

(a)



(b)

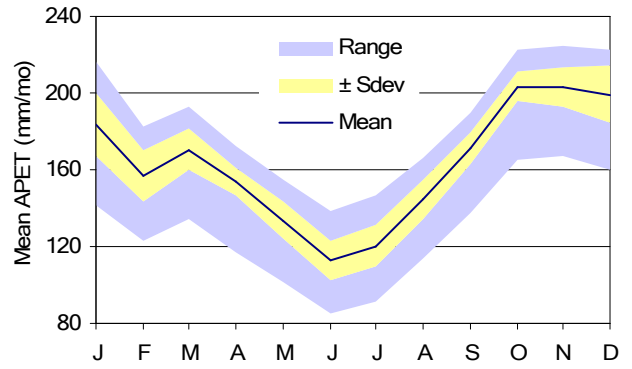


Figure 10. Long-term 77-year monthly (a) rainfall and (b) APET showing the project area maximum, minimum, mean and  $\pm$  one standard deviation of monthly rainfall and APET, respectively. The maximum and minimum values are the upper and lower bounds of the range, respectively

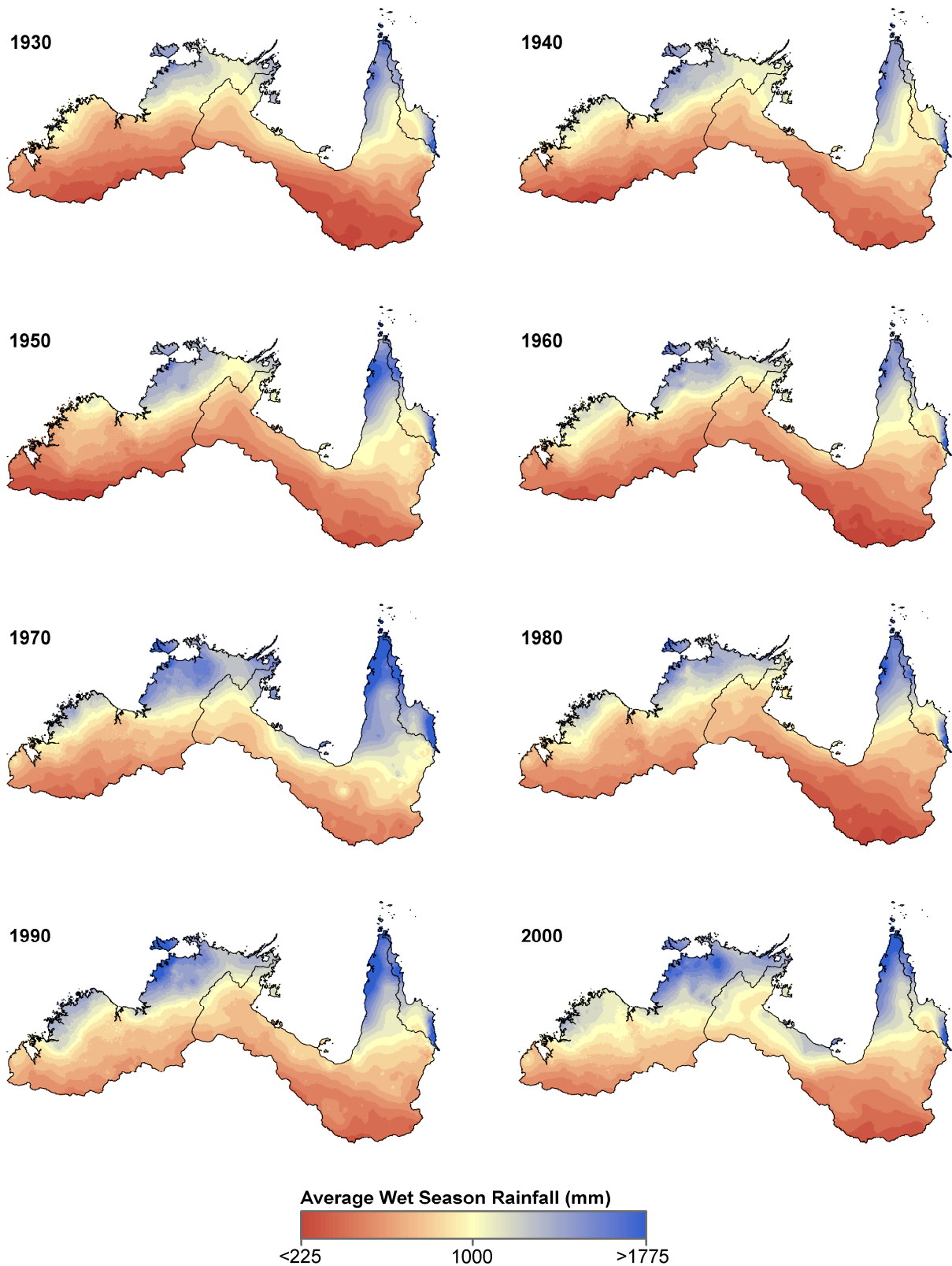


Figure 11. Decadal mean wet season rainfall. The decade labelled 1930 is the 1930/31 to 1939/40, and so on

For APET there is a strong north-south gradient across the divisions (Figure 9). Temporally for APET, there is a marked seasonality, with long-term variability around the mean (Figure 10b). The difference (calculated as rainfall minus APET) shows that on an annual basis much of the project area is water limited, as  $P - APET$  is negative (Figure 9g). Only one small pocket in the southern part of the Northern Coral region (i.e. around the Daintree) is energy-limited, as  $P - APET$  is positive (Figure 9g) on an annual time-step. Figure 9h shows that in the wet season the near coastal areas have relatively higher amounts of rainfall compared to APET, with Figure 9i showing that during the dry season APET is much

higher than rainfall, suggesting that evaporation from surface water storages in the project area in the dry season is large and needs to be planned for in water resource management schemes.

For rainfall, another characterisation of interest to hydrology is the coefficient of variation (CV), calculated as the standard deviation divided by the mean over the 77-year period; the spatial distribution of this is shown in Figure 12. For an annual time-step, for much of the project area the CV is <0.6 with values approaching 0.6 being further inland where mean annual rainfall is lowest. This pattern is expected following the global analysis of McMahon et al. (1992) who showed that drier areas experience the largest fluctuations in annual rainfall (hence have the highest CV values). The inverse relationship between rainfall and rainfall CV is clearly seen when the wet season (high rainfall and low rainfall CV) is compared to the dry season (low rainfall and high rainfall CV) in Figure 12b and c, respectively. In the dry season along the coast of the northern portion of the North-East Coast Drainage Division the rainfall CV is low, meaning that while winter rainfall is low (compared to summer rainfall) this rainfall has low inter-annual variability, resulting in a low CV.

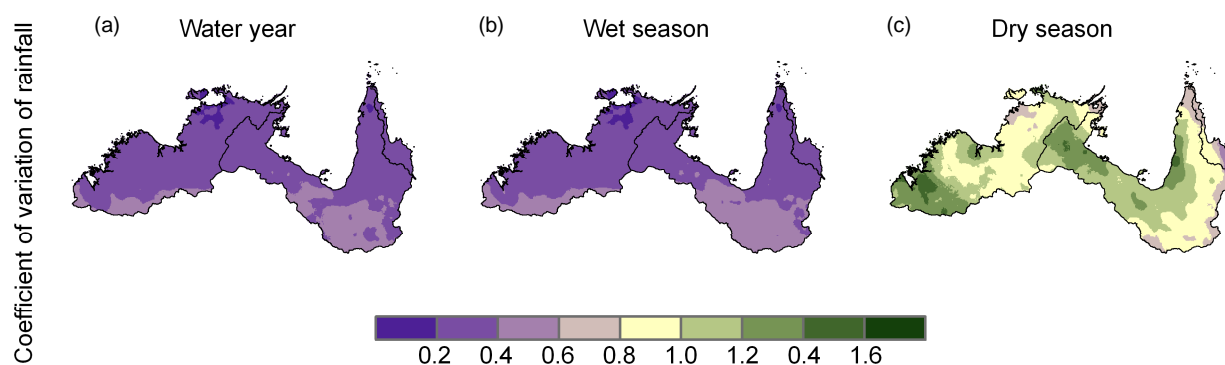


Figure 12. Coefficient of variation of rainfall for (a) water year; (b) wet season and (c) dry season

## 2.4 Rainfall, rainday and intensity trends

Rainfall trends were determined on a 0.05° grid-cell basis on annual, wet-season and dry-season scales for the 77-year period of Scenario A. This was performed by determining the slope of a linear regression (ordinary least squares) for each grid-cell; this method was recently used when analysing trends in all-Australian near-surface wind speeds (McVicar et al., 2008). Figure 13 shows the spatial distribution of these trends. It is illustrated that most of the Timor Sea Division and the western and northern portions of the Gulf of Carpentaria Division are experiencing increasing rainfall trends, both on an annual time-step (Figure 13a) and for the wet season (Figure 13b), which contributes >90 percent of the annual rainfall, see Table 1. Given this, the annual and wet-season mean rainfall trends are very similar, being 2.59 mm/year/year and 2.60 mm/season/year, respectively. Note, we are assessing the annual (or per annum) trend (or change) of rainfall which has units of mm per year, hence the units of the trend are mm per year per year, denoted mm/year/year. On an annual time-step the maximum and minimum rainfall trends are 17.25 mm/year/year and -4.56 mm/year/year, respectively. For the wet-season these values are 13.64 mm/season/year and -5.02 mm/season/year, respectively. The dry season trends, compared to the annual or wet season trends, are slight, and the area showing increase is approximately balanced by the area showing a decrease (Figure 13c), leading to a mean essentially 0.0 mm/season/year. The maximum positive trend, seen in the Northern Coral region, is 4.74 mm/season/year and the maximum negative trend is -1.72 mm/season/year.

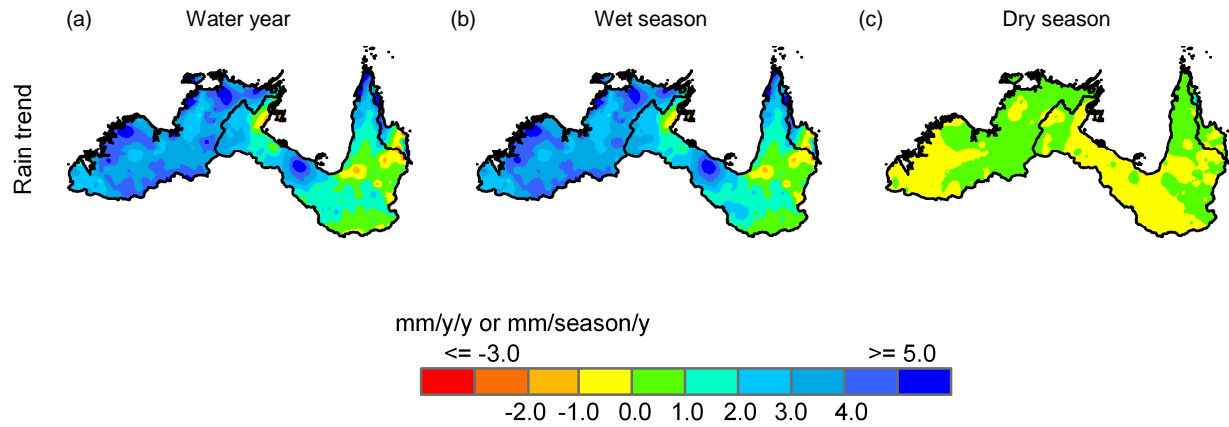


Figure 13. Spatial distribution of long-term rainfall trends for (a) the water year (1 September to 31 August), (b) the wet season (1 November to 30 April) and (c) the dry season (1 May to 31 October)

To calculate rainfall intensity the mean number of rainy days has been determined annually and for both the wet and dry seasons. To perform this calculation no threshold was applied to the amount of rainfall estimated in the SILO grid-cell for it to be counted as rainy, in other words a value of 0.0 mm/day is no-rain, and everything  $>0.0$  was considered a rainy day. While the spatial distribution of the number of rainy days could be considered an interim variable in the rainfall intensity calculation it provides additional characterisation of the rainfall regime (Figure 14). On an annual time-step the mean, maximum and minimum number of rainy days are 109.5 days, 222.9 days and 41.4 days, respectively. Figure 14a shows that most near-coastal areas north of  $15.5^{\circ}\text{S}$  receive rain for 120 days or greater during the year. In contrast, in the southern portion of the Flinders-Leichhardt region the number of rainy days is less than 60 days. During the wet season (Figure 14b) the mean number of rainy days is 94.3 days, with the maximum and minimum 140.6 days and 33.9 days, respectively. Considering that the wet season is 181 days (182 in leap years), this means that in some locations rain fell on over 75 percent of the days in the wet season. In January to March the proportion of rainy days is more extreme, and in the vicinity of Darwin over the 77-years rain is received nearly 90 percent of the days, the long-term monthly maximum number of rainy days of 27.23 days per January being found at  $132.60^{\circ}\text{E}$  and  $12.30^{\circ}\text{S}$  in the Van Diemen region some 200 km east of Darwin. During the dry season the mean number of rainy days is 15.1 days, with the maximum of 91.4 days located on the eastern sea-board of the Northern Coral region (Figure 14c), the minimum is 4.4 days located in the west of the South-East Gulf region.

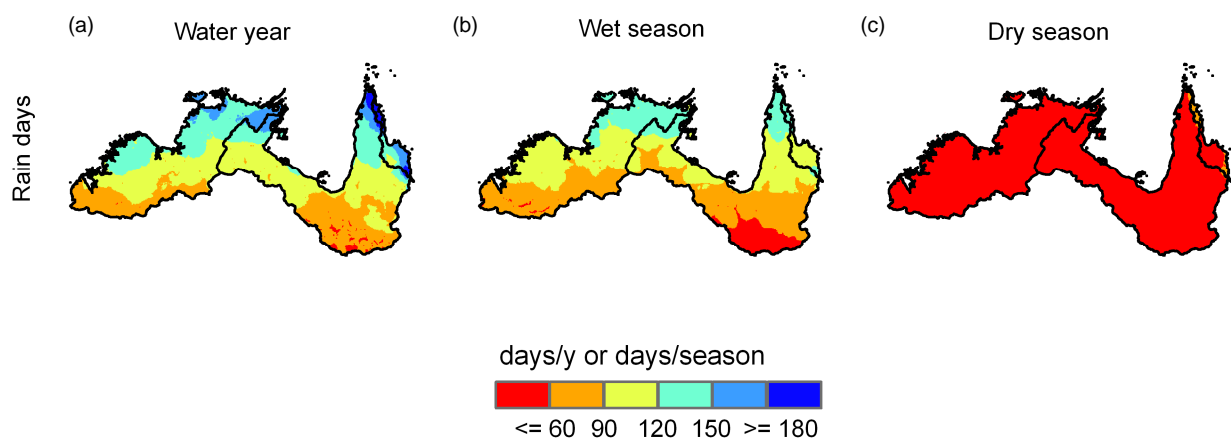


Figure 14. Spatial distribution of long-term number of rainy days for (a) the water year (1 September to 31 August), (b) the wet season (1 November to 30 April) and (c) the dry season (1 May to 31 October)

Rainfall intensity, calculated as rainfall per rain day (i.e. the data shown in Figure 9 divided by the data shown in Figure 14) is shown in Figure 15. On an annual time-step the rainfall intensity mean is 7.6 mm/rainday, with a maximum and minimum of 17.7 mm/rainday and 4.8 mm/rainday, respectively. As expected, most of the areas with high intensities are near-coastal, decreasing inland (Figure 15). During the wet season more intense rainfall is received, the rainfall intensity mean, maximum and minimum are 8.3 mm/rainday, 24.2 mm/rainday and 4.9 mm/rainday, respectively. While the annual and wet seasons spatial patterns of rainfall intensity are similar, differences are seen. For example, in the wet season most of Cape York receives rainfall with an intensity >8.0 mm/rainday, whereas annually this regions contracts to the western portion of Cape York adjacent to the Gulf of Carpentaria. In the dry season relatively (compared to the wet season) lower rainfall intensities are experienced, with the rainfall intensity mean, maximum and minimum being 3.5 mm/rainday, 10.6 mm/rainday and 1.0 mm/rainday, respectively. The areas of relatively high dry season rainfall intensity are located on the coast just north of Broome in the Fitzroy (WA) region and in the southern portion of the Flinders-Leichhardt region.

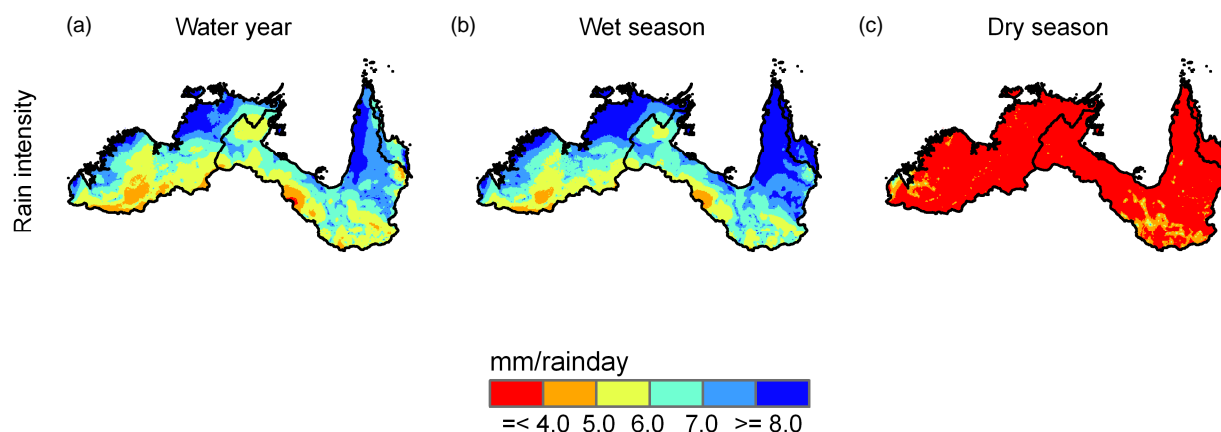


Figure 15. Spatial distribution of long-term rainfall intensity for (a) the water year (1 September to 31 August), (b) the wet season (1 November to 30 April); and (c) the dry season (1 May to 31 October)

The increase in rainfall shown in Figure 13 leads to the question: is the increase in rainfall due to: (1) an increase in the number of raindays; (2) an increase in the rainfall intensity; or (3) a combination of both. Trend analysis was performed by fitting a linear regression (ordinary least squares) to each grid-cell and determining the slope of the relationship for both the number of rain days (Figure 16) and rainfall intensity analysis (Figure 17) in the 77-year period. This was performed for the water year, wet season and dry season.

Figure 16 shows the spatial patterns of the trends in the number of rain days, and on an annual basis the mean value is only 0.11 raindays/year/year, with maximum and minimum values of 1.12 raindays/year/year and -1.37 raindays/year/year, respectively. For most of the project area, Figure 16a shows there is a patchy pattern of increasing and decreasing trends of number of rain days on an annual basis with the exception of most of the Timor Sea Drainage Division (where an increasing trend is seen). For the wet season the mean value is 0.41 raindays/season/year, with the maximum and minimum values being 1.16 raindays/season/year and -0.26 raindays/season/year, respectively. The spatial pattern of this trend reveals that most of northern Australia has experienced increasing number of rain days during the 77-year period (Figure 16b). For the dry season, which receives less than 10 percent of the annual rainfall (Table 1), the mean value is 0.07 raindays/season/y, with the extreme values being 0.77 raindays/season/y and -0.48 raindays/season/y, respectively (Figure 16c).

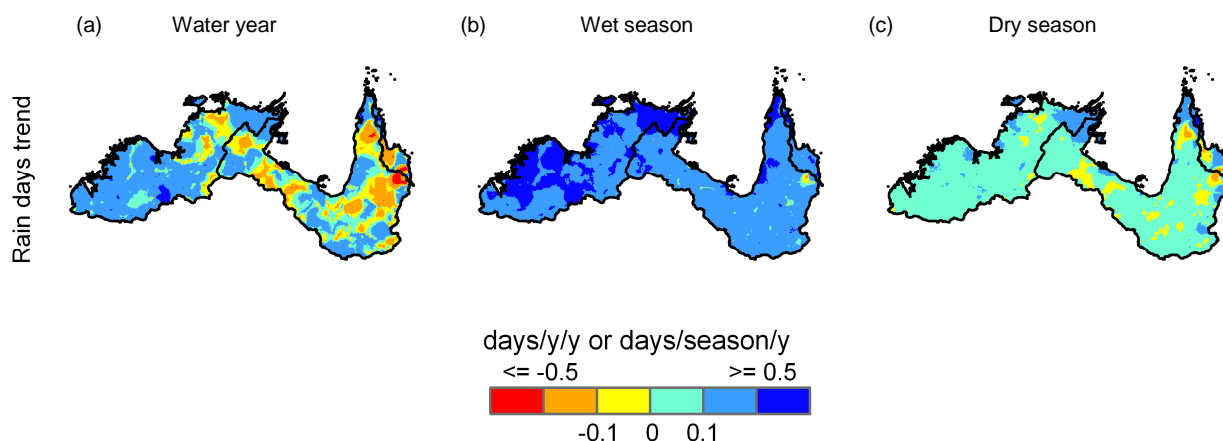


Figure 16. Spatial distribution of long-term trends in number of rain days for (a) the water year (1 September to 31 August); (b) the wet season (1 November to 30 April) and (c) the dry season (1 May to 31 October)

Figure 17 shows the distribution of the rainfall intensity trends. For the water year most of the area has an increasing trend (Figure 17a), the mean value is 0.016 mm/rainday/year. The maximum and minimum values are 0.123 mm/rainday/year and -0.164 mm/rainday/year, respectively. Figure 17b illustrates that in the wet season most of the area has an increasing trend of rainfall intensity, with the mean, maximum and minimum values being 0.019 mm/rainday/year, 0.123 mm/rainday/year and -0.166 mm/rainday/year, respectively. For the dry season much of the area has a decreasing, albeit slight, trend of rainfall intensity (Figure 17c), the mean value is -0.002 mm/rainday/year. In the dry season the maximum and minimum values are 0.145 mm/rainday/year and -0.161 mm/rainday/year, respectively.

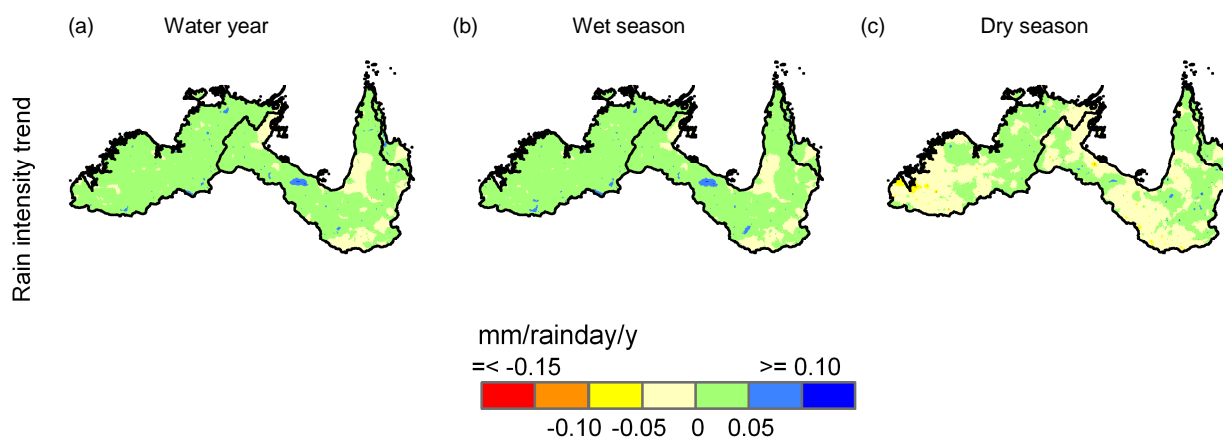


Figure 17. Spatial distribution of long-term trends in rainfall intensity for (a) the water year (1 September 31 August); (b) the wet season (1 November to 30 April) and (c) the dry season (1 May to 31 October)

The analysis presented in Figure 16 and Figure 17 shows that for water year the spatial pattern in the rainfall trend (Figure 13a) is more closely related to the changes in rainfall intensity trends (Figure 17a) than the trends in the number of rain days (Figure 16a). In the wet season (which contributes greater than 90 percent of the annual rainfall, Table 1) the increasing trend in rainfall (Figure 13b) is apparently due to increase in both the number of rain days (Figure 16b) and the rainfall intensity (Figure 17b). And, as for the annual analysis, the spatial pattern in the rainfall trends more closely corresponds with the spatial patterns of rainfall intensity trends. For the dry season, the rainfall trend (Figure 13c) is primarily explained by the trends in the rainfall intensity (Figure 17c); with the spatial distribution of the trends in rain days being negligible (Figure 16c). These results suggest that the increasing trend in rainfall intensity is the primary factor driving increasing rainfall trends over much of northern Australia; in line with climate change theory of a more intense hydrological cycle (e.g., Huntington, 2006).



### 3 Recent climate (Scenario B)

The recent climate scenario (Scenario B) is used to assess future water availability should the climate in the future prove to be similar to that of the most recent 11 years (i.e. 1 September 1996 to 31 August 2007). The recent mean annual rainfall averaged over the entire project area is 1001 mm, which is 17.8 percent higher than the historical 77-year mean of 850 mm, calculated over the period 1 September 1930 to 31 August 2007. Figure 18 shows the spatial differences of the two periods.

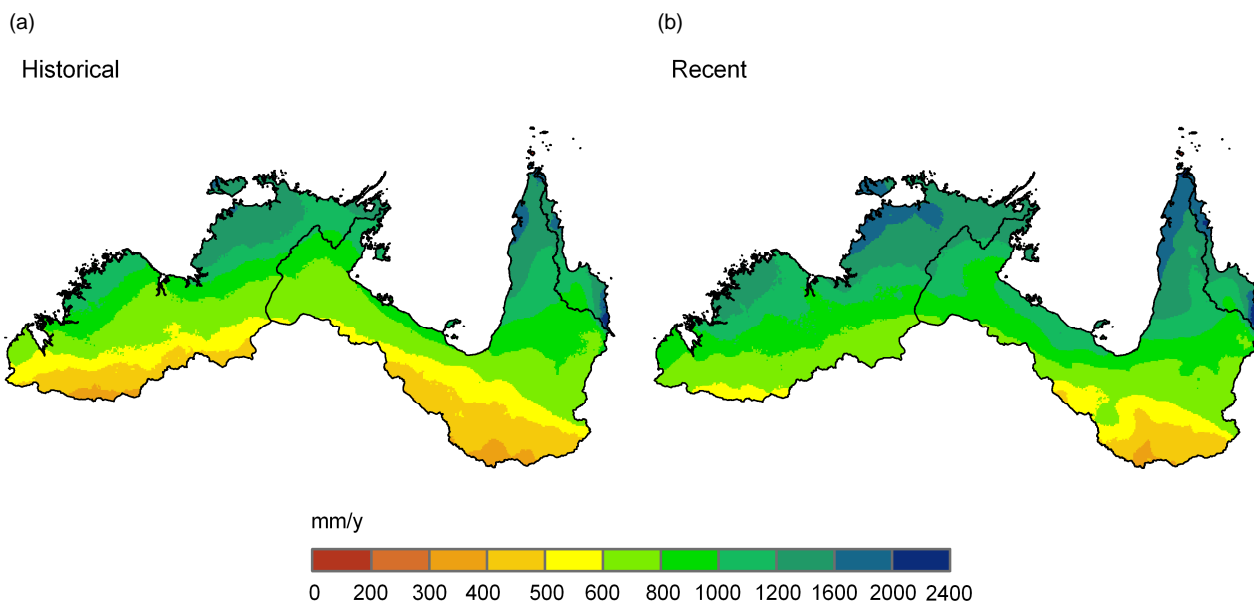


Figure 18. Historical and recent mean rainfall for the project area. Figure (a) is the historical rainfall calculated for the 77 years from 1 September 1930 to 31 August 2007 and figure (b) is the recent rainfall for the 11 years from 1 September 1996 to 31 August 2007

In calculating the differences between the climates of Scenario A ('historical') and Scenario B ('recent') only that portion of the historical record that does not overlap with the recent record was used. Hence, in the following, the historical period is 1 September 1930 to 31 August 1996 and is denoted 'historical\*'. The relative differences in rainfall between the two periods were calculated as  $P_{\text{recent}} - P_{\text{historical}^*} / P_{\text{historical}^*}$ , expressed as a percentage. To assess whether these differences were significant, a statistical test was performed using a two-sided, non-overlapping two-sample t-test with equal (pooled) variances across the two time periods:

$$t = \frac{(\bar{x}_1 - \bar{x}_2)}{\sqrt{s_p^2 \left( \frac{1}{n_1} + \frac{1}{n_2} \right)}}$$

where  $t$  is the Student's t-value,  $\bar{x}$  is the mean annual rainfall,  $s_p^2$  is the pooled variance, and  $n$  is the number of years. Subscript 1 denotes the 'historical\*' period (i.e. from 1 September 1930 to 31 August 1996; 66 years) and subscript 2 denotes the 'recent' period (i.e. 1 from September 1996 to 31 August 2007; 11 years). The degrees of freedom is  $n_1 + n_2 - 2$ .

The pooled variance,  $s_p^2$ , is calculated as:

$$s_p^2 = \frac{(n_1 - 1)s_1^2 + (n_2 - 1)s_2^2}{n_1 + n_2 - 2},$$

where  $s_1^2$  and  $s_2^2$  are the variances for the two non-overlapping periods defined above.

The relative difference shows that all of the Timor Sea Division has received increases in rainfall for the most recent 11-years (i.e. 1 September 1996 to 31 August 2007) compared to the 66 years from 1 September 1930 to 31 August 1996 (Figure 19a). The majority of the division is significantly wetter at the  $\alpha = 0.05$  level, with greater than 50 percent of the area being significantly wetter at the  $\alpha = 0.01$  level (Figure 19b).

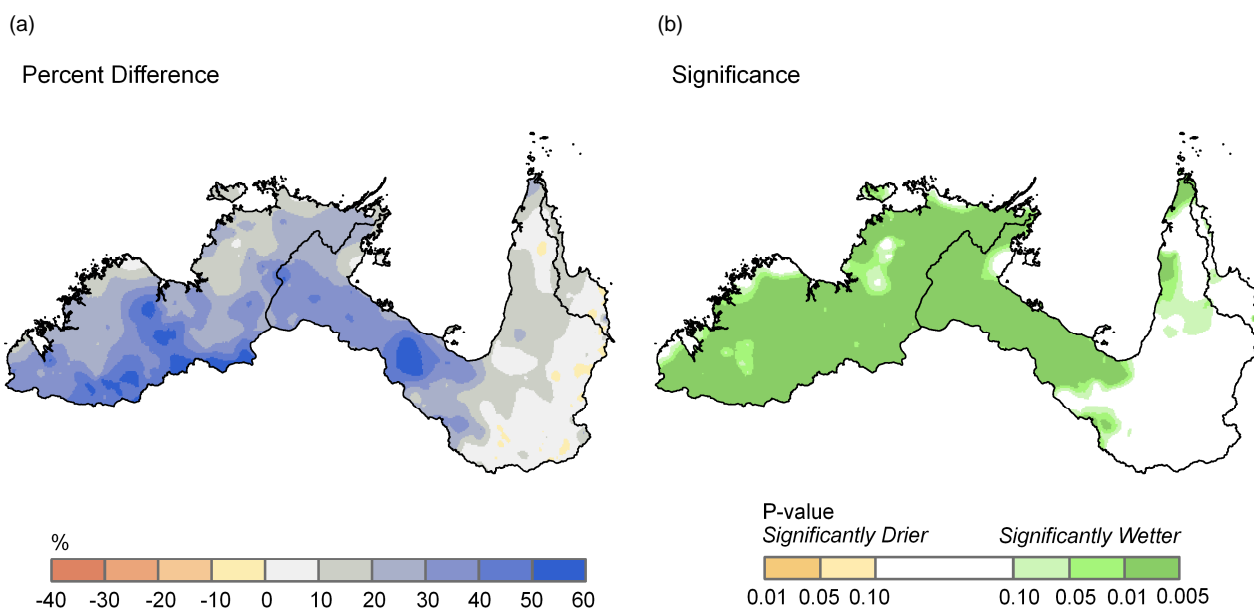


Figure 19. Comparison of 'historical' and 'recent' mean water year rainfall for the project area. Figure (a) shows the percentage relative differences between the 'historical' and 'recent' periods. Figure (b) is the statistical significance results between the 'historical' and 'recent' periods, calculated using a two-sided, non-overlapping two-sample t-test. The 'historical' period is from 1 September 1930 to 31 August 1996 (i.e. 66 years) and the 'recent' period is from September 1996 to 31 August 2007 (i.e. 11 years)

Characterisations of Scenario B rainfall and APET for each of the project reporting areas are provided in Table 5 and Table 6, respectively. For rainfall, comparing the Scenario A (Table 1) and Scenario B (Table 5) shows an unequivocal increase of the recent past (last 11 years) compared to the historical past (last 77 years) with rainfall increasing in each of the 13 reporting regions. The increase ranges from 55 mm/year in the South-West Gulf region to 228 mm/year in Kimberley region, averaged across the two different scenario periods. There is little change in the seasonality of rainfall between the two scenarios, with the smallest change being a 1 percent decrease and the largest change being a 2 percent increase.

For APET, when comparing the Scenario A (Table 3) and Scenario B (Table 6) values at an all NASY level, there are decreases of 7 mm/year, commensurate with increasing rainfall. At a regional level both increases and decreases are seen, varying from a decrease of 37 mm/year for the Mitchell region to an increase of 27 mm/year for the Van Diemen region. There is essentially no change in the seasonality of APET between the two scenarios, the changes are zero percent at the all NASY, and only range between -1 and 1 percent at the regional level, with the majority (8 of 13) regions also having no change in the APET seasonality between the two scenarios.

Table 5. Scenario B rainfall characteristics of northern Australia, for the 17 areas. All units are mm, with the exception of the column labelled '% wet of total' which is the ratio of the total wet season rainfall to the total water year rainfall (expressed as a percentage). Note that the sum of the seasonal values do not equal the water year values because the combined wet season–dry season period (Nov–Oct) is different to the water year period (Sep–Aug)

Areas	Long-term annual				Wet / Dry seasonal information		
	Mean	Std	Max	Min	Wet mean	Dry mean	% Wet of total
	mm						percent
NASY*	1001	351	3963	372	948	49	95%
TS	1070	317	2072	532	1016	51	95%
GC	890	319	2120	372	843	42	95%
NE	1443	417	3963	954	1336	95	93%
01FI	762	130	1240	532	712	48	93%
02KI	1178	153	1551	825	1123	52	95%
03OB	921	226	1807	612	867	51	94%
04DA	1232	191	1831	815	1183	47	96%
05VD	1606	162	2072	1244	1538	61	96%
06AR	1350	99	1593	1058	1296	53	96%
07RO	1018	159	1499	729	975	41	95%
08SW	848	191	1250	480	807	33	96%
09FL	553	111	965	372	503	45	91%
10SE	805	146	1179	533	758	42	94%
11MI	1035	189	1739	694	981	47	95%
12WC	1551	256	2120	1127	1494	51	96%
13NC	1443	417	3963	954	1336	95	93%

\*the all-project-area

Table 6. Scenario B APET characteristics of northern Australia, for the 17 areas. All units are mm, with the exception of the column labelled '% wet of total' which is the ratio of the total wet season APET to the total water year APET (expressed as a percentage). Note that the sum of the seasonal values do not always equal the water year values because the combined wet season–dry season period (Nov–Oct) is different to the water year period (Sep–Aug)

Areas	Long-term annual				Wet / dry seasonal information		
	Mean	Std	Max	Min	Wet mean	Dry mean	% Wet of total
	mm						percent
NASY*	1947	70	2119	1567	1055	857	55%
TS	1975	51	2119	1794	1056	883	54%
GC	1930	71	2075	1567	1063	834	56%
NE	1832	45	1900	1570	972	827	54%
01FI	2021	40	2072	1804	1128	857	56%
02KI	1964	50	2109	1794	1039	890	53%
03OB	1988	31	2119	1811	1084	868	55%
04DA	1933	25	1974	1846	999	898	52%
05VD	1963	35	2005	1815	982	945	50%
06AR	1898	23	1980	1828	952	912	51%
07RO	1933	26	1986	1823	1016	882	53%
08SW	1926	22	1981	1853	1065	827	56%
09FL	1946	70	2060	1693	1132	782	59%
10SE	1983	85	2075	1665	1106	844	56%
11MI	1868	77	1980	1567	1010	826	55%
12WC	1854	37	1911	1642	955	866	52%
13NC	1832	45	1900	1570	972	827	54%

\*the all-project-area

## 3.1 Rainfall recurrence intervals

The rainfall average recurrence interval (ARI) is the average waiting time until an independent 11-year wet (or dry) sequence would occur that is equal to or wetter (drier) than the last 11 years (i.e. Scenario B). Note that estimates of the ARIs are calculated under an assumption of climate stationarity. As rainfall in some of the project area can not be considered stationary over the Scenario A time period (i.e. increasing trends in rainfall since 1930 are present for most the Timor Sea Drainage Division and the western and northern portions of the Gulf of Carpentaria Drainage Division, refer to Figure 13 and Section 2.4) it is expected that the method will result in extremely large ARIs. In this case, the large ARIs are indicative of non-stationary (trending) rainfall, and subsequent bias in the model parameters. In other words, it is likely that the wet conditions observed in recent years will occur sooner than is estimated by the ARI for those rainfall stations showing significant upward trends in rainfall.

Rainfall ARIs provide a measure of the rarity of a rainfall event, with the metric being reported in the period of recurrence between certain rainfall patterns and are calculated through a simulation approach. For each rainfall station, Scenario A rainfall was modelled with the lag-one autoregressive model of Frost et al. (2007). This model allows for non-Gaussian distributions using Box-Cox transformation and considers parameter uncertainty using Bayesian methods with Markov Chain Monte Carlo parameter estimation. The prior distribution of the Box-Cox lambda parameter is bounded between – 2 and 2. Frost et al.'s (2007) model was used to generate 100 replicates of 100,000 years of 'water year' rainfall. The ARI for Scenario B (defined as the most recent 11 years, that is from 1 September 1996 to 31 August 2007) rainfall was then calculated directly from the 100,000-year water year replicate as the mean time between successive upcrossings (i.e. crossings from below) of a threshold equal to the mean of the last 11 years rainfall. As the distribution of the ARI estimates can be highly skewed, particularly for the higher ARIs, the median ARI from the 100 estimates was reported as the ARI for Scenario B rainfall; full details of method used to calculate and interpret the ARIs are found in Potter et al. (2008).

Due to the computational requirement for running the ARI algorithm the analysis was first performed at meteorological stations and the results interpolated to produce a surface, as opposed to running the algorithm on the SILO data. The number of rainfall stations to run the average recurrence intervals (ARI) algorithm on was determined by firstly identifying the number of BoM stations recording rainfall in each of the 13 regions comprising the project area, and the combined area. Also to ensure that the resultant ARI metric was interpolated (as opposed to extrapolated), for the project area the ARI was calculated at the isolated BoM stations in the area and including a 2 degree (~ 200 km) buffer around the area (denoted NASY Buff in Table 7 below). Results, presented in Table 7, show that at strict levels of completeness (e.g. >90 percent) there are several regions that do not have a single adequate rainfall station. Consequently the threshold was relaxed to be 70 percent complete, as at this level at least one rainfall station was present in each region; there are 146 stations in the project area increasing to 279 when including all those within the buffer. For this analysis the buffer was 2 degrees outside the outer boundary of the project area. At the stations missing rainfall data were infilled from the SILO surfaces so that continuous daily rainfall records were presented to the algorithm used to calculate the ARI.

Table 7. Number of rainfall stations passing completeness thresholds in each region, all the project area and an associated buffered area

%	01FI	02KI	03OB	04DA	05VD	06AR	07RO	08SW	09FL	10SE	11MI	12WC	13NC	NASY	NASYBuff
60	25	1	22	4	5	3	7	5	49	24	12	6	15	178	342
65	23	1	20	4	4	3	7	5	44	21	12	5	12	161	309
70	21	1	20	3	4	3	3	5	38	21	12	5	10	146	279
75	20	0	17	2	4	3	2	5	34	21	10	3	7	128	247
80	15	0	12	2	2	1	1	5	29	19	10	3	6	105	211
85	13	0	9	2	2	1	1	4	26	14	7	3	6	88	177
90	6	0	7	0	1	1	0	3	20	11	6	3	5	63	129
95	2	0	2	0	1	1	0	2	12	7	5	1	2	35	77

The ARIs shown in Figure 20 quantify the probability of occurrence of Scenario B rainfall in the context of the variability of Scenario A rainfall. Results show that ARIs of the last 11 years with the context of the last 77 years are less than 50 years along the eastern coast of the North-East Coast Drainage Division and the south-eastern portion of the Gulf of

Carpentaria Division. However, in the western part of the Gulf of Carpentaria Drainage Division and for the most of the Timor Sea Division rainfall ARIs of the last 11 years with the context of the last 77 years are generally large (i.e. >100 years and in some cases exceeding 300 years). A spatial surface of the ARIs was generated using Kriging interpolation and the input data available from the isolated BoM stations (Figure 20), noting that the ARI analysis is conducted at stations outside the area so the resultant surface is generated using interpolation not extrapolation. Results of this interpolation are shown in Figure 21 where the output surface clearly shows the east-west divide in rainfall ARIs experienced across the project area. This spatial pattern has general accordance with the trends in rainfall shown in Figure 13.

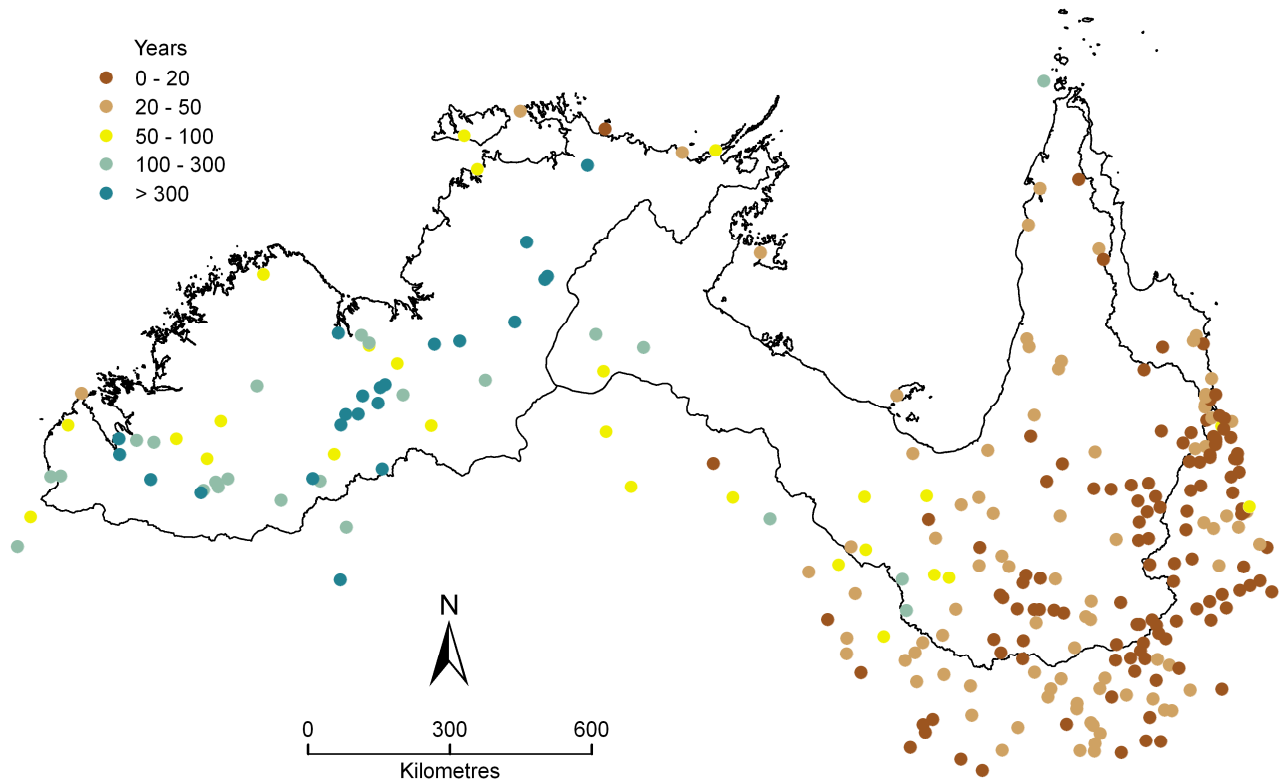


Figure 20. Average recurrence intervals for rainfall for the Scenario B period relative to the Scenario A period at the locations of BoM stations

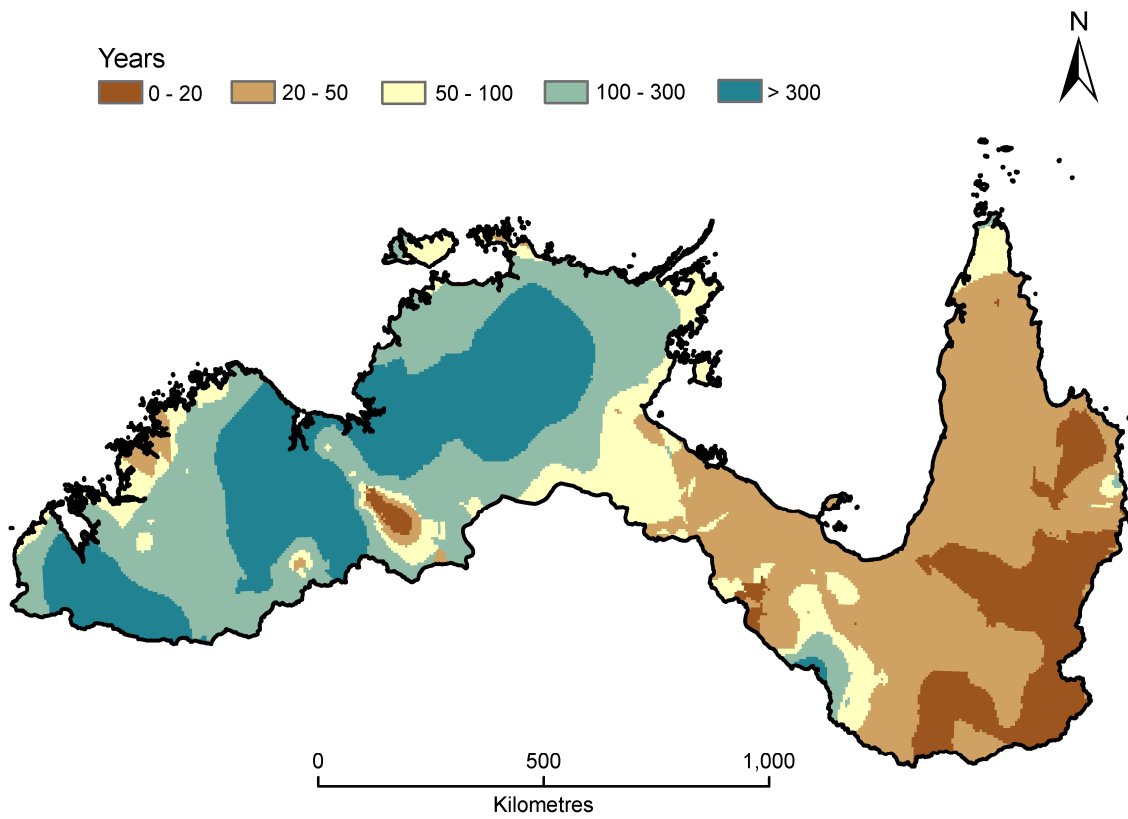


Figure 21. Surface of average recurrence intervals for rainfall for the Scenario B period relative to the Scenario A period

## 4 Future climate (Scenario C)

### 4.1 Global warming and the Fourth Assessment Report of the Intergovernmental Panel on Climate Change

This section briefly summarises the global warming projections leading to the three global warming scenarios used for this project. A comprehensive picture of the present state of knowledge on global climate change can be found in the Fourth Assessment Report (AR4) of the Intergovernmental Panel on Climate Change (IPCC 2007) and online at <http://www.ipcc.ch>. A recently released report (CSIRO and Bureau of Meteorology, 2007) provides detailed future projections of Australian climate and discusses past climate characteristics and drivers of Australian climate.

There is an increasing body of research that supports a picture of a warming world with significant changes in regional climate systems. Eleven of the last 12 years rank among the 12 warmest years in the instrumental record of global surface temperature (since 1850) and the linear warming trend over the last 50 years is about 0.13°C per decade (IPCC, 2007). However, since 1976, the global temperature has risen more sharply at 0.18°C per decade (WMO, 2006). The global average air temperature over the last 150 years is shown in Figure 22. Based on many lines of evidence including the widespread warming of the atmosphere and ocean, together with ice mass loss, the IPCC (2007) concluded that most of the observed increase in the global average temperature since the mid-20th century is very likely due to the observed increase in anthropogenic greenhouse gas concentrations.

The global climate system is highly complex, and therefore it is inappropriate to simply extrapolate past trends to predict future conditions. To estimate future climate change, scientists have developed emission scenarios for greenhouse gases and aerosols. The greenhouse gas emissions considered here are those due to human activities, such as energy generation, transport, agriculture, land clearing, and industrial processes. To provide a basis for estimating future climate change, Working Group III of the IPCC prepared 40 greenhouse gas and sulfate aerosol emission scenarios for the 21<sup>st</sup> century that combine a variety of assumptions about demographic, economic and technological factors likely to influence future emissions. Described fully in the Special Report on Emission Scenarios (SRES) (IPCC, 2000), each scenario represents a variation within one of four 'storylines' (A1, A2, B1 and B2, see Table 8) with projected carbon dioxide, methane, nitrous oxide and sulfate aerosol emissions associated with each of the scenarios.

Increasing concentrations of greenhouse gases affect the radiative balance of the Earth. The balance between incoming solar radiation and outgoing heat radiation defines the Earth's radiative budget and average temperature. Radiative forcing is the term given to an externally imposed change in the radiation balance, such as changes in atmospheric concentrations of greenhouse gases. Carbon dioxide gas dominates the radiative forcing, as it absorbs longwave radiation that would otherwise be outward longwave radiation from the Earth surface (through the atmosphere) to space. Thus increases in the concentration of carbon dioxide gas results in atmospheric warming.

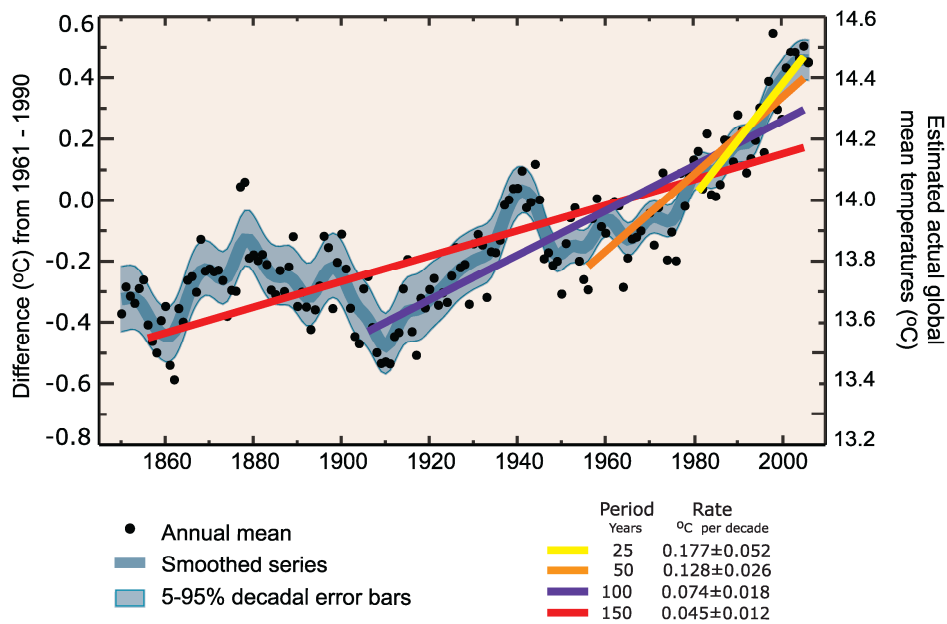


Figure 22. Global average temperature over the last 150 years (from IPCC, 2007)

Table 8. Storylines from the Intergovernmental Panel on Climate Change (2000) Special Report on Emission Scenarios (SRES)

A1. The A1 storyline describes a future world of very rapid economic growth, a global population that peaks in mid-century and declines thereafter, and the rapid introduction of new and more efficient technologies. Major underlying themes are convergence among regions, capacity building and increased cultural and social interactions, with a substantial reduction in regional differences in per capita income. The A1 story line develops into three scenario groups that describe alternative directions of technological change in the energy system. They are distinguished by their technological emphasis: fossil intensive (A1FI), non-fossil energy sources and technologies (A1T), or a balance across all sources (A1B) (where balanced is defined as not relying too heavily on one particular energy source, on the assumption that similar improvement rates apply to all energy supply and end use technologies).

A2. The A2 storyline describes a very heterogeneous world. The underlying theme is self reliance and preservation of local identities. Fertility patterns across regions converge very slowly, which results in continuously increasing population. Economic development is primarily regionally oriented and per capita economic growth and technological change more fragmented and slower than other storylines.

B1. The B1 storyline describes a convergent world with the same global population, that peaks in mid-century and declines thereafter, as in the A1 storyline, but with rapid change in economic structures toward a service and information economy, with reductions in material intensity and the introduction of clean and resource efficient technologies. The emphasis is on global solutions to economic, social and environmental sustainability, including improved equity, but without additional climate initiatives.

B2. The B2 storyline describes a world in which the emphasis is on local solutions to economic, social and environmental sustainability. It is a world with continuously increasing global population, at a rate lower than A2, intermediate levels of economic development, and less rapid and more diverse technological change than in the B1 and A1 storylines. While the scenario is also oriented towards environmental protection and social equity, it focuses on local and regional levels.

An illustrative scenario was chosen for each of the six scenario groups A1B, A1FI, A1T, A2, B1 and B2. All were considered equally sound by the IPCC.

The SRES scenarios do not include additional climate initiatives, which means that no scenarios are included that explicitly assume implementation of the United Nations Framework Convention on Climate Change or the emissions targets of the Kyoto Protocol.

The Summary for Policymakers in the AR4 (IPCC, 2007) provides estimates of global warming for the year 2100 for six emission scenarios (B1, A1T, B2, A1B, A2 and A1F). The range of warming is based on 23 global climate models (GCMs) and results from a hierarchy of independent models and observational constraints. Important uncertainties, including the possibility of significant further amplification of climate change due to carbon cycle feedbacks, are also considered. The lower end of the warming range corresponds to the mean warming minus 40 percent, while the upper end of the range is the mean warming plus 60 percent. The range of global warming by 2100 is 1.1 °C to 6.4 °C.

Equivalent global warming values for ~2030 are not provided by the IPCC (2007). The values required for this project and for broader Australian projections have been derived in a way that is consistent with the approach used by the AR4 for 2100. The result is three predictions of the temperature change by ~2030 relative to ~1990: a low global warming of 0.7 °C (low end of SRES B1), medium global warming of 1.0 °C (average of the low and high global warming scenarios), and high global warming of 1.3 °C (high end of SRES A1T).

## 4.2 Methods used to simulate a 2030 climate

The method implemented here to generate the Scenario C climate data is based upon that used in the CSIRO Murray-Darling Basin Sustainable Yield (MDBSY) project, and the material herein draws heavily from Chiew et al. (2008). There are a variety of possible methods to obtain future catchment-scale climate data to drive hydrological models (see Chiew (2006b) for an overview of methods). Statistical and dynamic downscaling methods that relate large synoptic-scale atmospheric variables to catchment-scale rainfall can potentially provide more reliable future rainfall inputs to drive hydrological models. However, the use of downscaling methods was not possible given the time constraints of this project. Additionally, downscaling methods may not necessarily provide more reliable future rainfall than the method used in this project because: (i) downscaling research is still developing and has not been used for hydrologic investigations of this scale; (ii) it is difficult to calibrate the downscaling method for a large region like northern Australia; and (iii) there are limited archived daily GCM simulations from which to downscale to provide the range of uncertainties in the future climate.

The future climate scenario (Scenario C) provides projections of possible conditions around the year 2030 under three different potential global warming scenarios. This is achieved by using 'scaling factors', derived from GCM outputs, to rescale the 1930 to 2007 historical climate data for each warming scenario.

Three global warming scenarios for ~2030 relative to ~1990 are used based on projected greenhouse gas emissions: high, median and low emissions. These three scenarios are inferred from the AR4 (IPCC 2007) and the latest climate change projections for Australia (CSIRO and Bureau of Meteorology, 2007). The increase in global average near-surface air temperatures resulting from low, median and high emissions scenarios for ~2030 relative to ~1990 used in this project are 0.7, 1.0 and 1.3 °C, respectively. The corresponding values for MDBSY were 0.45, 1.03 and 1.60 °C, respectively. The slight difference in values used here compared to those used in MDBSY is due to increased understanding of global temperature rises associated with projected low, medium and high emissions, that continues to evolve as earth system science advances.

Broadly, the method used to derive Scenario C climate projections is outlined below and in Figure 23. For more methodological detail, see Chiew et al. (2008).

- 1. Derive scaling factors for rainfall, net radiation, air temperatures and relative humidity**  
Archived monthly simulations from 15 AR4 GCMs (Table 9) were analysed to produce scaling factors that denote the percent change in rainfall, solar radiation, maximum and minimum air temperature, and relative humidity per °C warming (i.e. globally averaged air temperature). For each of these climate variables, seasonal scaling factors were produced for each grid cell in the project area. For rainfall daily scaling factors were also obtained. In total there are 15 sets of seasonal scaling factors – 1 set from each GCM.
- 2. Calculate an interim 2030 APET and derive scaling factors for APET**  
The GCMs do not produce projections of future APET and so APET scaling factors could not be derived directly from the GCM outputs. Instead, interim projections of future solar radiation, maximum and minimum air temperature, and vapour pressure were calculated using respective rescaling factors and assuming a 1 °C rise in global air temperature (noting that the GCMs produce percent change in relative humidity per °C warming; they do not produce a percent change in vapour pressure per °C

warming). This necessitated that the percent change in relative humidity per °C warming was used as input and the relative humidity vapour pressure relationship (seen in equations 1 and 2) was inverted to derive the required percent change in vapour pressure per °C warming required for the APET calculations. The four scaling factors (i.e. solar radiation, maximum and minimum air temperature, and vapour pressure) were then used to create an interim ~2030 APET. Scaling factors for APET were derived from the simulated future APET.

### 3. Produce projections of 2030 climate by rescaling the historical climate data

Each set of scaling factors was multiplied by the amount of projected temperature increase (0.7, 1.0 and 1.3 °C) and then used to rescale historical climate variables to simulate possible 2030 climates. Rescaling of rainfall used both seasonal and daily scaling factors. In total, 45 different projections of future climate were produced.

Table 9. List of 15 Global Climate Models used

Global Climate Models	Modelling group, Country	Horizontal resolution (km)
CCCMA T47	Canadian Climate Centre, Canada	~250
CCCMA T63	Canadian Climate Centre, Canada	~175
CNRM	Meteo-France, France	~175
CSIRO-MK3.0	CSIRO, Australia	~175
GFDL 2.0	Geophysical Fluid, Dynamics Lab, USA	~200
GISS-AOM	NASA/Goddard Institute for Space Studies, USA	~300
IAP	LASG/Institute of Atmospheric Physics, China	~300
INMCM	Institute of Numerical Mathematics, Russia	~400
IPSL	Institut Pierre Simon Laplace, France	~275
MIROC-M	Centre for Climate Research, Japan	~250
MIUB	Meteorological Institute of the University of Bonn, Germany Meteorological Research Institute of KMA, Korea	~400
MPI-ECHAM5	Max Planck Institute for Meteorology DKRZ, Germany	~175
MRI	Meteorological Research Institute, Japan	~250
NCAR-CCSM	National Center for Atmospheric Research, USA	~125
NCAR-PCM1	National Center for Atmospheric Research, USA	~250

Monthly scaling factors were calculated for rainfall (and other climate variables) for the period 1870 to 2100 by plotting the simulated rainfall (or other climate variable) against the simulated global average air temperature. An ordinary linear regression is fitted through the data points and the slope of the linear regression is the scaling factor which gives the change in rainfall (or other climate variable) per degree of global warming. The scaling factors were then multiplied by the change in temperature for each of the global warming scenarios for ~2030 relative to ~1990 to obtain changes for rainfall (and other climate variables) for the different global warming scenarios. This was performed for each of the 15 GCMs, for each season for each GCM grid-cell. The 77-year historical daily climate data with 0.05° x 0.05° (~ 5 km x 5 km) resolution grids were then scaled by the monthly scaling factors for each climate variable.

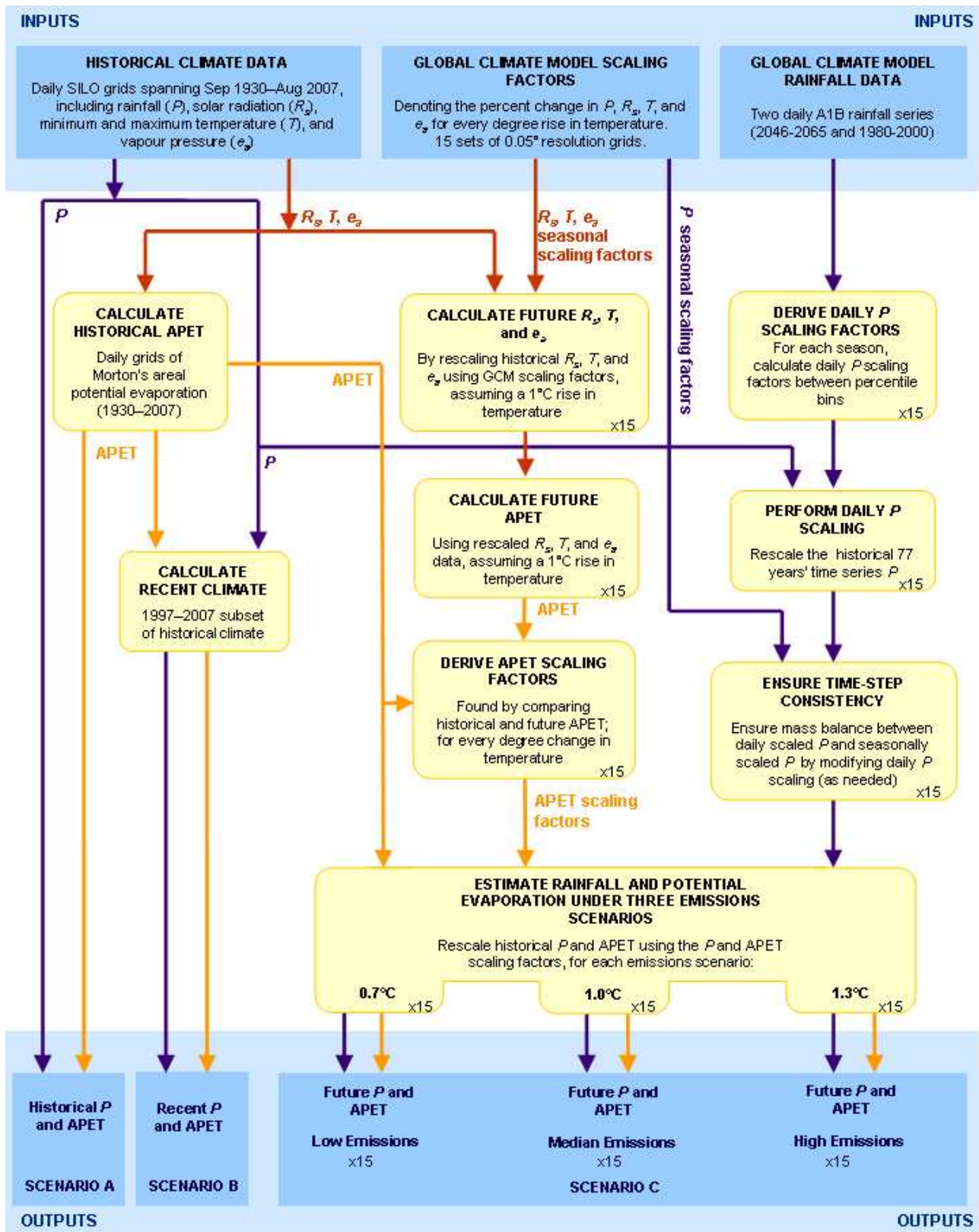
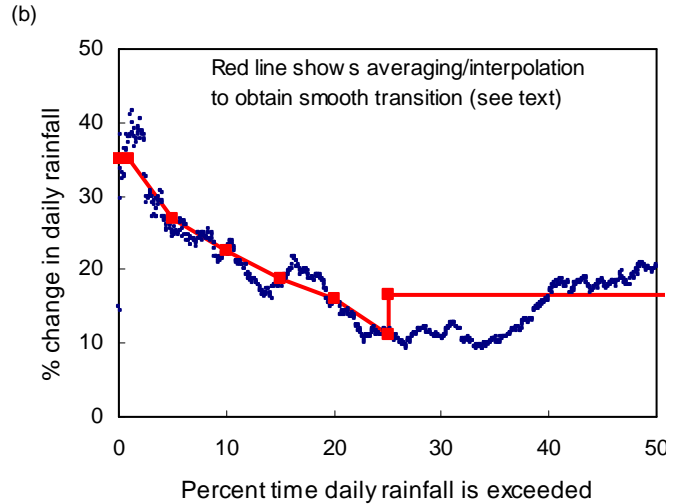
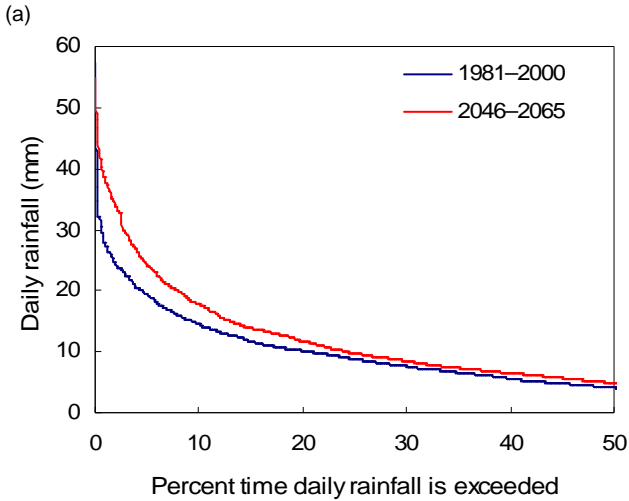


Figure 23. Diagram summarising the methods used to calculate Scenario C data. The inter-relationships with the historical data used in Scenario A and B are highlighted

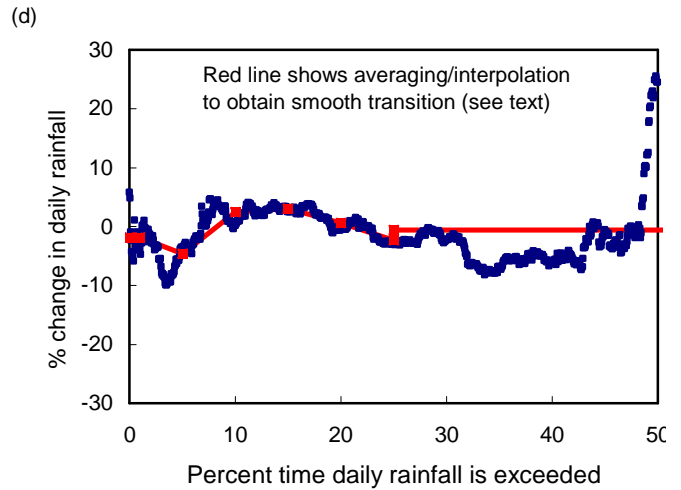
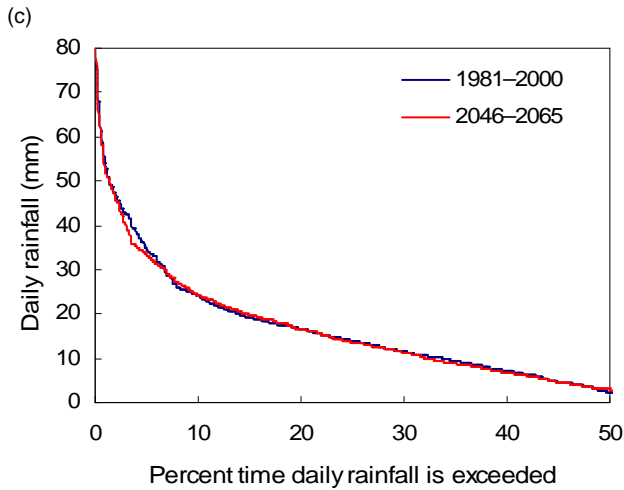
To account for changes in the future daily rainfall distribution, an additional percentile scaling factor was applied to daily rainfall on a seasonal basis. The scaling factors for the different rainfall percentiles/amounts were determined by comparing daily rainfall simulations from the 15 GCMs for a single SRES A1B run for two 20-year time slices, 2046 to 2065 and 1981 to 2000 (see Figure 24 a, c and e). The method used compares the 2046 to 2065 and 1981 to 2000 daily rainfall distributions, and develops a smooth transition in the 'daily scaling' factors, the percent changes are estimated by

averaging the rainfall amounts over percentile ranges: 1<sup>st</sup> percentile (all points less than 2<sup>nd</sup> percentile), 5<sup>th</sup> percentile (all points between 2.5<sup>th</sup> and 7.5<sup>th</sup> percentiles), 10<sup>th</sup> percentile (all points between 7.5<sup>th</sup> to 12.5<sup>th</sup> percentiles), and every five percentile range downwards to the 'lowest category', where all the small rainfall amounts are considered together. This lowest category bound is defined by the percentile at which the observed rainfall is less than 1 mm, or the 30<sup>th</sup> percentile if the percentile at which the observed rainfall is less than 1 mm is less than the 30<sup>th</sup> percentile. This is performed as rainfall events less than 1 mm, or those below the 30<sup>th</sup> percentile, are not important for runoff generation. All rainfall events below the lowest category bound were lumped together and used to determine the single value of percent change. The percent changes at the discrete percentile values were then interpolated to obtain the percent changes for all the rainfall percentiles (see Figure 24 b, d and f). For each of the 15 GCMs and each of the three global warming scenarios, the above daily scaling factors were used to scale the different daily rainfall amounts in the 77-year daily rainfall series to obtain a daily rainfall series for a ~2030 climate relative to a ~1990 climate. The entire series was then scaled, using a different constant factor for each of the four seasons, to ensure that the mean rainfalls in the four seasons were the same as those determined using the seasonal scaling factors. This is because the seasonal scaling factors were determined using a large number of data points from several ensemble runs from the archived GCM continuous monthly simulations over more than 200 years, while the archived GCM daily simulations used to estimate the daily scaling factors were available only for two time slices from limited modelling runs. In addition, because of the large spatial resolution of GCMs, the monthly simulations were more realistic than the daily simulations. This daily scaling was only implemented for rainfall, as this is the most important variable for runoff generation; and while some locations may experience lower annual total rainfall the frequency of high intensity rainfall may increase resulting in increases in runoff for these conditions.

NASY Point 1 (11.0°S, 142.25°E) – Summer (DJF)



NASY Point 2 (16.0°S, 142.25°E) – Summer (DJF)



NASY Point 3 (21.0°S, 142.25°E) – Summer (DJF)

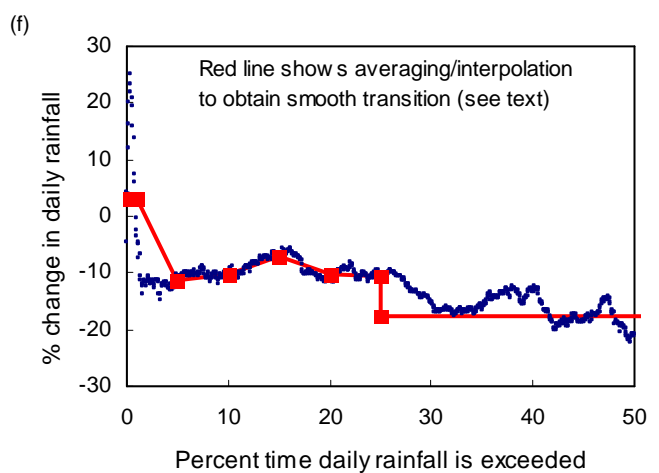
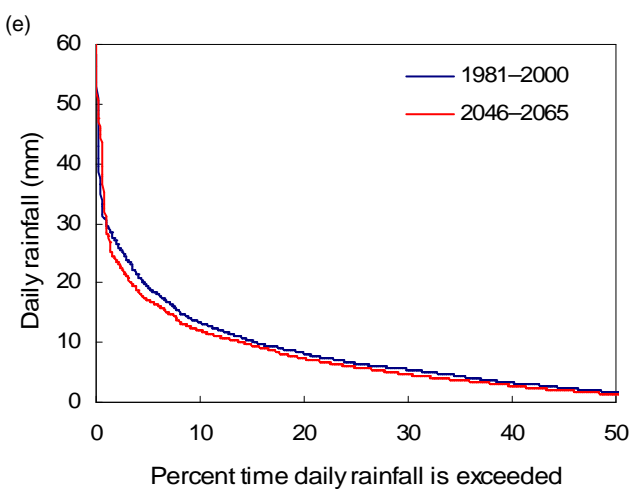


Figure 24. Schematic explaining the daily scaling factors for rainfall from three grid-cells (NASY points 1, 2 and 3) for summer. Daily rainfall exceedance plots comparing the 1982–2000 GCM simulation with the 2046 to 2065 GCM simulation are shown in (a), (c) and (e). The functions used to fit the binned data are shown in (b), (d) and (f)

As the future climate series (Scenario C) were obtained by scaling the historical daily climate series for the 1931 to 2007 northern Australia water-year (Scenario A), the daily climate series for Scenarios A and C have the same length of data (77 years) and the same sequence of daily climate (for example, potential changes in the frequency and timing of daily rainfall were not considered). Scenario C is therefore not a forecast climate at 2030, but a 77-year daily climate series based on 1931 to 2007 data for projected global near-surface air temperatures at ~2030 relative to ~1990.

The method used here takes into account two types of uncertainties. The first uncertainty is in the global warming projection, due to the uncertainties associated with projecting greenhouse gas emissions and predicting how sensitive the global climate is to changing greenhouse gas concentrations by accounting for both positive- and negative-feedbacks in a system that is highly inter-connected. The second uncertainty is in GCM modelling of local climate in the project area. The method separately accounts for different changes in each of the four seasons for rainfall and APET as well as changes in the daily rainfall distribution. The consideration of changes in the daily rainfall distribution is important because many GCMs indicate that future extreme rainfall in an enhanced greenhouse climate is likely to be more intense (e.g., O’Gorman and Schneider 2009), even in some regions where decreasing mean-seasonal or mean-annual rainfalls are projected. As high rainfall events generate large runoff, the use of simpler methods that assume the entire rainfall distribution change in the same way would lead to an underestimation of projected total runoff.

The method used here is similar to, but not the same as, the approach used by CSIRO and Bureau of Meteorology (2007) <<http://www.climatechangeinaustralia.gov.au>> to provide the climate change projections for Australia. The key differences are: (i) this project uses 15 of the 23 IPCC AR4 GCMs, while the CSIRO and BoM projections use all 23 GCMs; (ii) this project assesses the extreme range of global warming by ~2030; and (iii) this project also considers changes in the daily rainfall distribution.

## 4.3 Characterising simulated climate change

The simulation of the approximate 2030 climate yielded 15 sets of 2030 rainfall and APET projections for each of the three emissions scenarios, as well as the equivalent number of datasets of the input variables used to calculate APET. It is important to note that this section provides a study-wide characterisation of the changes in simulated ~2030 climate relative to ~1990 climate generated with the medium (1.0 °C) emissions scenario, starting with air temperature, followed by rainfall, the APET input variables and then APET itself. Thus this section does not aim to characterise the simulated ~2030 climate, rather it is the changes in simulated ~2030 climate relative to ~1990 climate that are presented.

### 4.3.1 Characterising simulated air temperature change

Figure 25 shows the change in mean annual near-surface air temperature for ~2030 relative to ~1990 from the 15 GCMs for the medium global warming scenario. The projections for the medium global warming scenario generally show a temperature increase of 0.6 to 1.5 °C, generally with the western part of the project area showing greater increases. Note that none of the GCMs predict a cooling anyway – in that the legend does not need to be negative.

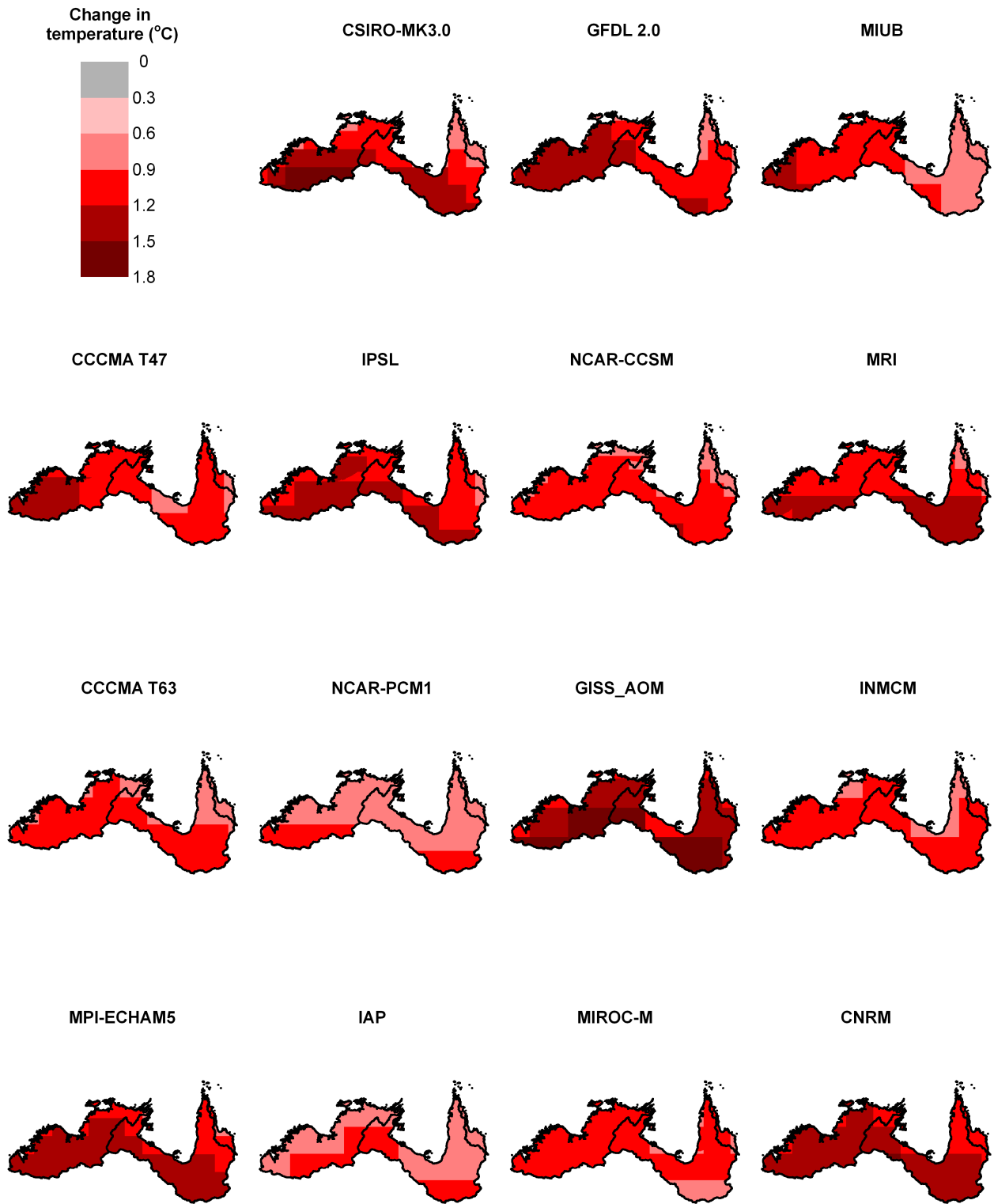


Figure 25. Change in mean annual near-surface air temperature for ~2030 relative to ~1990 for the project area from the 15 GCMs for the medium global warming scenario

### 4.3.2 Characterising simulated rainfall change

As rainfall is the key variable impacting rainfall-runoff modelling, we characterise changes in rainfall that are simulated to occur at ~2030 relative to ~1990 from the 15 GCMs. Figure 26 shows appreciable scatter in the simulated changes in annual rainfall that are projected to occur over the project area. Given the challenging nature of forecasting rainfall a week into the future it is not surprising that there are differences when predicting rainfall over 20 years into the future. In addition to rainfall amounts, rainfall characteristics (including intensity) are key elements governing the amount of runoff generated for a certain amount of rainfall.

For annual rainfall Figure 27a shows that for much of the project area the number of GCMs showing an increase is essentially equal to the number of GCMs showing a decrease – the grey colour seen in this figure. Much of Cape York and in the vicinity of the Joseph Bonaparte Gulf shows that approximately two-thirds (or 10 of the 15) GCMs estimate increases in ~2030 annual rainfall relative to ~1990 annual rainfall. Mainly towards the southern extent of the area the opposite holds, that is, approximately two-thirds (or more correctly 9 of the 15) GCMs estimate decreases in ~2030 annual rainfall relative to ~1990 annual rainfall. Figure 27b shows that for much of the near-coastal portions of the area, with two 'hot-spots' located in Cape York and in the vicinity of the Joseph Bonaparte Gulf, the overwhelming majority of GCMs simulate increases in the most intense 1 percent of rainfall when comparing the ~2030 simulated rainfall percentiles relative to ~1990 rainfall percentiles. In the southern part of the area many (i.e. 9 to 11 of the 15) GCMs estimate decreases in the most intense 1 percent of rainfall when comparing the ~2030 simulated rainfall percentiles relative to ~1990 rainfall percentiles. For the 5 percent and 10 percent rainfall percentile analysis (Figure 27c and d, respectively) less striking contrasts are seen, with much of the area having 6 to 9 GCMs in agreement, though some isolated pockets where more GCMs are in agreement (both increases and decreases) are seen. Figure 27d shows that in some areas (e.g. near Darwin and on Cape York), two-thirds (or 10 of the 15) GCMs simulate decreases in the most intense 10 percent of rainfall when comparing the ~2030 simulated rainfall percentiles relative to ~1990 rainfall percentiles. Interestingly these same areas had increases in the 1 percent analysis. As most rainfall occurs during the wet-season (Table 1), with what is traditionally defined as summer (December, January and February) being generally the wettest (Table 2) the percentage change of simulated summer rainfall for ~2030 relative to ~1990 summer rainfall for the 15 GCMs is shown in Figure 28.

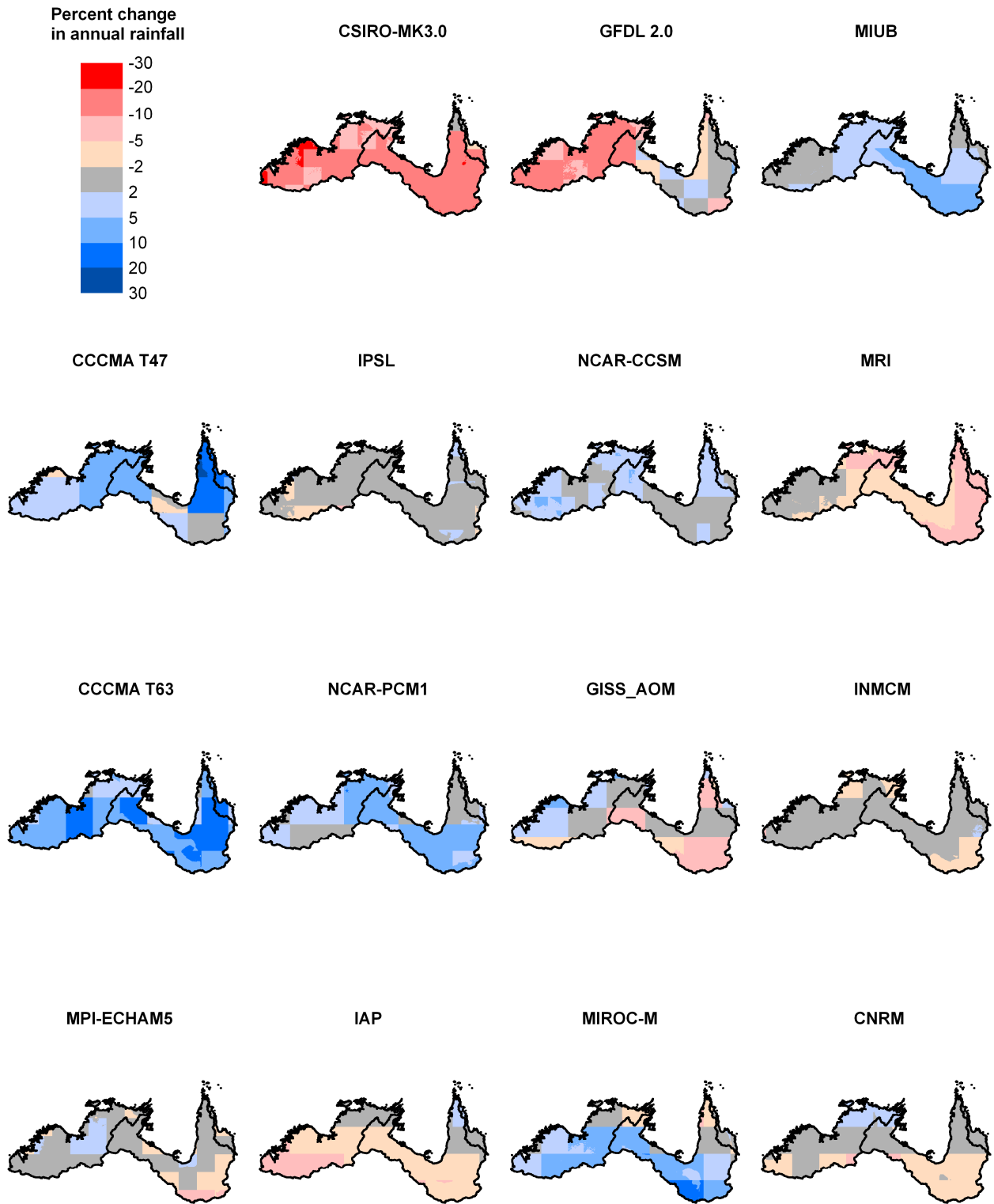


Figure 26. Percent change in mean annual rainfall for ~2030 relative to ~1990 for the project area from the 15 GCMs for the medium global warming scenario

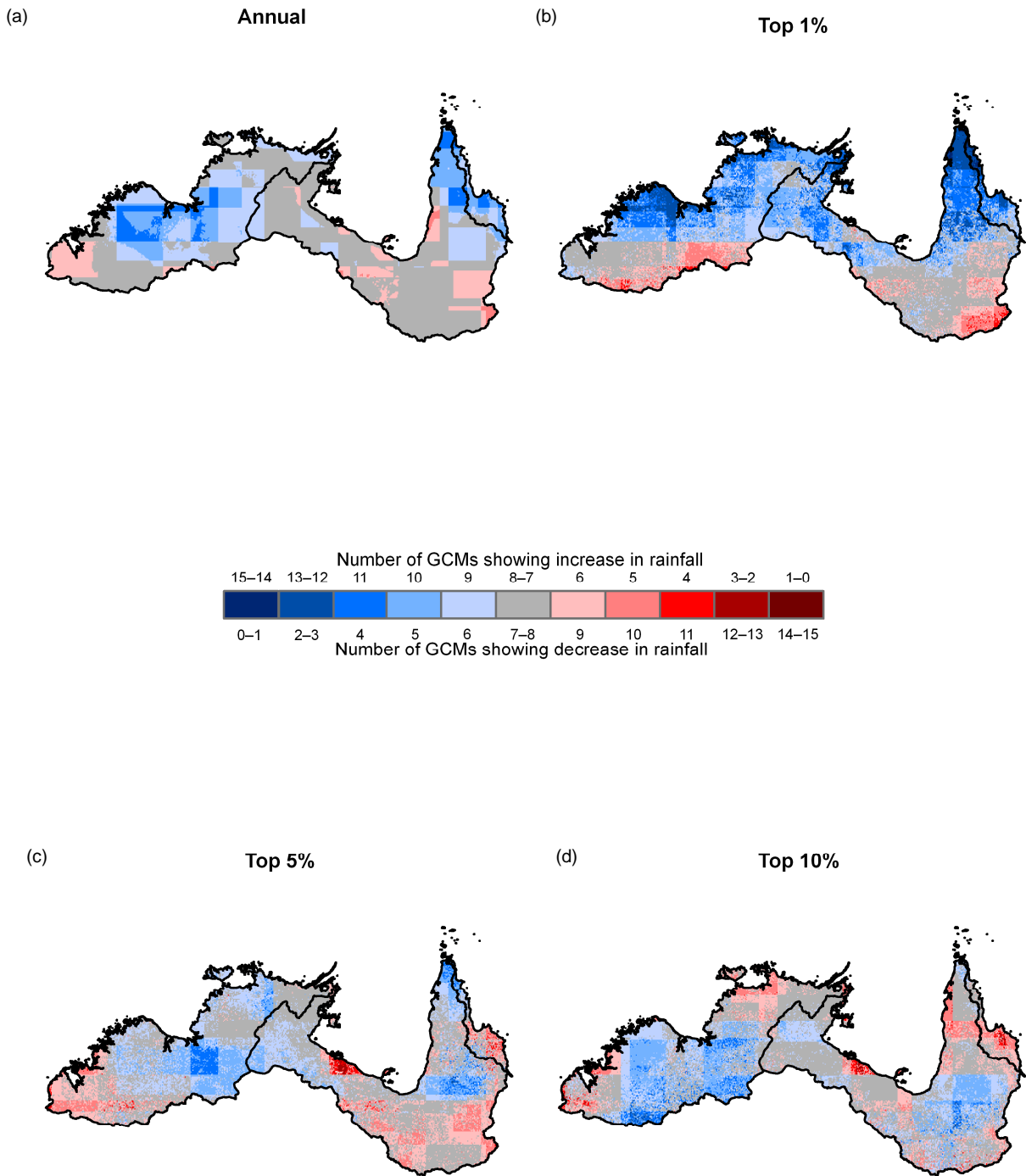


Figure 27. Number of GCMs showing decreases (or increases) in: (a) future mean annual rainfall; (b) highest 1 percent of rainfall (c) highest 5 percent of rainfall and (d) highest 10 percent of rainfall, when simulated ~2030 outputs are compared to ~1990 rainfall levels. All 15 GCMs are used

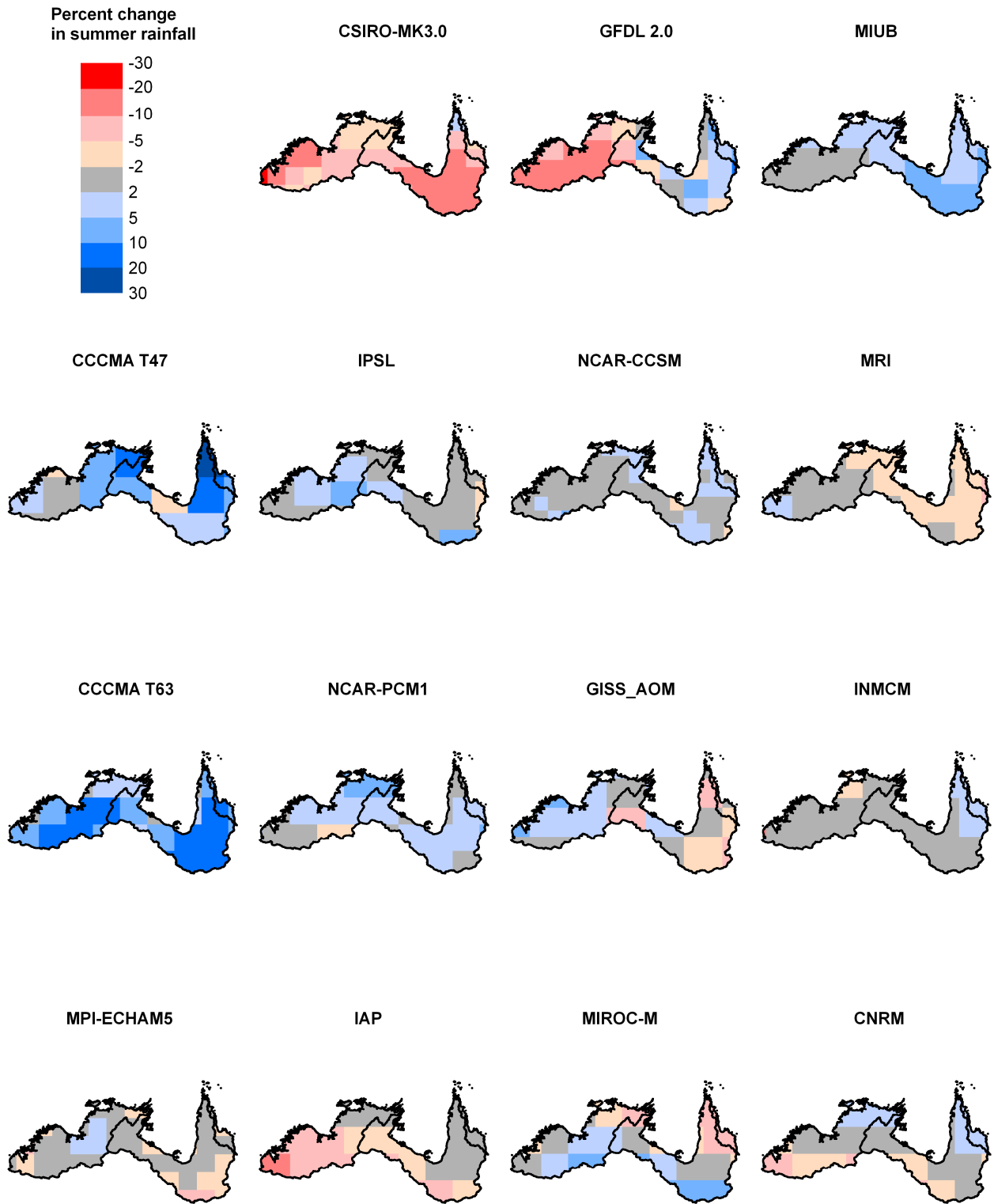


Figure 28. Spatial distribution of percent change in mean summer rainfall for ~2030 relative to ~1990 for the project area from the 15 GCMs for the medium global warming scenario. Summer is defined by the months December, January and February

### 4.3.3 Characterising simulated APET change

Given the simulated rises in air temperature in ~ 2030 shown in Figure 25, and rescaling other variables used to estimate APET, using the four-step method outlined in Section 4.2, APET is derived for ~2030 relative to ~1990. This method is schematically shown in Figure 23. This uses the simulated rises in air temperature (Figure 25), relative humidity (Figure 29) and incoming solar radiation (Figure 30).

Figure 29 illustrates the percent changes in mean annual near-surface relative humidity for ~2030 relative to ~1990 from the 15 GCMs for the medium global warming scenario. Most GCMs predict very small changes (i.e. in the range of +1 percent to -1 percent) in relative humidity. This is expected, as rises in air temperature (which increase the atmosphere's ability to hold water vapor) are offset by a corresponding rise in specific humidity, so the relative humidity remains near constant. Figure 30 shows the percent changes in mean annual near-surface incoming solar radiation, for ~2030 relative to ~1990 from the 15 GCMs for the medium global warming scenario. Most of the GCMs show very small changes (i.e. in the range of +1 percent to -1 percent), with those showing larger differences most likely resulting in differing implementations of cloud formation processes in the individual GCMs.

Figure 31 shows the resultant mean annual changes in APET and shows that, using Morton's formulation, projected APET increases generally 2 to 4 percent. This change has been predominantly driven by the increase in air temperature, which affects Morton's wet area potential both directly via its influence on surface temperature and indirectly via its affect on vapour pressure and on long-wave radiation. However, Morton's formulation of APET does not incorporate the effects of wind speed, even though wind speed is a key variable in the aerodynamic component of evapotranspiration. Recently (McVicar et al., 2008) showed that all of northern Australia has experienced declines in wind speed of approximately 0.01 m/second/year over the last 30 years, and this has been shown to be the primary factor driving the observed decreases of pan evaporation across much of Australia, including northern Australia over the same time period (Roderick et al., 2007). The effect of decreasing wind speed is to moderate the effect rising temperatures will have on potential evaporation rates. As a consequence, the projections of APET here will be higher than they would be if a fully physical potential formation were to be used (that is, one that incorporates net radiation, humidity, wind speed and temperature).

From current research, it is emerging that the optimal potential evaporation formulations for looking at long-term dynamics in potential are the fully physical, Penman-based formulations (e.g. Penman, 1948; Monteith, 1981). However, there continues to be some scientific debate about the validity of various formulations of PET. For the purposes of the rainfall-runoff modelling performed here Morton's formulation is a pragmatic choice as all the required input data are available over the temporal extent of the modelling and are produced by GCMs. Additionally, it should be noted that rainfall-runoff models are much more sensitive to changes in rainfall than PET. Chiew (2006a) presented a 'rule-of-thumb' that a 1 percent change in mean annual rainfall generally amplified to a 2 to 3.5 percent change in mean annual runoff, whereas a 1 percent change in mean annual PET generally leads to a 0.5 to 0.8 percent change in mean annual runoff. More precise figures of the sensitivity of runoff generation caused by changes in both rainfall and APET for the north of Australia are presented in the regional reports.

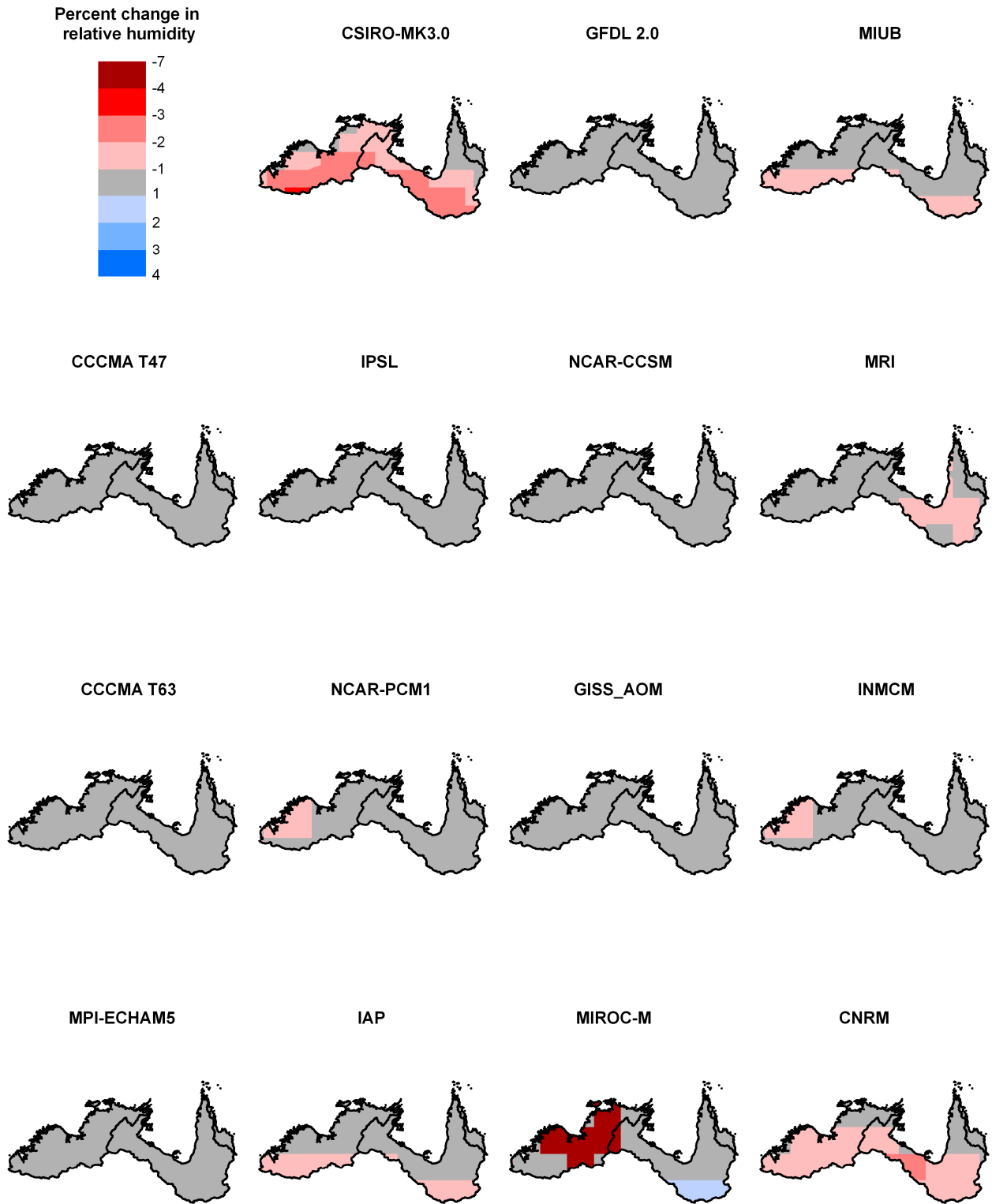


Figure 29. Percent change in mean annual near-surface relative humidity for ~2030 relative to ~1990 for the project area from the 15 GCMs for the medium global warming scenario

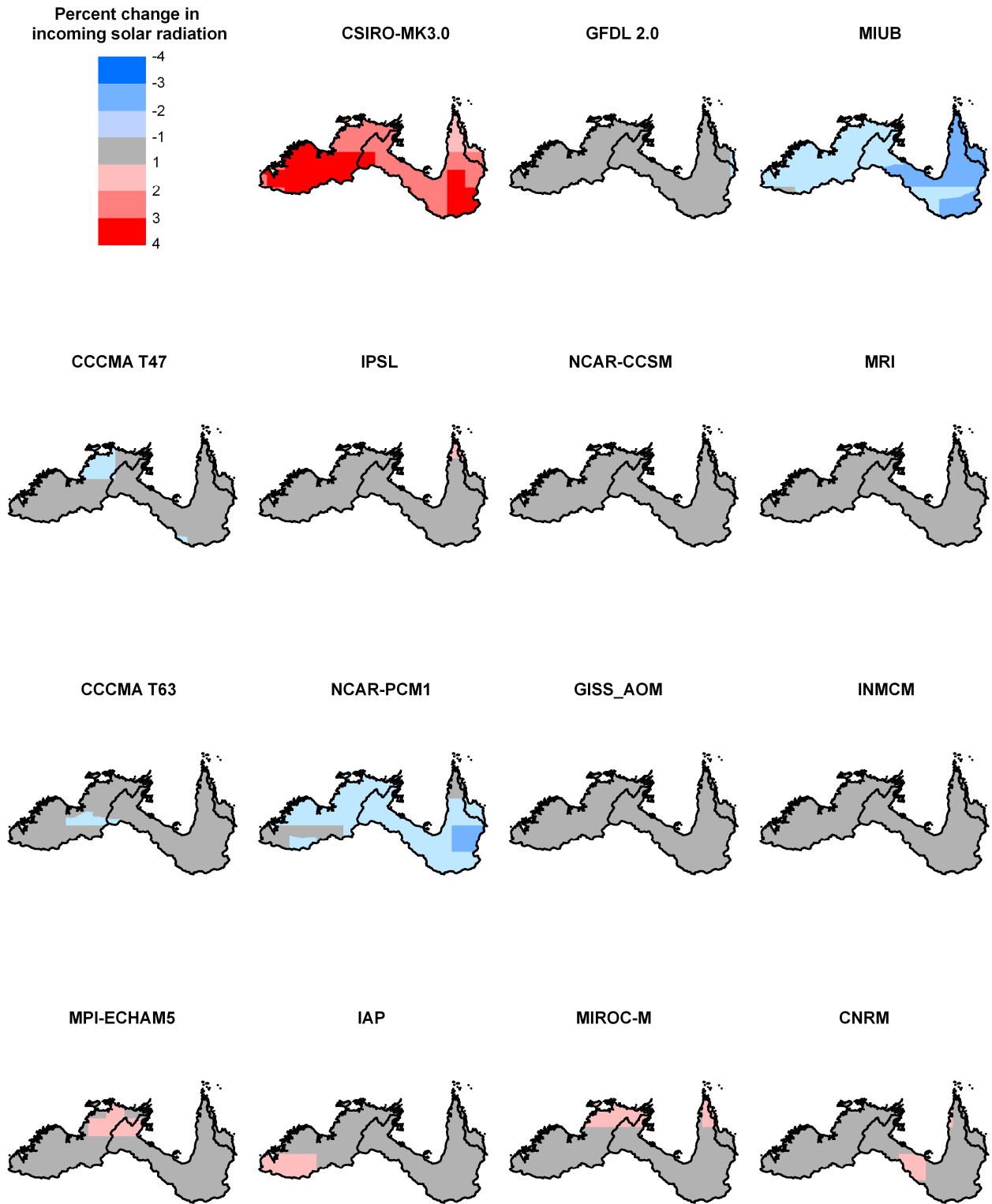


Figure 30. Percent change in mean annual near-surface incoming solar radiation for ~2030 relative to ~1990 for the project area from the 15 GCMs for the medium global warming scenario

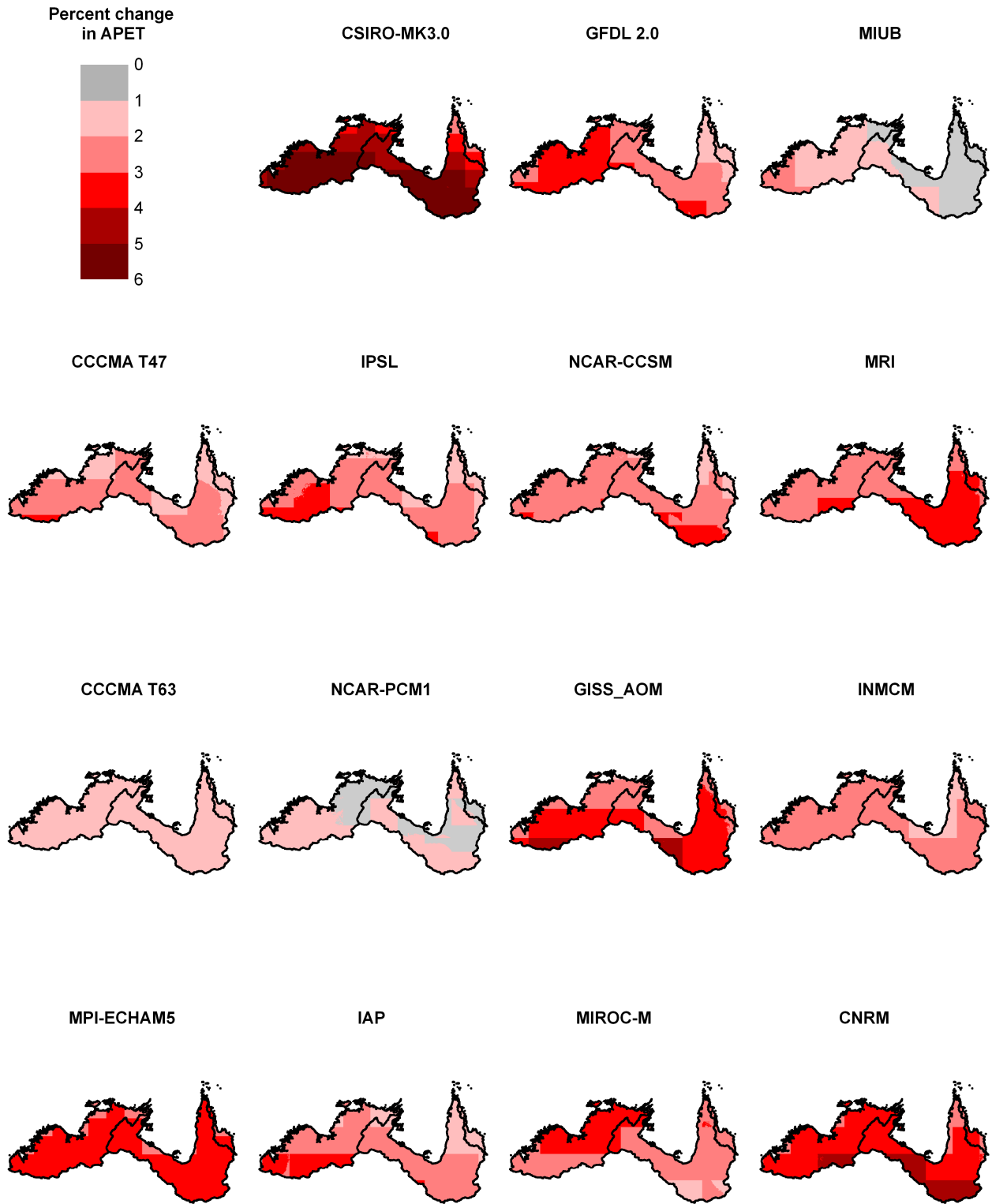


Figure 31. Percent change in mean annual areal potential evapotranspiration for ~2030 relative to ~1990 for the project area from the 15 GCMs for the medium global warming scenario

## 4.4 Identifying three representative 2030 climates—Cwet, Cmid and Cdry

The range of P and APET for the ~2030 climates relative to ~1990 levels for the three warming scenarios for the 15 GCMs (i.e. 45 in total) are shown for the project area for P (see Figure 32 and Table 10) and APET (see Figure 33 and Table 11). Some notable features emerge, including: (1) for P all warming scenarios have GCMs that predict both increases and decreases in rainfall (see Figure 32 and Table 10); (2) in contrast, for APET all GCMs in all three warming scenarios predict increased APET (see Figure 33 and Table 11); (3) the absolute relative changes of P are projected to be greater than APET for all warming scenarios (see Figure 32, Table 10 and contrast results with Figure 33, Table 11); (4) for P the high global warming scenario predicts greater absolute extreme values than the medium global warming scenario, which in-turn predicts greater extreme values than the low global warming scenario (see Figure 32 and Table 10); and (5) for APET the high global warming scenario consistently predicts larger change than the medium global warming scenario which, in turn, predicts consistently larger change than the low global warming scenario (see Figure 33 and Table 11). The spatial distributions of the percent simulated change for the medium warming scenario for each GCM compared against the historical Scenario A data are provided for P and APET in Figure 26 and Figure 31, respectively.

As the three emissions scenarios each produce 15 different projections of ~2030 P and APET, three climate projections were identified from the 45 which were considered to represent the breadth of range in the simulated ~2030 climates. The three representations identified are: a relatively wet ~2030 climate ('Cwet'), a mid-range ~2030 climate ('Cmid'), and a relatively dry ~2030 climate ('Cdry'). As the high warming scenario generally produced the wettest and driest climate simulations, the scenario Cwet and Cdry climates were selected from the 15 climate simulations produced using the high warming (+1.3°C) scenario. Scenario Cwet was identified at the second wettest climate (i.e. second highest average annual P) from within the 15 high warming scenario climate projections (see Table 10). Scenario Cmid was identified as the median climate (i.e. eight highest average annual P) from within the 15 medium warming scenario climate projections (see Table 10). Cdry was the second driest climate (i.e. second lowest average annual P) from within the 15 high warming scenario climate projections (the high warming scenario is used, not the low warming scenario, as the high warming scenario produced the largest changes in P – refer to Figure 32 and Table 10). This selection procedure was applied separately to each region, each division and to the whole project area (Table 12). This means that adjacent reporting areas can have ~2030 climates generated from different GCMs, and that the representative ~2030 climate for a division may not be the same as the aggregate of the representative climates of all its constituent regions.

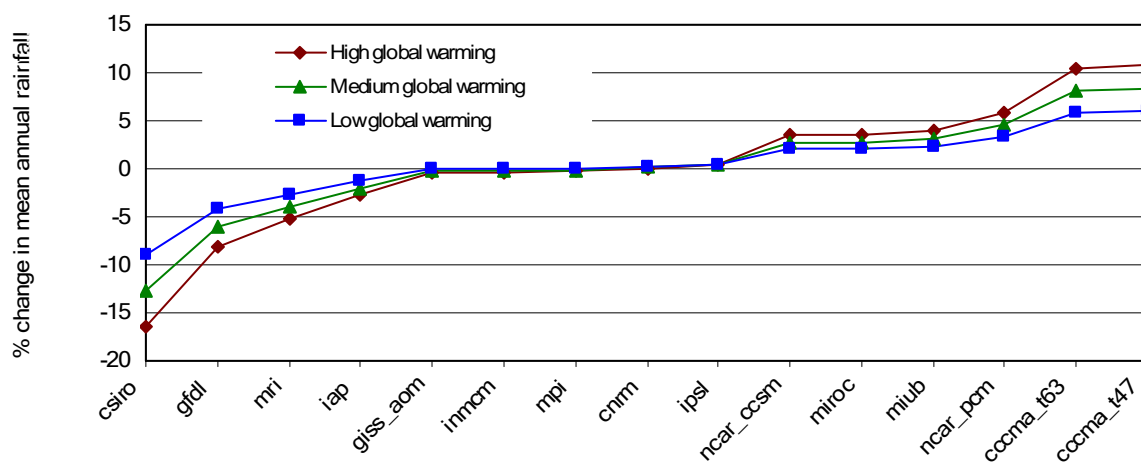


Figure 32. Percent change in mean annual rainfall for the 15 GCMs using the high, medium and low global warming scenarios for the project area. The GCMs are ordered by their percent change for the high global warming scenario from lowest (on the left) to highest (on the right). The values for this data are provided below in Table 10, and the spatial distributions of P percent simulated change for the 15 GCMs for the medium warming scenario are shown in Figure 26

Table 10. Mean annual rainfall and percent rainfall change over the project area for the 15 GCMs using the high, medium and low global warming scenarios. The rainfall percent change is calculated as (GCM rainfall – historical rainfall) / historical rainfall and expressed as a percentage. The historical rainfall value is derived from Scenario A results and is 850 mm/year (see Table 1). The mean annual rainfall change data are plotted in Figure 32. Scenario Cwet (high scenario GCM = cccma\_t63) Cmid (medium scenario GCM = cnrm) and the Cdry (high scenario GCM = gfdl) are bolded. The spatial distributions of P percent simulated change for the 15 GCMs for the medium warming scenario are shown in Figure 26

High global warming			Medium global warming			Low global warming		
GCM	Rainfall	Rainfall	GCM	Rainfall	Rainfall	GCM	Rainfall	Rainfall
	mm/y	percent change		mm/y	percent change		mm/y	percent change
csiro	708	-16.56%	csiro	741	-12.79%	csiro	774	-8.87%
<b>gfdl</b>	<b>781</b>	<b>-8.05%</b>	<b>gfdl</b>	<b>797</b>	<b>-6.13%</b>	<b>gfdl</b>	<b>813</b>	<b>-4.21%</b>
mri	805	-5.14%	mri	816	-3.90%	mri	827	-2.65%
iap	826	-2.72%	iap	832	-2.03%	iap	838	-1.34%
giss_aom	846	-0.42%	giss_aom	847	-0.26%	giss_aom	848	-0.10%
inmcm	846	-0.34%	inmcm	847	-0.20%	inmcm	849	-0.06%
mpi	847	-0.24%	mpi	848	-0.12%	mpi	849	-0.01%
cnrm	850	0.08%	<b>cnrm</b>	<b>850</b>	<b>0.12%</b>	cnrm	850	0.16%
ipsl	852	0.39%	ipsl	852	0.36%	ipsl	852	0.33%
ncar_ccsm	879	3.47%	ncar_ccsm	872	2.73%	ncar_ccsm	866	1.99%
miroc	879	3.57%	miroc	873	2.81%	miroc	866	2.05%
miub	882	3.87%	miub	875	3.04%	miub	868	2.21%
ncar_pcm	899	5.87%	ncar_pcm	888	4.57%	ncar_pcm	877	3.28%
<b>cccma_t63</b>	<b>938</b>	<b>10.51%</b>	<b>cccma_t63</b>	<b>918</b>	<b>8.15%</b>	<b>cccma_t63</b>	<b>898</b>	<b>5.78%</b>
cccma_t47	941	10.84%	cccma_t47	920	8.40%	cccma_t47	900	5.96%

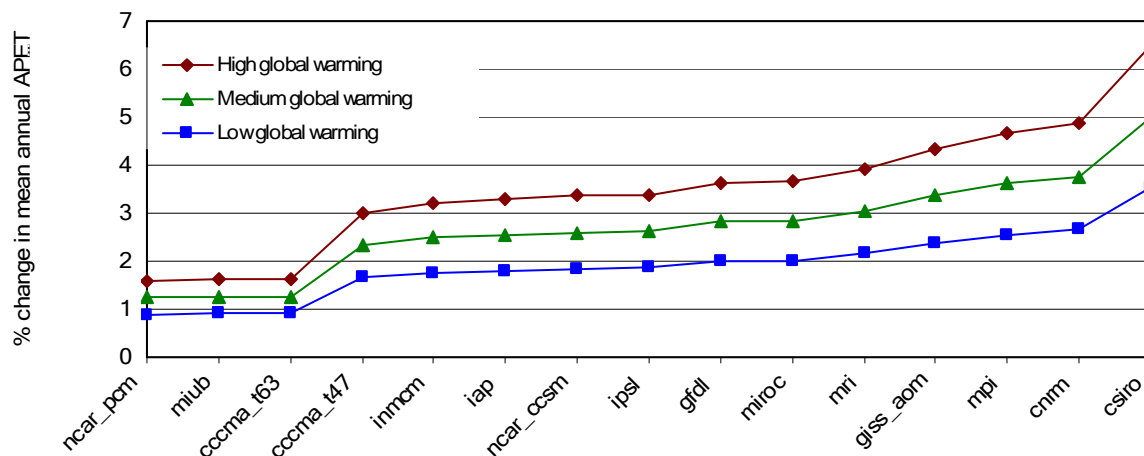


Figure 33. Percent change in mean annual APET for the 15 GCMs using the high, medium and low global warming scenarios for the project area. The GCMs are ordered by their percent change for the high global warming scenario from lowest (on the left) to highest (on the right). The values for these data are provided below in Table 11, and the spatial distributions of APET percent simulated change for the 15 GCMs for the medium warming scenario are shown in Figure 31

Table 11. Mean annual APET and percent APET change over the project area for the 15 GCMs using the high, medium and low global warming scenarios. The APET percent change is calculated as (GCM APET – historical APET) / historical APET and expressed as a percentage. The historical APET value is derived from Scenario A and is 1954 mm/year (see Table 3). The mean annual APET change data are plotted in Figure 33. Scenario Cwet (high scenario GCM = cccma\_t63) Cmid (medium scenario GCM = cnrm) and the Cdry (high scenario GCM = gfdl) are bolded; noting this decision is based on P not APET. The spatial distributions percent simulated change for the 15 GCMs for the medium warming scenario are shown in Figure 31

High global warming			Medium global warming			Low global warming		
GCM	APET	APET	GCM	APET	APET	GCM	APET	APET
	mm/y	percent change		mm/y	percent change		mm/y	percent change
ncar_pcm	1984	1.58%	ncar_pcm	1977	1.23%	ncar_pcm	1970	0.89%
miub	1985	1.62%	miub	1978	1.26%	miub	1971	0.91%
<b>cccma_t63</b>	<b>1985</b>	<b>1.62%</b>	cccma_t63	1978	1.26%	cccma_t63	1971	0.91%
cccma_t47	2011	2.99%	cccma_t47	1998	2.32%	cccma_t47	1985	1.65%
inmcm	2016	3.22%	inmcm	2002	2.50%	inmcm	1988	1.77%
iap	2017	3.29%	iap	2003	2.55%	iap	1988	1.81%
ncar_ccsm	2019	3.36%	ncar_ccsm	2004	2.60%	ncar_ccsm	1989	1.84%
ipsl	2019	3.38%	ipsl	2004	2.62%	ipsl	1989	1.86%
<b>gfdl</b>	<b>2024</b>	<b>3.64%</b>	gfdl	2008	2.82%	gfdl	1992	2.00%
miroc	2025	3.67%	miroc	2009	2.84%	miroc	1992	2.01%
mri	2030	3.92%	mri	2012	3.03%	mri	1995	2.15%
giss_aom	2038	4.35%	giss_aom	2019	3.37%	giss_aom	2000	2.38%
mpi	2045	4.68%	mpi	2024	3.62%	mpi	2003	2.56%
cnrm	2048	4.87%	<b>cnrm</b>	<b>2027</b>	<b>3.76%</b>	cnrm	2005	2.66%
csiro	2080	6.49%	csiro	2051	5.01%	csiro	2022	3.53%

Over the all-project-area, there is more variation in the projections of rainfall than in the projections of APET (Table 12, and contrast the projected changes presented in Figure 32, Table 10 with those in Figure 33, Table 11). The range in projected water-year rainfall varies between 781 and 939 mm/year compared to its historical average of 850 mm/year. APET is projected to range between 1985 and 2027 mm/year compared to a historical average of 1954 mm/year. Water year rainfall under the Scenario Cwet climate may increase by 10 percent and APET increase by 2 percent. Under the Scenario Cmid climate, yearly rainfall may potentially remain unchanged (i.e. 0 percent change when rounded to the nearest integer) and APET to increase by 4 percent, and, under the Scenario Cdry climate, to decrease by 8 percent and increase by 4 percent, respectively. The changes in rainfall are projected to occur almost exclusively in the wet season, whereas changes in APET are projected to occur more uniformly across the two seasons. Regionally, the differences between scenarios Cwet and Cdry rainfall projections generally range between 150 to 250 mm/year and those of APET generally range between 20 and 80 mm/year (Table 12). For rainfall regionally, the average difference between scenarios Cwet and Cdry is 194 mm/year, the largest and smallest differences are projected to occur in the Van Diemen and Flinders-Leichhardt regions, being 305 mm/year and 91 mm/year, respectively (see Table 12). Whereas for APET regionally, the average difference between scenarios Cwet and Cdry is 44 mm/year, the largest and smallest differences are projected to occur in the Daly and Kimberley regions, being 102 mm/year and 8 mm/year, respectively (see Table 12).

Table 12. Annual and seasonal averaged P and APET for historical conditions and for scenario Cwet, Cmid and Cdry 2030 climate simulations. Note that the sum of the seasonal values do not always equal the water year values because the combined wet season–dry season period (Nov–Oct) is different to the water year period (Sep–Aug)

	Scenario	GCM	Rainfall			APET		
			Water year	Wet season	Dry season	Water year	Wet season	Dry season
			mm/y or mm/season					
NASY*	Historical		850	802	48	1954	1068	886
	Cwet	CCCMA T63	939	877	51	1985	1075	908
	Cmid	CNRM	850	793	47	2027	1106	918
	Cdry	GFDL 2.0	781	729	42	2025	1104	917
TS	Historical		868	822	46	1979	1068	911
	Cwet	CCCMA T47	942	884	47	2044	1098	944
	Cmid	CNRM	875	818	46	2052	1106	944
	Cdry	GFDL 2.0	743	695	39	2063	1115	945
GC	Historical		779	735	44	1939	1076	863
	Cwet	CCCMA T63	872	815	47	1970	1083	884
	Cmid	INMCM	777	725	43	1987	1099	884
	Cdry	MRI	727	682	36	2020	1119	897
01NE	Historical		1338	1233	105	1853	989	864
	Cwet	CCCMA T63	1508	1383	108	1880	994	884
	Cmid	INMCM	1350	1226	108	1893	1009	881
	Cdry	MRI	1218	1118	87	1921	1028	890
02FI	Historical		577	534	43	2023	1140	883
	Cwet	MIROC-M	612	562	42	2095	1175	915
	Cmid	INMCM	579	530	42	2077	1167	906
	Cdry	GFDL 2.0	469	423	39	2109	1189	915
03KI	Historical		950	898	53	1994	1069	926
	Cwet	GISS-AOM	1006	938	55	2068	1102	963
	Cmid	CNRM	959	894	53	2065	1105	957
	Cdry	GFDL 2.0	819	765	44	2076	1114	959
04OB	Historical		730	689	41	1988	1092	896
	Cwet	CCCMA T47	798	747	41	2054	1123	928
	Cmid	INMCM	741	692	39	2037	1117	917
	Cdry	GFDL 2.0	632	587	37	2081	1143	933
05DA	Historical		1019	975	44	1942	1015	927
	Cwet	NCAR-PCM1	1131	1057	63	1967	1017	949
	Cmid	GISS-AOM	1032	978	44	2003	1045	957
	Cdry	CSIRO MK3.0	892	856	26	2069	1088	979
06VD	Historical		1390	1327	63	1936	972	964
	Cwet	NCAR-PCM1	1531	1428	84	1957	973	984
	Cmid	IPSL	1396	1318	62	1977	991	986
	Cdry	CSIRO MK3.0	1226	1176	35	2043	1034	1008
07AR	Historical		1186	1140	46	1898	958	941
	Cwet	NCAR-PCM1	1266	1201	51	1918	959	958
	Cmid	IAP	1202	1143	45	1931	973	957
	Cdry	CSIRO MK3.0	1060	1017	30	1995	1013	981
08RO	Historical		843	805	38	1928	1023	906
	Cwet	CCCMA T63	932	882	41	1959	1030	928
	Cmid	CNRM	843	797	38	2001	1061	937
	Cdry	GFDL 2.0	765	724	34	1996	1060	934
09SW	Historical		670	631	39	1961	1103	858
	Cwet	MIROC-M	732	683	40	2022	1134	884
	Cmid	IPSL	668	624	37	2009	1125	880
	Cdry	MRI	632	593	32	2041	1143	894
10FL	Historical		493	437	56	1939	1134	805
	Cwet	MIROC-M	547	481	59	1993	1160	828
	Cmid	GFDL 2.0	492	432	54	1994	1159	830
	Cdry	GISS-AOM	456	398	51	2038	1186	847
11SE	Historical		750	710	40	1980	1109	871
	Cwet	CCCMA T47	855	803	42	2035	1132	899
	Cmid	GFDL 2.0	750	702	39	2026	1128	894
	Cdry	MRI	698	657	32	2065	1153	908

\*the all-project-area

	Scenario	GCM	Rainfall			APET		
			Water year	Wet season	Dry season	Water year	Wet season	Dry season
			mm/y or mm/season					
12MI	Historical		965	917	48	1905	1036	870
	Cwet	CCCMA T63	1098	1034	51	1935	1041	891
	Cmid	MIROC-M	970	909	49	1960	1067	889
	Cdry	MRI	885	836	38	1982	1078	901
13WC	Historical		1417	1370	47	1874	974	900
	Cwet	CCCMA T63	1570	1502	48	1902	979	921
	Cmid	NCAR-PCM1	1435	1369	48	1897	982	913
	Cdry	MRI	1320	1265	39	1944	1013	929
14NC	Historical		1338	1233	105	1853	989	864
	Cwet	CCCMA T63	1508	1383	108	1880	994	884
	Cmid	INMCM	1350	1226	108	1893	1009	881
	Cdry	MRI	1218	1118	87	1921	1028	890

The spatial distributions of projected 2030 P and APET for the project area are presented in Figure 34 and Figure 35, respectively. The ~2030 simulated rainfall is projected to retain the strong north–south gradient in the wet season, but with latitudinal shifts for a given mean annual rainfall depending on the emissions scenario: a southwards shift under Scenario Cwet and a northwards shift under Scenario Cdry, compared to its location historically (Figure 34). Under the Scenario Cmid and Scenario Cdry climates, projections also suggest that there may be changes in the rainfall gradient caused by relatively greater decreases in rainfall occurring along the northern coastlines than over project area’s south (see Figure 34). Figure 35 shows that the spatial patterns in projected APET reflect those of historical APET, being highly regionalised. The greatest APET changes are simulated to occur at the base of the Gulf of Carpentaria and south and east of the Kimberley region.

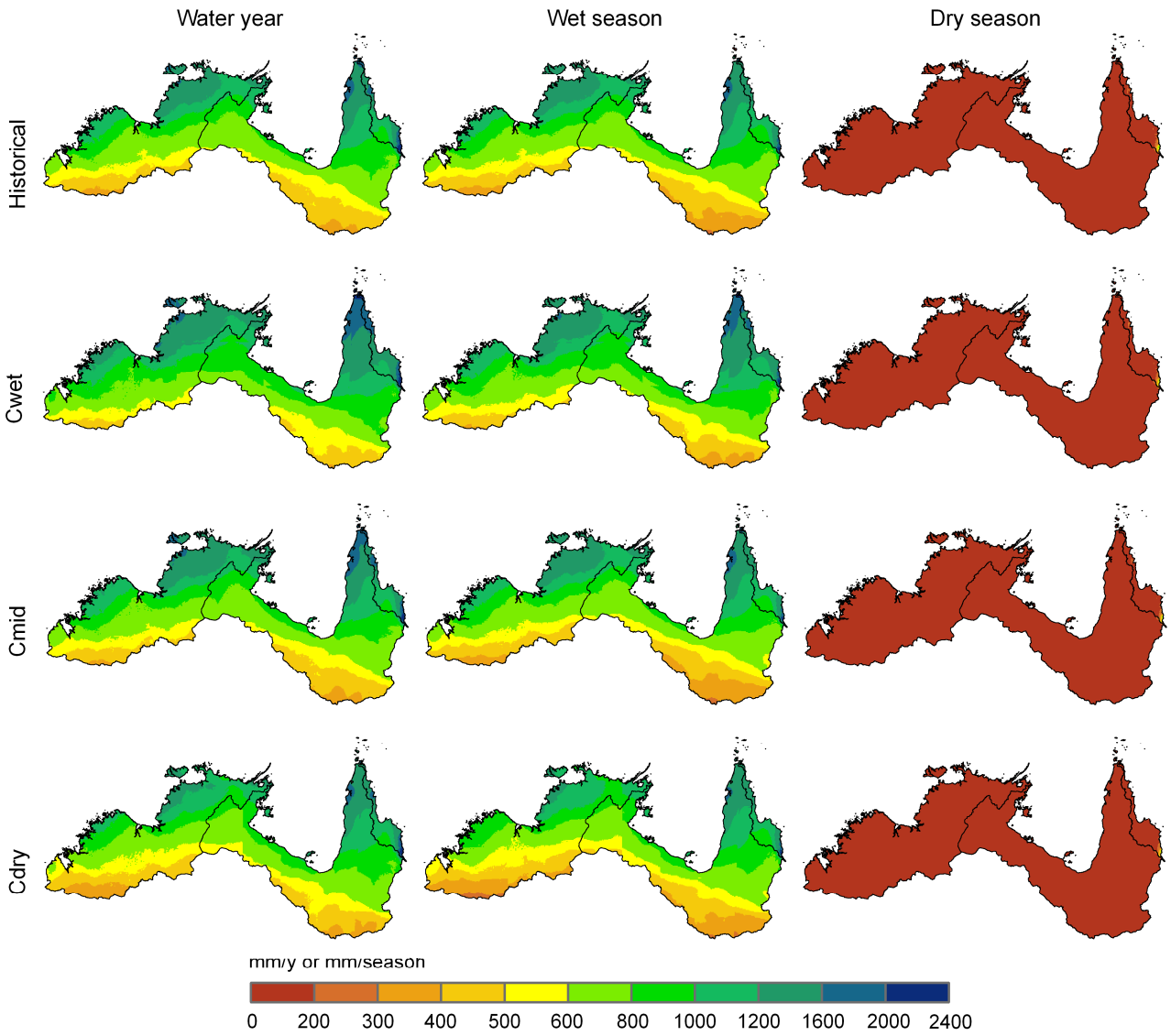


Figure 34. Water year, wet season and dry season rainfall for the project area under historical climate and scenarios Cwet, Cmid and Cdry 2030 climate projections

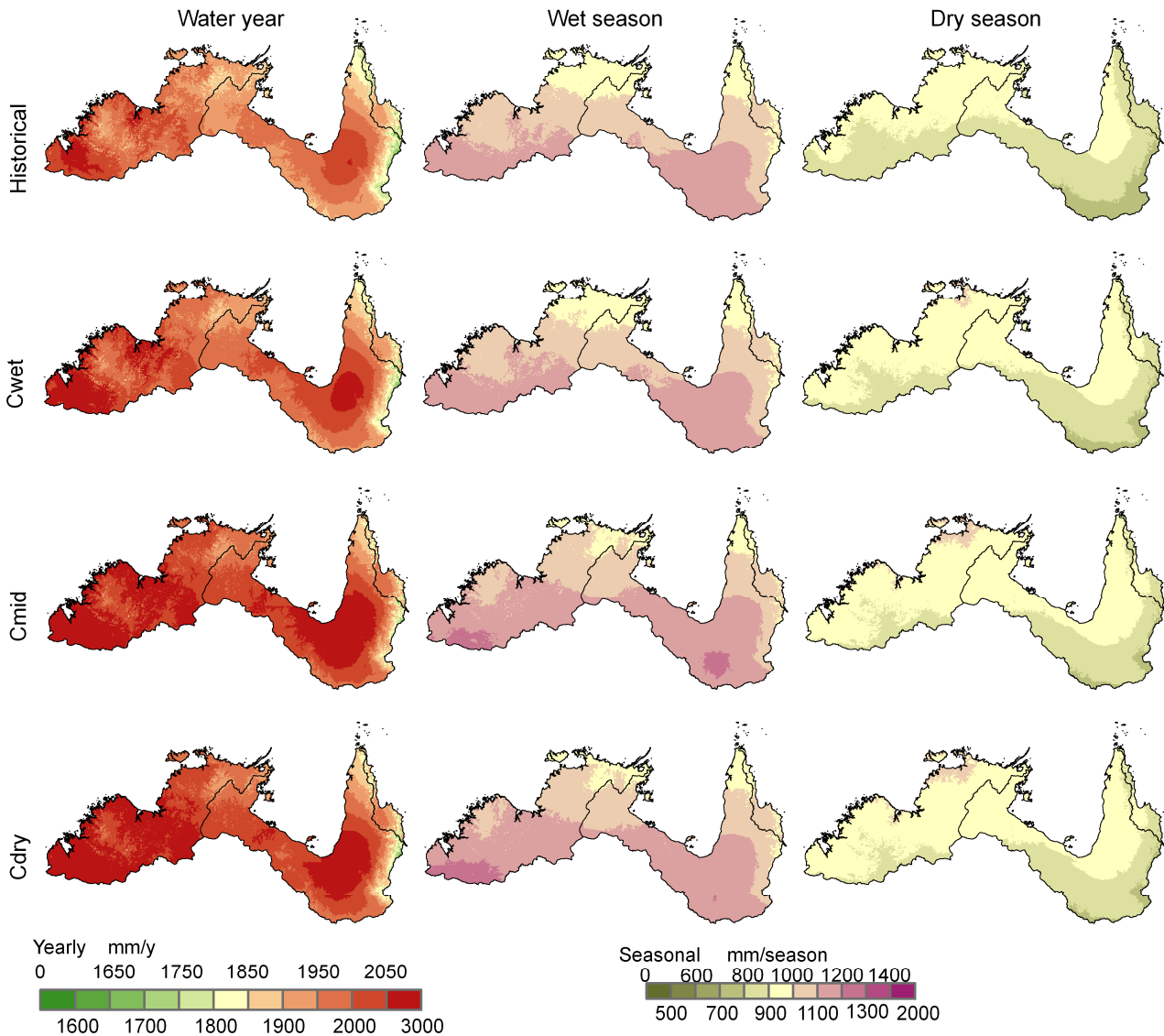


Figure 35. Water year, wet season and dry season APET for the project area under historical climate and scenarios Cwet, Cmid and Cdry 2030 climate projections

On a regional basis, the relative differences between the three ~2030 climate simulations and the historical climate (Figure 36) highlight the spatial patterns of projected change. Under Scenario Cwet, the rainfall is projected to increase by over 6 percent for all regions other than the two most western regions (the Fitzroy (WA) and Kimberley). The lower relative change in these two regions is likely linked to the recent (i.e. 1980 onwards) large increasing trends of rainfall which are included in the historical (Scenario A) rainfall statistics that the ~2030 climate simulations are compared to generate this analysis. Rainfall for Scenario Cmid straddles a zero percent change, varying regionally from a 3 percent decrease to a 3 percent increase. Under Scenario Cdry, all regions are projected to become drier, by at least 6 percent and especially in the Timor Sea Drainage Division with decreases ranging from 12 to 18 percent (Figure 36). As previously noted, changes in APET are projected to be more moderate than those in rainfall, and under all climate scenarios for all regions increases are projected – with most projected increases being in the range of zero to 6 percent (see Figure 36). Under Scenario Cwet, it is interesting to note that the APET projections have the expected complimentary regional pattern to Scenario Cwet rainfall.

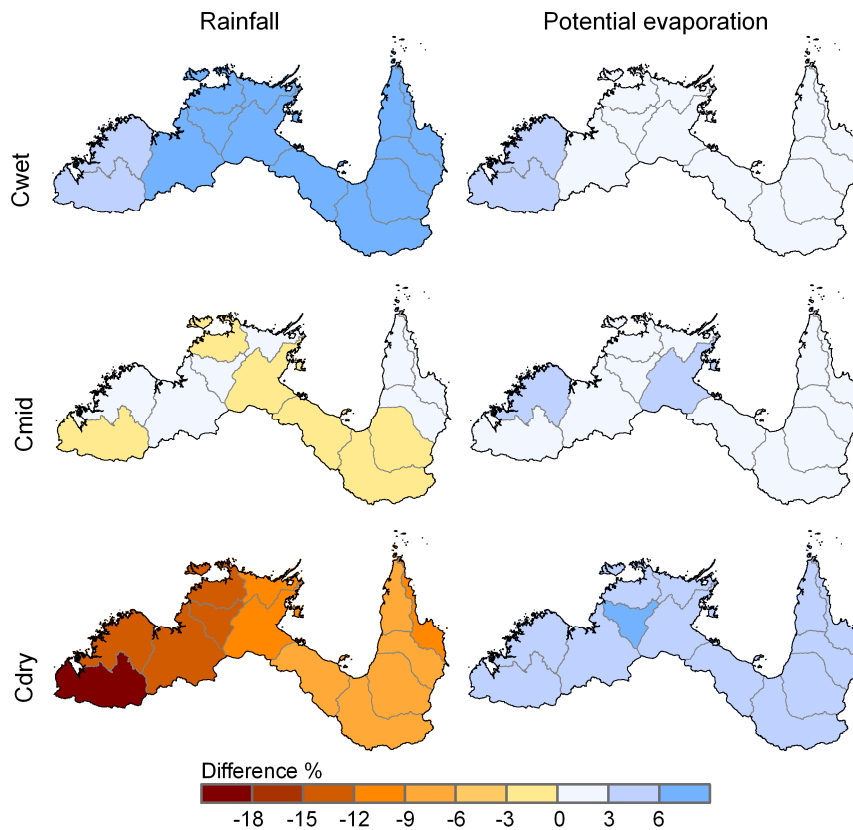
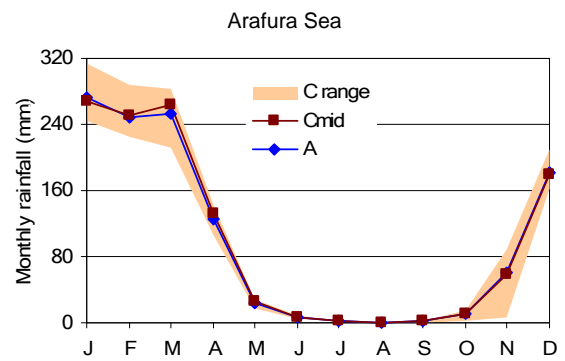
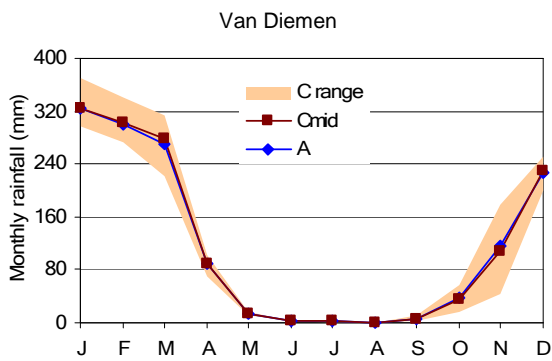
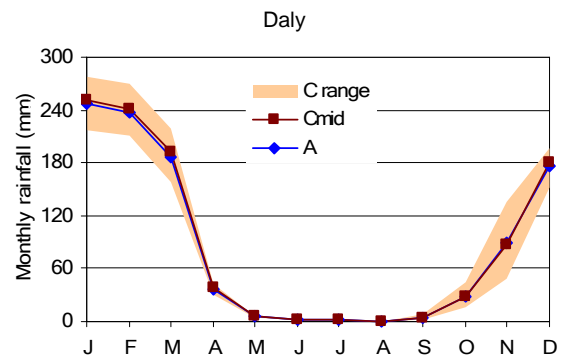
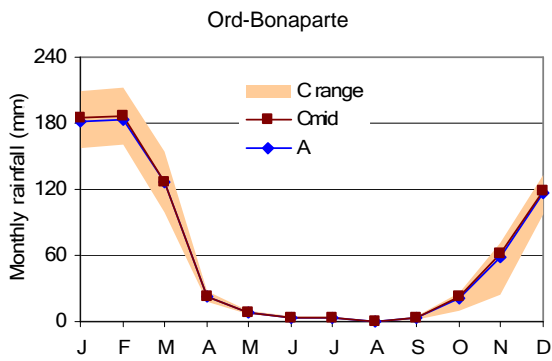
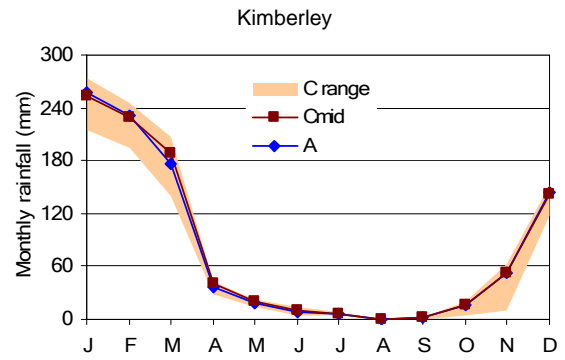
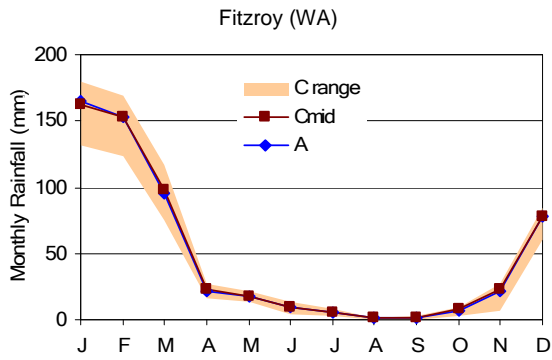
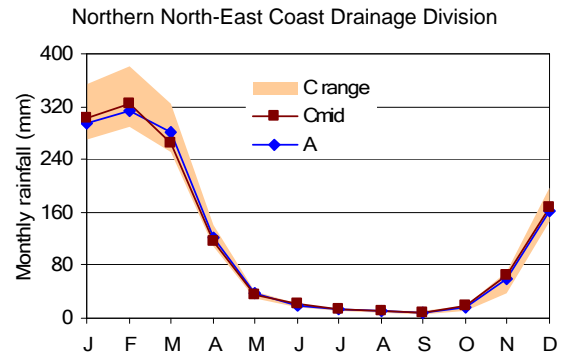
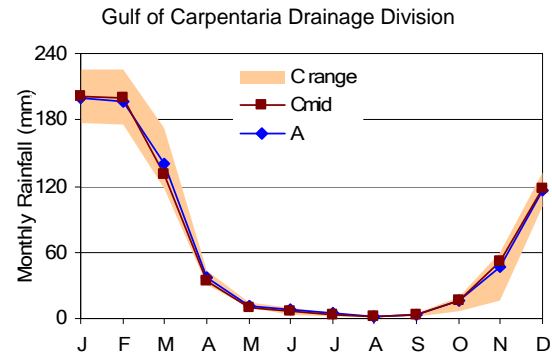
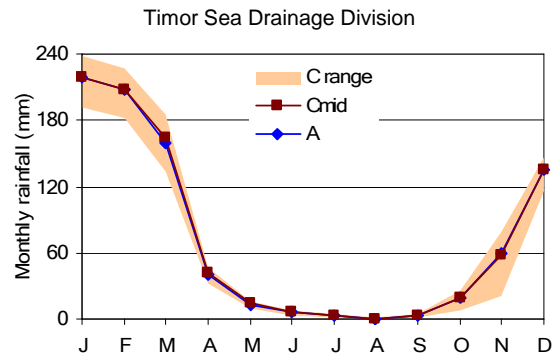
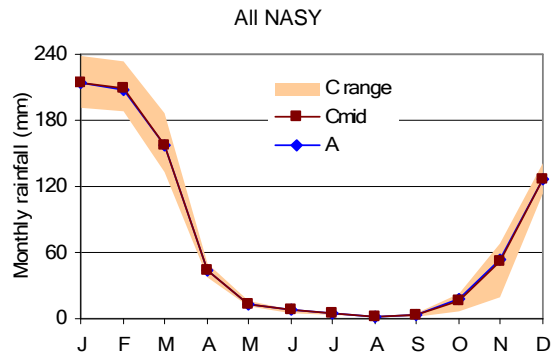


Figure 36. The relative difference in rainfall and areal potential evapotranspiration under scenarios Cwet, Cmid and Cdry relative to historical climate

Figure 37 and Figure 38 show that long-term monthly mean of Scenario Cmid ~2030 simulated rainfall, respectively, do not differ much from historical values. Historical rainfall lies well within the projected range in values from all 45 modelled climates (see Figure 37). The seasonality of rainfall is projected to change slightly only in that any changes in rainfall will occur in the wet season. However, there is appreciable variation in the rainfall projections in the wet season months (mainly November to March for most regions), with the range in any given region varying by approximately 50 to 100 mm/month. The largest monthly range in rainfall values from all 45 modelled climates was 135 mm/month in November in the Van Diemen region (see Figure 37). In contrast, historical APET is projected to lie at, or just below, the lower bound of the ~2030 projected range in APET values from all 45 modelled climates (Figure 38). The seasonality of APET is likely to remain the same as changes are projected to occur uniformly across the year – as seen by the difference between scenario A and Cmid being approximated by a single offset for most regions throughout the year. The largest monthly range in APET values from all 45 modelled climates was 22 mm/month in December in the South-East Gulf region.



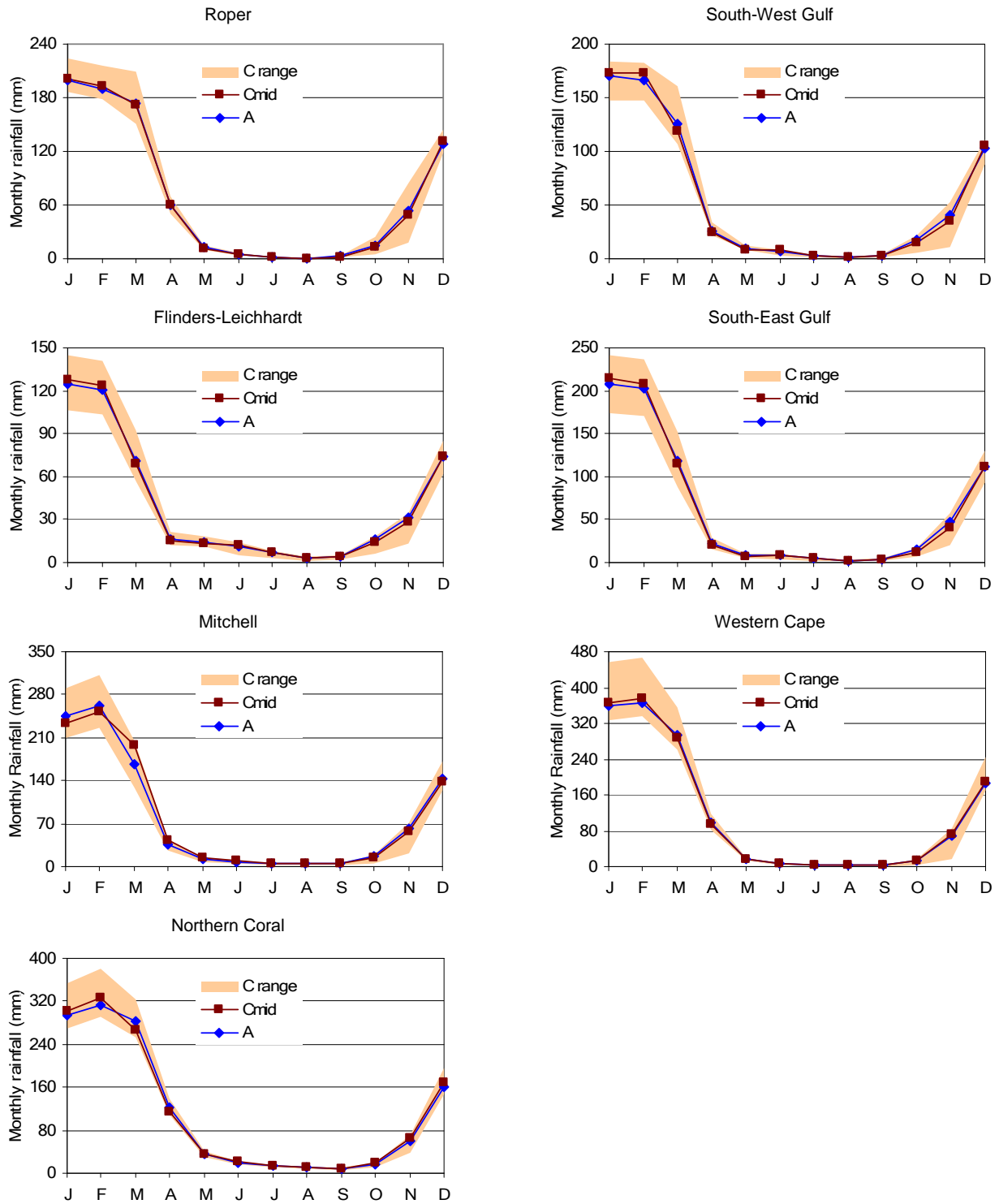
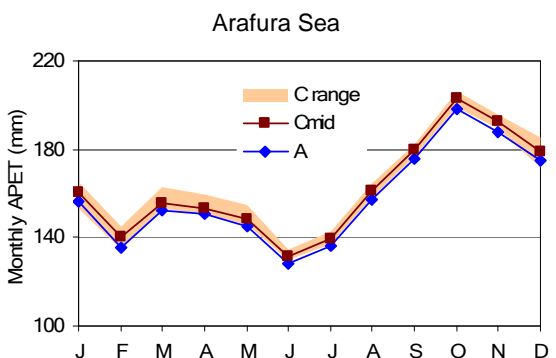
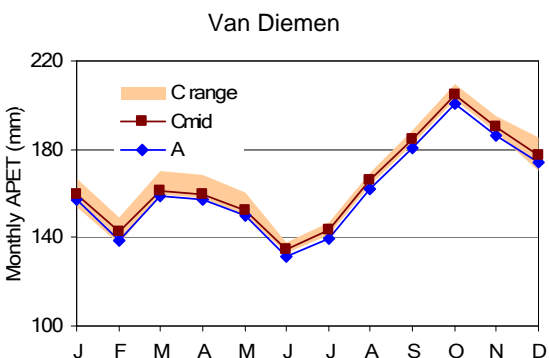
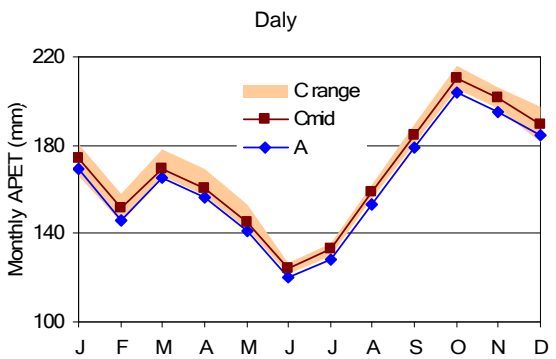
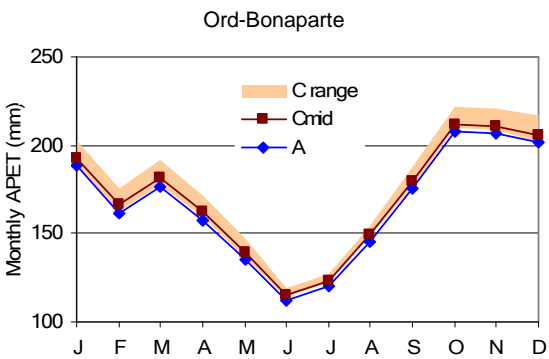
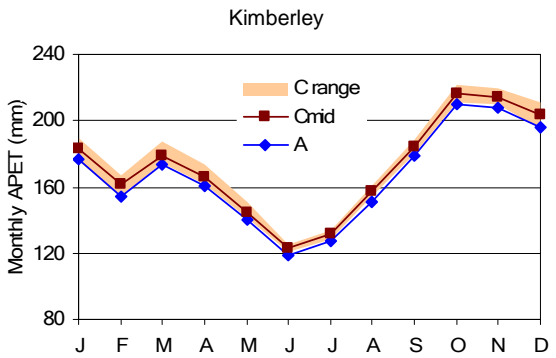
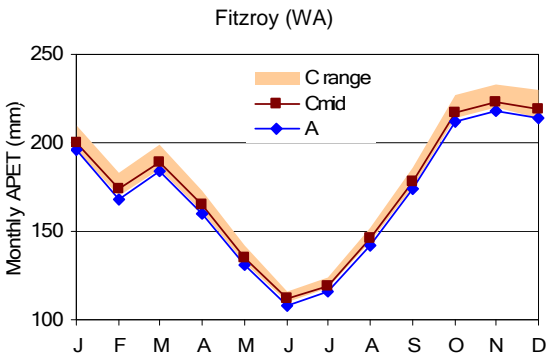
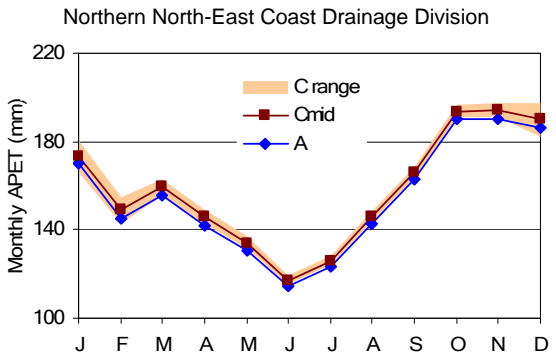
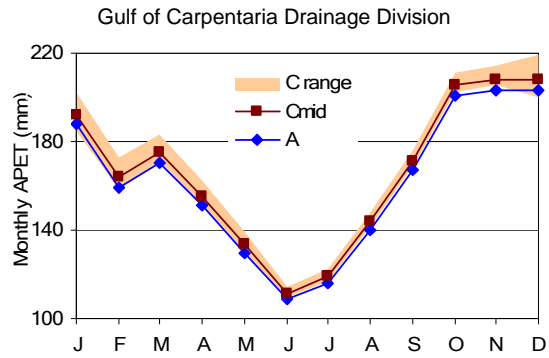
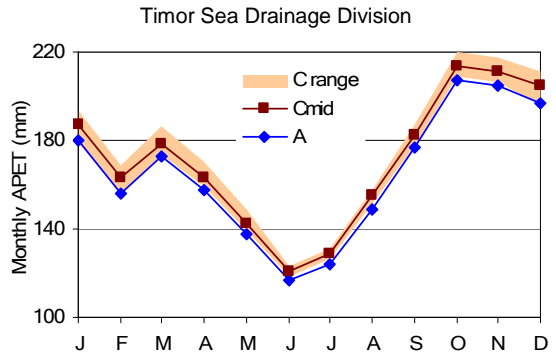
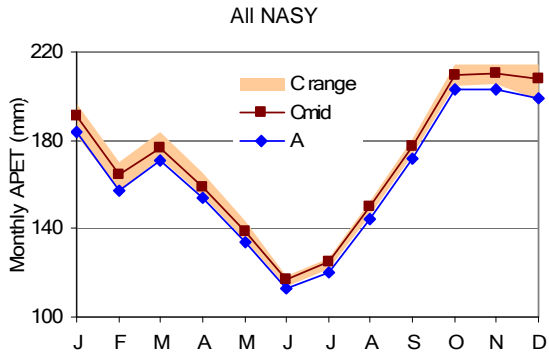


Figure 37. Mean monthly rainfall across northern Australia, reported for the 17 areas under historical climate (i.e. Scenario A – labelled A) and Scenario C. The range of Scenario C values (C range) is the highest and lowest value from all 45 future ~2030 climate variants (i.e. the 15 GCMs and the high, medium and low emission scenarios)



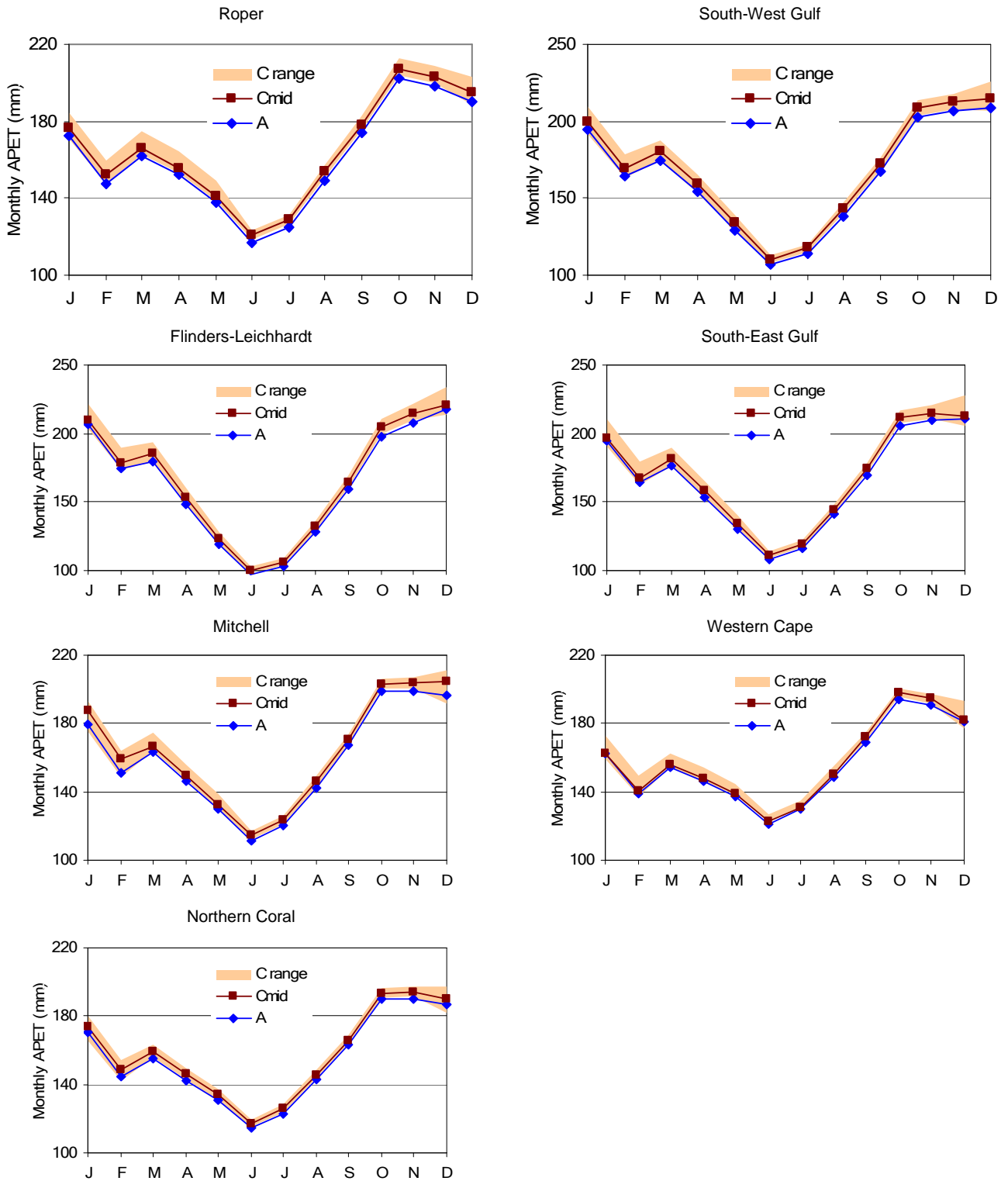


Figure 38. Mean monthly APET across northern Australia, reported for the 17 areas under historical climate (i.e. Scenario A – labelled A) and Scenario C. The range of Scenario C values (C range) is the highest and lowest value from all 45 future ~2030 climate variants (i.e. the 15 GCMs and the high, medium and low emission scenarios)



## 5 Confidence levels

A variety of metrics are calculated to characterise the level of confidence associated with the input data for the scenarios. These metrics do not perform 'confidence level' analysis in the strict statistical meaning of this term; here the term is used more generally as a basis to provide some characterisation of the confidence, or uncertainty, involved in each scenario.

As rainfall is the variable with the greatest uncertainty when interpolating, and is the primary variable controlling runoff (Chiew, 2006a), it is important to understand the confidence associated with it when interpreting rainfall-runoff modelling results. While both Australia-wide error statistics and long-term average maps of error have been reported (Jeffrey et al., 2001) that provide indicative levels of confidence of the data used in the construction of scenarios A, B and C, here the combined spatio-temporal dynamics are analysed. This is achieved by combining, for each decade, both the distance between each grid-cell to the nearest 10 input stations and the completeness of the records of these closest stations into a single metric – called the 'distance-completeness' index.

The distance-completeness index is a unitless metric, scaled consistently over the entire period, providing a quantitative measure illustrating the dynamics of the underpinning observation network. The completeness of record for each decade of the nearest 10 meteorological stations to each grid cell were weighted using a Gaussian distance function:

$$w = \exp(-d/h)^2$$

where  $w$  is the vector of weighting factors for the nearest 10 observation stations;  $d$  is a vector of the distance between the grid cell and the nearest 10 observation locations, and  $h$  is the 'bandwidth', which for this case was set to approximately 250 km (defined by 50 0.05° grid cells). The maximum value of the 10 nearest station's distance-weighted completeness value was then recorded at the grid cell, which provides an index of confidence of the gridded meteorological data at every geographic location. Within the distance-completeness index, stations with a higher completeness of record have a larger spatial footprint of influence. The index is scaled between 0.0 and 1.0, with a value of 1.0 being obtained for any SILO grid-cell in which a Bureau of Meteorology station is located that recorded rainfall data for every day of the decade. The index decreases as the distance to an observation increases, and/or the completeness of the recorded rainfall decreases.

Figure 39 shows the distance-completeness index for rainfall for the period of the study. The analysis reveals that coverage of BoM stations increases through time series with the majority of the area having values  $>0.5$  since the 1930s and only minimal areas having values less than  $<0.5$  since the 1970s. While characterising the confidence of rainfall is of primary interest (due to the influence it has on daily rainfall-runoff modelling), we also show the decadal distance-completeness index for maximum daily air temperature (Figure 40) as this indicates the relative confidence of an input to the Morton's areal potential evapotranspiration used here. Over time, the distance-completeness index for maximum daily air temperature has been generally increasing, as the density of BoM observations has increased. As expected, the distance-completeness index for maximum daily air temperature (Figure 40) is less than that for rainfall (Figure 39). This is due to the BoM establishing and maintaining a rainfall observation network with greater density than the air temperature observation network. This is done purposefully to capture high localised variance in time and space of rainfall compared to air temperature. Note that the distance-completeness index does not consider the underlying spatial and temporal auto-correlations of the climate variables that are interpolated.

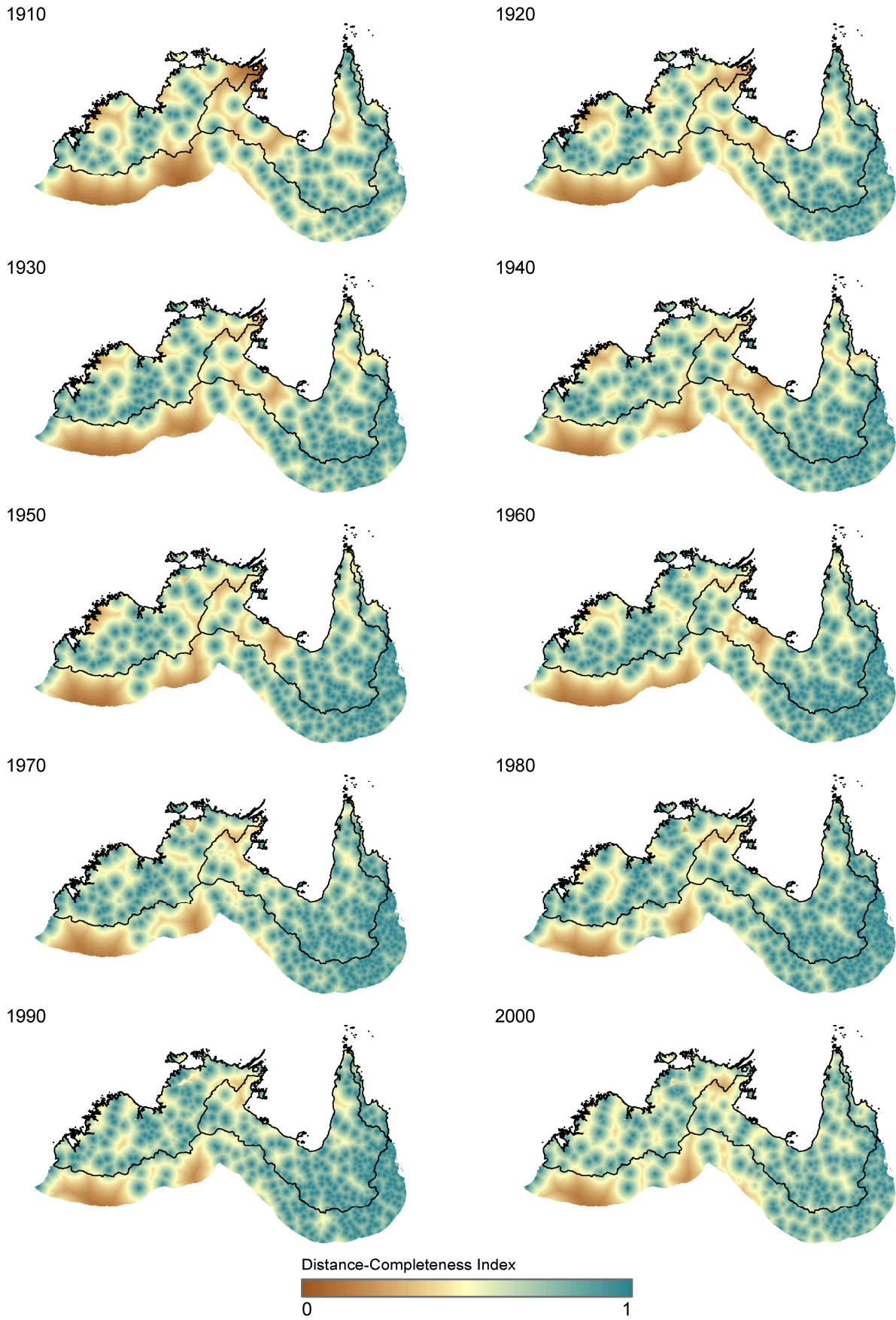
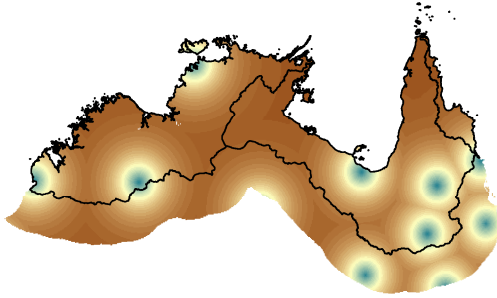
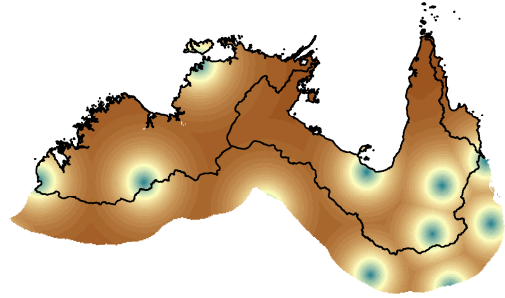


Figure 39. Decadal maps of the distance-completeness index for rainfall. A value of 1.0 means the location is at a station with a complete rainfall record, and the index decreases with distance away from stations and/or with decreasing completeness of rainfall record. The decade labelled 1910 is defined from 1 January 1910 to 31 December 1919, and so on

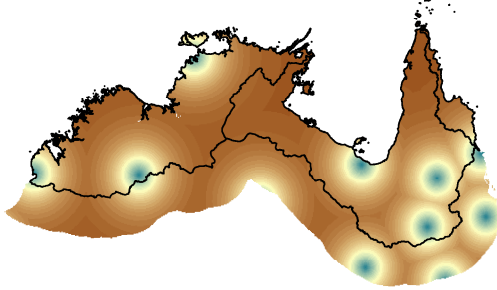
1910



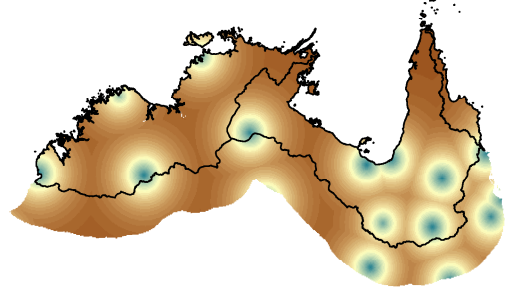
1920



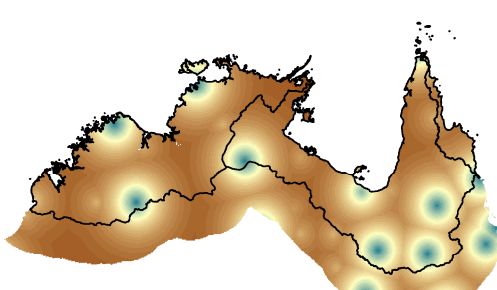
1930



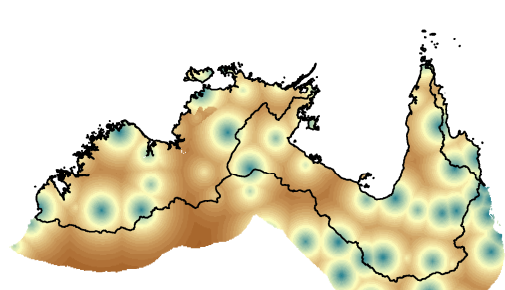
1940



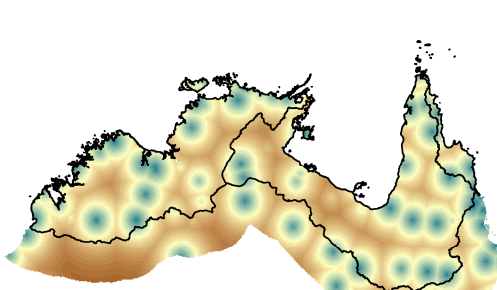
1950



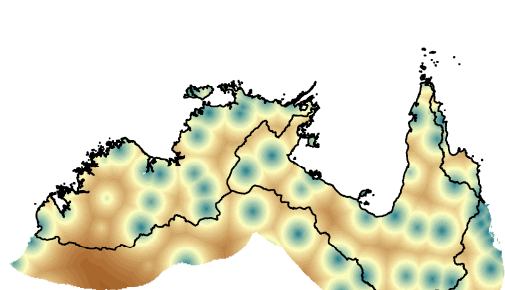
1960



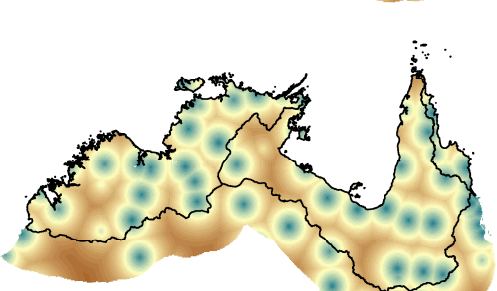
1970



1980



1990



2000

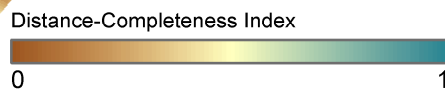
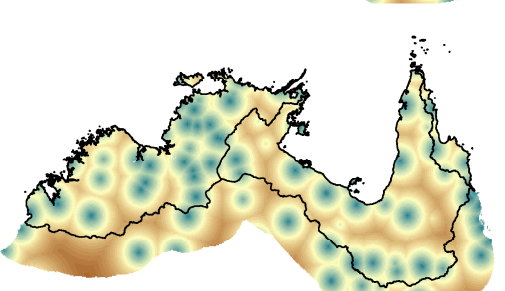


Figure 40. Decadal maps of the distance-completeness index for maximum air temperature. A value of 1.0 means the location is at a station with a complete record, and the index decreases with distance away from stations and/or with decreasing completeness of record. The decade labelled 1910 is defined from 1 January 1910 to 31 December 1919, and so on

## 6 Conclusions

Scenario A's 77-year record (1 September 1930 to 31 August 2007) was based on the SILO database developed and maintained in real-time by the Queensland Climate Change Centre of Excellence. Scenario B is used to assess future water availability should the climate in the future prove to be similar to that of the most recent 11 years (i.e. 1 September 1996 to 31 August 2007). Scenario C is used to assess a range of climate conditions around the year 2030. Forty-five future climate variants, each with 77 years of daily climate sequences, are used. The future climate variants come from scaling the historical climate data to represent ~2030 climate, based on analyses of 15 global climate models (GCMs) and three global warming scenarios from the Fourth Assessment Report (AR4) of the Intergovernmental Panel on Climate Change (IPCC, 2007).

The mean annual rainfall, averaged over the 77-year period for the entire project area is 850 mm. There is a predominant north-south rainfall gradient over much of the area, where rainfall is highest in near-coastal areas (with some isolated locations receiving on average in excess of 3,000 mm/year) and lowest in the south (less than 350 mm). Over the entire area, 94 percent of the rainfall occurs in the wet season defined from November to April the following year. The 77-year mean annual areal potential evapotranspiration averaged across the entire project area is 1954 mm, varying from 2116 mm in the south to 1584 mm in the north. On a mean annual basis, as potential evapotranspiration is greater than rainfall, most of the project area is a water-limited landscape, noting there are pockets where on a mean annual basis rainfall is greater than potential evapotranspiration and so hydrologically are considered energy-limited. However, due to the high wet season rainfall that is extremely intense, significant river flows occur, mainly in the wet season. Over the 77-year period rainfall trends are increasing, and this is primarily due to an increase in rainfall intensity, with the number of rain-days per year being fairly constant.

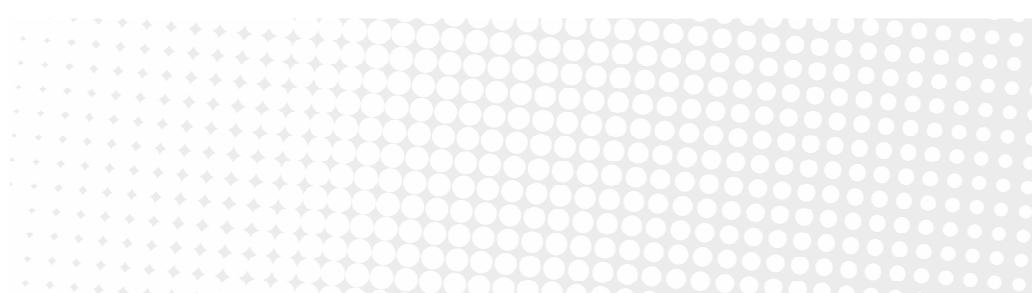
The mean annual rainfall averaged over the project area in the most recent 11 years is 1001 mm, which is 17.8 percent higher than the 77 year mean of 850 mm. The increases are seen primarily in the Timor Sea Drainage Division (the western part of the study area) whereas for much of the Gulf of Carpentaria Drainage Division and the northern portion of the North-East Coast Drainage Division rainfall in the most 11 years is similar to that of the previous 77 years.

There is considerable uncertainty in the global warming projections and in the projections of how global warming affects local rainfall, simulations of potential evapotranspiration shows less variance. There are very significant differences in the future annual rainfall simulations between the 15 GCMs, and in the wet season months, regional projections of rainfall can vary by up to 100 mm/month. Over the whole project area, the range in projected water-year rainfall varies between 758 and 873 mm/year compared to its historical average of 850 mm/year. Potential evapotranspiration was projected to range between 1920 and 1972 mm/year compared to a historical average of 1954 mm/year. Water year rainfall under a Scenario Cwet rainfall may increase by 3 percent and potential evapotranspiration decrease by 2 percent, compared to historical values. Under Scenario Cmid, yearly rainfall may potentially decrease by 3 percent and potential evapotranspiration to increase by 1 percent, and, under the Scenario Cdry, to decrease by 11 percent and increase by 1 percent, respectively. The changes in rainfall are projected to occur predominantly in the wet season, whereas changes in potential evapotranspiration are projected to occur more uniformly across the two seasons. Regionally, the differences between the rainfall projections under scenarios Cwet and Cdry are between 50 and 200 mm/year and those of potential evapotranspiration are less than 50 mm/year. While the output from the 15 GCMs are not in agreement, making confident future climate projections problematic, it should be noted that the majority of the GCMs show increases in the highest percentile of rainfall in ~ 2030 compared to the ~ 1990 levels, especially in near-coastal areas. This suggests an increased frequency in large intense rainfall events in these areas generating similarly intense runoff, potentially increasing flood recurrence in these areas.

An assessment of the network of meteorological stations established and maintained by the Bureau of Meteorology that form the underlying input into the SILO database was performed at each grid-cell by coupling the distance to the 10 closest stations with the decadal completeness of the meteorological record at those 10 stations. This assessment illustrates that the coverage of Bureau of Meteorology stations has increased through time with only minimal areas having 'distance-completeness' values less than <0.5 since the 1970s.

## 7 References

- Allen RG, Pereira LS, Raes D and Smith M (1998) Crop evapotranspiration - Guidelines for computing crop water requirements. FAO Irrigation and Drainage Paper 56, Rome, Italy, 300 pp. Available at <<http://www.fao.org/docrep/X0490E/X0490E00.htm>>
- Chiew FHS (2006a) Estimation of rainfall elasticity of streamflow in Australia. *Hydrological Sciences Journal* 51, 613-625.
- Chiew FHS (2006b) An overview of methods for estimating climate change impact on runoff. Launceston, Tasmania.
- Chiew FHS and Leahy C (2003) Comparison of evapotranspiration variables in Evapotranspiration Maps of Australia with commonly used evapotranspiration variables. *Australian Journal of Water Resources* 7, 1-11.
- Chiew FHS, Teng J, Kirono D, Frost AJ, Bathols JM, Vaze J, Viney NR, Young WJ, Hennessy KJ and Cai WJ (2008) Climate data for hydrologic scenario modelling across the Murray-Darling Basin. A report to the Australian Government from the CSIRO Murray-Darling Basin Sustainable Yields Project. CSIRO, Australia, 35 pp.
- CSIRO and Bureau of Meteorology (2007) Climate change in Australia. Technical report, <[www.climatechangeinaustralia.gov.au](http://www.climatechangeinaustralia.gov.au)>
- Donohue RJ, McVicar TR and Roderick ML (2009) Climate-related trends in Australian vegetation cover as inferred from satellite observations, 1981–2006. *Global Change Biology* 15, 1025-1039.
- Frost AJ, Thyer MA, Srikanthan R and Kuczera G (2007) A general Bayesian framework for calibrating and evaluating stochastic models of annual multi-site hydrological data. *Journal of Hydrology* 340, 129-148.
- Huntington TG (2006) Evidence for intensification of the global water cycle: Review and synthesis. *Journal of Hydrology* 319, 83-95.
- IPCC (2007) Climate Change 2007: The Physical Basis. Contributions of Working Group 1 to the Fourth Assessment Report of the Intergovernmental Panel on Climate Change. Cambridge University Press <[www.ipcc.ch](http://www.ipcc.ch)>
- IPCC (2000) Emissions scenarios. A Special Report of Working Group III of the Intergovernmental Panels on Climate Changes. [Nakicenovic N and Swart R (eds.)]. Cambridge University Press, UK. pp570.
- Jeffrey SJ (2006) Error analysis for the interpolation of monthly rainfall used in the generation of SILO rainfall datasets: <<http://www.nrw.qld.gov.au/silo/pdf/interpUpdate.pdf>>
- Jeffrey SJ, Carter JO, Moodie KB and Beswick AR (2001) Using spatial interpolation to construct a comprehensive archive of Australian climate data. *Environmental Modelling and Software* 16, 309-330.
- McMahon TA, Finlayson BL, Haines BL and Srikanthan R (1992) Global Runoff - Continental Comparisons of Annual Flows and Peak Discharges. edition. Catena, Cremligen-Destedt, 166 pp.
- McVicar TR and Jupp DLB (1999) Estimating one-time-of-day meteorological data from standard daily data as inputs to thermal remote sensing based energy balance models. *Agricultural and Forest Meteorology* 96, 219-238.
- McVicar TR, Van Niel TG, Li L, Hutchinson MF, Mu X and Liu Z (2007) Spatially distributing monthly reference evapotranspiration and pan evaporation considering topographic influences. *Journal of Hydrology* 338, 196-220.
- McVicar TR, Van Niel TG, Li LT, Roderick ML, Rayner DP, Ricciardulli L and Donohue RJ (2008) Wind speed climatology and trends for Australia, 1975-2006: Capturing the stilling phenomenon and comparison with near-surface reanalysis output. *Geophysical Research Letters* 35, L20403. doi:10.1029/2008GL035627.
- Morton FI (1983) Operational estimates of areal evapotranspiration and their significance to the science and practice of hydrology. *Journal of Hydrology* 66, 1-76.
- O'Gorman PA and Schneider T (2009) The physical basis for increases in precipitation extremes in simulations of 21st-century climate change. *Proceedings of the National Academy of Sciences* 106, 14773-14777. 10.1073/pnas.0907610106.
- Potter N, Chiew F, Frost A, Srikanthan R, McMahon T, Peel M and Austin J (2008) Characterisation of recent rainfall and runoff in the Murray-Darling Basin. A report to the Australian Government from the CSIRO Murray-Darling Basin Sustainable Yields Project. CSIRO, Canberra, Australia, 40 pp.
- Prescott JA (1940) Evaporation from water surface in relation to solar radiation. *Transactions of the Royal Society of South Australia* 64, 114-125.
- Roderick ML, Rotstayn LD, Farquhar GD and Hobbins MT (2007) On the attribution of changing pan evaporation. *Geophysical Research Letters* 34, L17403. doi:10.1029/2007GL031166.
- Rotstayn LD, Cai W, Dix MR, Farquhar GD, Feng Y, Ginoux P, Herzog M, Ito A, Penner JE, Roderick ML and Wang M (2007) Have Australian rainfall and cloudiness increased due to the remote effects of Asian anthropogenic aerosols? *Journal of Geophysical Research - Atmospheres* 112, D09202. doi:10.1029/2006JD007712.
- Rotstayn LD, Keywood MD, Forgan BW, Gabric AJ, Galbally IE, Gras JL, Luhar AK, McTainsh GH, Mitchell RM and Young SA (2008) Possible impacts of anthropogenic and natural aerosols on Australian climate: A review. *International Journal of Climatology* doi: 10.1002/joc.1729, published online 18/6/2008.
- Suppiah R (1992) The Australian summer monsoon: a review. *Progress in Physical Geography* 16, 283-318
- Suppiah R and Hennessy KJ (1998) Trends in Total Rainfall, Heavy Rain Events and Dry Days in Australia, 1910-1990. *International Journal of Climatology* 10, 1141-1164.



### Contact Us

Phone: 1300 363 400

+61 3 9545 2176

Email: [enquiries@csiro.au](mailto:enquiries@csiro.au)

Web: [www.csiro.au](http://www.csiro.au)

### Your CSIRO

Australia is founding its future on science and innovation. Its national science agency, CSIRO, is a powerhouse of ideas, technologies and skills for building prosperity, growth, health and sustainability. It serves governments, industries, business and communities across the nation.